AD NUMBER

AD848605

NEW LIMITATION CHANGE

TO

Approved for public release, distribution unlimited

FROM

Distribution authorized to U.S. Gov't. agencies and their contractors; Administrative/Operational use; Nov 1968. Other requests shall be referred to Aerospace Medical Research Laboratories, Wright-Patterson Air Force Base, Ohio 45433.

AUTHORITY

AMRL ltr, 3 May 1971

AMRL-TR-68-94

SLIP NET MOBILITY JOINTS FOR PRESSURE SUITS

A. F. FRASER
P. R. PREISWERK

Astro Research Corporation

NOVEMBER 1968

AEROSPACE MEDICAL RESEARCH LABORATORIES
AEROSPACE MEDICAL DIVISION
AIR FORCE SYSTEMS COMMAND
WRIGHT-PATTERSON AIR FORCE BASE, OHIO

NOTICES

When US Government drawings, specifications, or other data are used for any purpose other than a definitely related Government procurement operation, the Government thereby incurs no responsibility nor any obligation whatsoever, and the fact that the Government may have formulated, furnished, or in any way supplied the said drawings, specifications, or other data, is not to be regarded by implication or otherwise, as in any manner licensing the holder or any other person or corporation, or conveying any rights or permission to manufacture, use, or sell any patented invention that may in any way be related thereto.

Federal Government agencies and their contractors registered with Defense Documentation Center (DDC) should direct requests for copies of this report to:

DDC
Cameron Station
Alexandria, Virginia 22314

Non-DDC users may purchase copies of this report from:

Chief, Storage and Dissemination Section
Clearinghouse for Federal Scientific & Technical Information (CFSTI)
Sills Building
5285 Port Royal Road
Springfield, Virginia 22151

Organizations and individuals receiving reports via the Aerospace Medical Research Laboratories' automatic mailing lists should submit the addressograph plate stamp on the report envelope or refer to the code number when corresponding about change of address or cancellation.

Do not return this copy. Retain or destroy.

700 - February 1969 - CO455 - 64-1420

AMRL-TR-68-94

SLIP NET MOBILITY JOINTS FOR PRESSURE SUITS

A. F. FRASER
P. R. PREISWERK

FOREWORD

This report was prepared by members of the staff of Astro Research Corporation, Santa Barbara, California, under Contract AF 33615-67-C-1586 and in support of Project 7164, "Aerospace Protective Technology," and Task 716411, "Aerospace Pressure Outfits". The work was initiated under the direction of Dr. Hans U. Schuerch. During the course of the research, Dr. Allister Fraser joined the Astro staff and took over as principal investigator on this program. Mr. Peter Preiswerk made a major contribution in testing and analysis. Miss Lilly Gloor and Mr. John Thompson fabricated all test specimens and the deliverable components. This report covers the contract period between April 1, 1967 and May 31, 1968. The research reported in this paper was sponsored by the Aerospace Medical Research Laboratories, Aerospace Medical Division, Air Force Systems Command, Wright-Patterson Air Force Base, Ohio, under the contract monitor Mr. J. Donald Bowen. The Astro Research Corporation report number is ARC-R-286.

This technical report has been reviewed and is approved.

Wayne H. McCandless
Technical Director
Biomedical Laboratory
Aerospace Medical Research Laboratories

SUMMARY

A program was conducted to determine experimentally the properties of slip-net materials and configurations and to apply these results to the design and fabrication of pressure-suit elements having near-zero-constraint mobility. A materials survey was completed, and "Dacron" tufbraid was selected as the material best suited for study on this program. A series of tests were performed in order to obtain load-displacement data. The basic test specimen was a pressurized cylindrical tube. The tests included cantilever bending, torsion, and an attempt at pure bending. The last category of tests was only partially successful. Fatigue tests were run on the basic Dacron fiber material in configurations typical of a slip-net fabric.

On the basis of the results of these tests, an integrated design of an entire arm was made; this included a shoulder, upper arm, elbow, forearm, and wrist. The entire arm was fabricated and installed in a Gemini II space suit. Tests were run to evaluate the characteristics of the delivered design of each component in the arm assembly. The performance was found to be better than the original Gemini-suit soft components. The hard disconnect and wrist bearing for torsion in the Gemini suit is superior to the soft component.

It is recommended that slip-net components be further developed for application in high-altitude suits as well as space suits.

TABLE OF CONTENTS

LIST OF FIGURES

SECTION I, INTRODUCTION

The increased requirements of recent space and high-altitude missions of the military and space agencies has precipitated the need for pressure-constraint garments capable of excellent performance characteristics. One of the major requirements is for an increase in mobility and a decrease in the forces required for limb motion. Attempts have been made to improve these two functions with hard suits, soft suits, and combinations of the two. All these approaches have both desirable and undesirable properties. For example, the soft suits are more comfortable to wear unpressurized when not in use, but require relatively large forces to accomplish motion when pressurized. Hard suits have been made which allow motion with virtually no force over a range of motion; however, they tend to be heavy, bulky, and hard to manage when donned but not pressurized(1). Because of the many different mission requirements in space and at high altitude, all these concepts are under active investigation in Government and industrial laboratories.

One concept for soft-suit joints which shows promise of improved mobility and lower required forces is a three-layer fabric system which permits relative motion among layers during deformation. This three-layer mobile fabric system is termed a slip net. The concept evolved from the study of pressure-containing filament-wound cylinders capable of large deformations. Under ideal conditions the fibers within the three-layer fabric reorient during deformation so that the pressure loads are balanced and no change in internal volume occurs. Consequently no work is done on the contained gas, and deforming as well as sustaining forces are at a minimum.

The aim of the program described in this report is to obtain basic data on slip-net performance in bending, torsion, and bending by side load, and to apply these data to the design and fabrication of component parts of a soft pressure suit. The parts made during this program are a wrist, a forearm, an elbow, and a shoulder.

---

(1) For a discussion of the pros and cons of different concepts see "Space Suits" by Matthew I. Radnofsky; International Science and Technology, February 1967.

SECTION II, DELIVERED COMPONENTS

This effort culminated in the design, fabrication, and evaluation of integrated shoulder, elbow, forearm, and wrist components. The entire assembly was installed in a Gemini G-2C-14 space suit. Figure 1 shows this assembly, and figures 2 and 3 are closeup views of the modified shoulder-arm and wrist-forearm sections, respectively.

The final design shown in figures 1 - 3 makes use of the knotted slip-net 1-1/2-turn fabric in the wrist, elbow, and shoulder components, and 1/2-turn braided fabric in the forearm and upper arm. Details of the design, technical evaluation, and testing of the final deliverable assembly are given in following sections. However, because the best measure of any constraint layer is obtained by its use, a description of the current deliverable assembly in use, and comparison with the Gemini shoulder-arm section is appropriate.

The modified Gemini G-2C-14 space suit was donned and pressurized to approximately 4 psig. The tester moved his right (modified) shoulder, elbow, forearm, and wrist through all possible motions and performed the same motions with his left (unmodified) shoulder, elbow, forearm, and wrist. The motions were performed simultaneously when possible, otherwise sequentially.

Wrist

The slip-net wrist initially fabricated with a cloth-backed zipper was satisfactory in all respects. It allowed essentially unconstrained bending motion and could be left in deformed positions without sustaining forces. Bending motion was easier and more confortable than in the Gemini-glove wrist. The maximum position to which the wrist could be deformed and left with no sustaining force is shown in figure 4. The performance was degraded when the deliverable zipper (a pressure-sealing zipper, B.F. Goodrich Company Style 530) was installed. However, the performance of the deliverable wrist is still better than the Gemini-glove wrist.

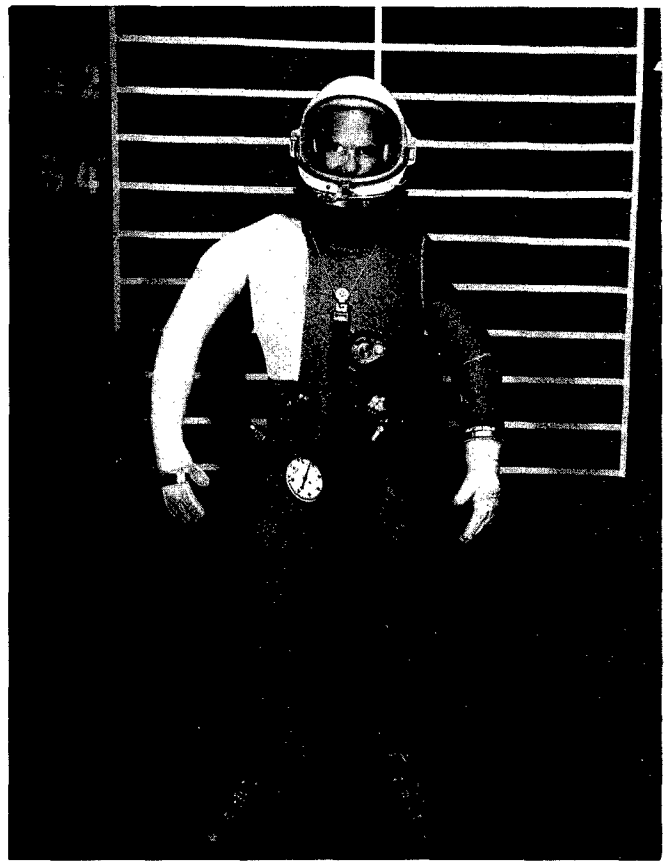

Figure 1. Integrated Assembly Installed in Gemini G-2C-14 Space Suit

Figure 2. Shoulder and Upper Arm Components

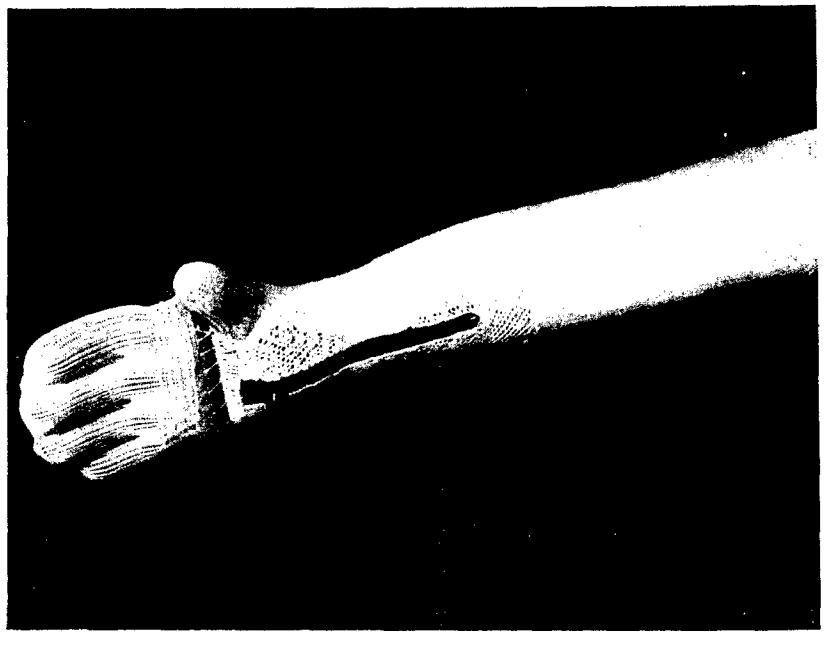

Figure 3. Wrist, Forearm and Elbow Components

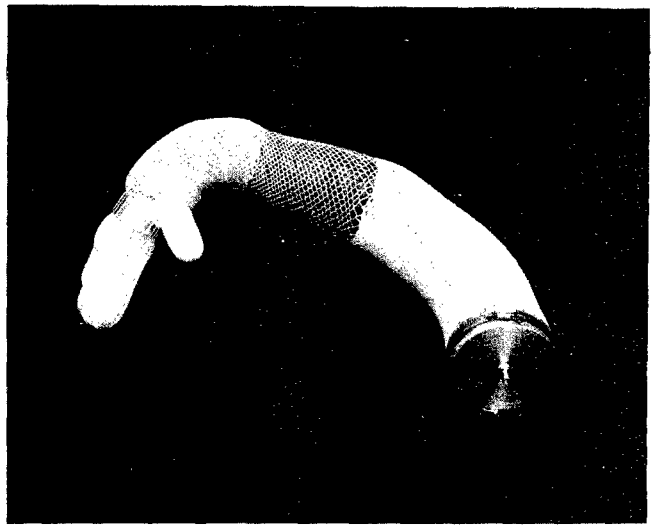

Figure 4. Maximum Zero-Load Wrist Position

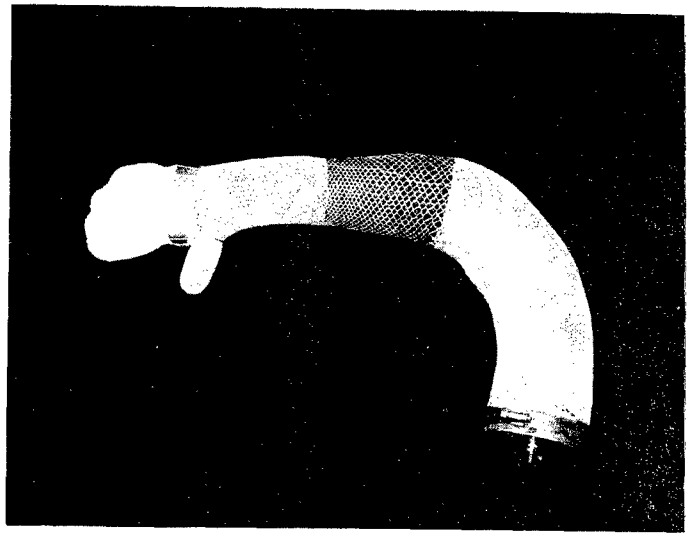

Figure 5. Maximum Zero-Load Elbow Position

Forearm

The function of the braided single-layer fabric used in the forearm is to supply torsional compliance to allow twisting of the wrist-forearm. For moderate twisting motions (0° - 40°), the force required is not excessive, and deformed positions can be maintained with little or no sustaining force. However, for larger twisting motions, the required force is excessive and quickly tiring. The wrist disconnect in the Gemini suit is far superior to the fabric in all of its functions.

Elbow

The slip-net elbow is comfortable, allows easy bending and restoring motion, and can be maintained in a bent position of up to 100° from the straight position with no sustaining force. This is shown in figure 5. It is more compliant than the Gemini elbow; and though the range of elbow motion is unchanged by the modification, the Gemini elbow requires application of force to maintain displaced positions.

Shoulder

The combination slip-net shoulder with braided single-net upper arm is significantly better than the shoulder in the Gemini suit. This is demonstrated in figure 6 in which both arms are raised as far as possible. The slip-net shoulder allows motion of the hand to the top of the helmet. This motion is impossible using the Gemini shoulder. In general, forward, backward, up, and down motions are less constrained in the slip-net shoulder, and maximum attainable motions are larger. The tester felt, however, that improvements in the shoulder design are required. This is substantiated by the fact that slip action does not permeate back into the slip net away from the immediate vicinity of the shoulder joint. The improved freedom of motion over the Gemini shoulder comes from action between the slip-net shoulder and the braided upper arm rather than true slip action throughout the entire chest-back area as anticipated.

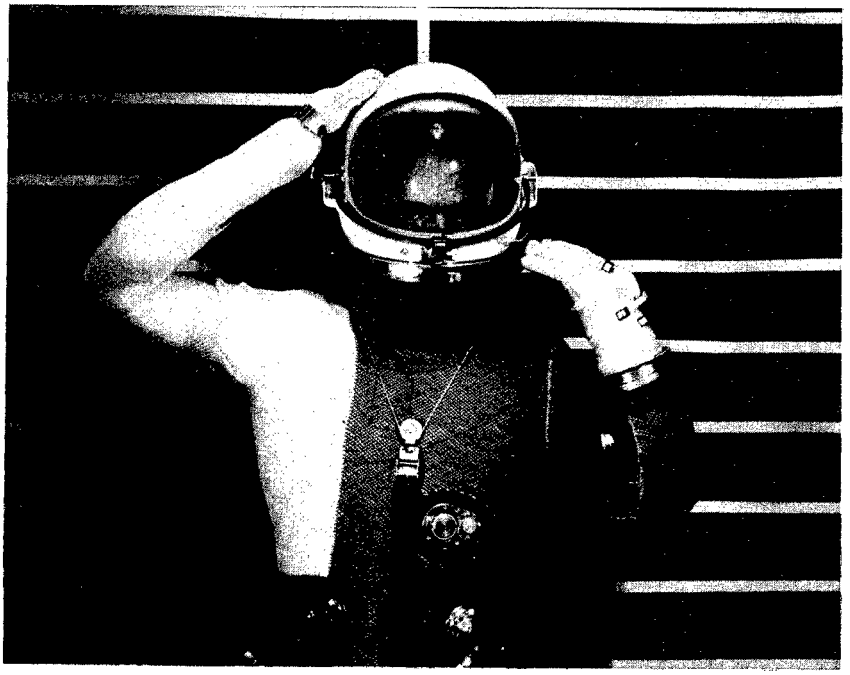

Figure 6. Limits of Upward Motion of Slip Net (left) and Gemini G-2C-14 (right) shoulder

SECTION III, SLIP-NET CONCEPT AND DEVELOPMENT

The fundamental slip-net design and the modifications to it which were developed during this experimental program account for the improved functional performance of the final design over earlier soft-suit components.

A slip net consists of three separate fabric layers in most design applications. At joints where large deformations are required, such as wrists, elbows, and shoulders, the two outer layers are free to slip and redistribute loads so that minimum forces are required to maintain the joint in a deformed state.

When properly designed and fitted, the constraint to motion of a slip-net joint is due primarily to friction forces between layers, thus minimum effort on the part of the user is required to attain the deformed states.

A sketch of a typical slip net is shown in figure 7[2]. The bladder serves as an impermeable barrier to the contained pressurized air or oxygen while the three fabric layers carry the structural loads in the system. The bottom circumferential layer carries a portion of the tangential load; however, its prime function is to deliver dimensional stability. The fibers in the outer two fabric layers are laid up on a bias, one being the mirror image of the other when viewed along the axis of the tube in figure 7. During deformation, slip occurs between layers, and the bias angles in the outer two layers change to accommodate the deformation. The pressure-containing function is not disturbed, however, and the system therefore performs as a pressure-containing mechanism.

The major problem in reducing the slip-net concept to engineering practice was overcome by the elimination of a bunching instability inherent in the basic slip-net design. The problem arises because the slip net functions by relative movement of the two outer layers and a resultant redistribution of membrane loads to accommodate deformations. If the relative motion in an actual

---

2. Detailed sketches of the local geometry of the braided fabric with 1-1/2 turns (used in the slip-net components) and 1/2 turn (used in the slip-net components) are shown in the sketches of figures 28 and 29.

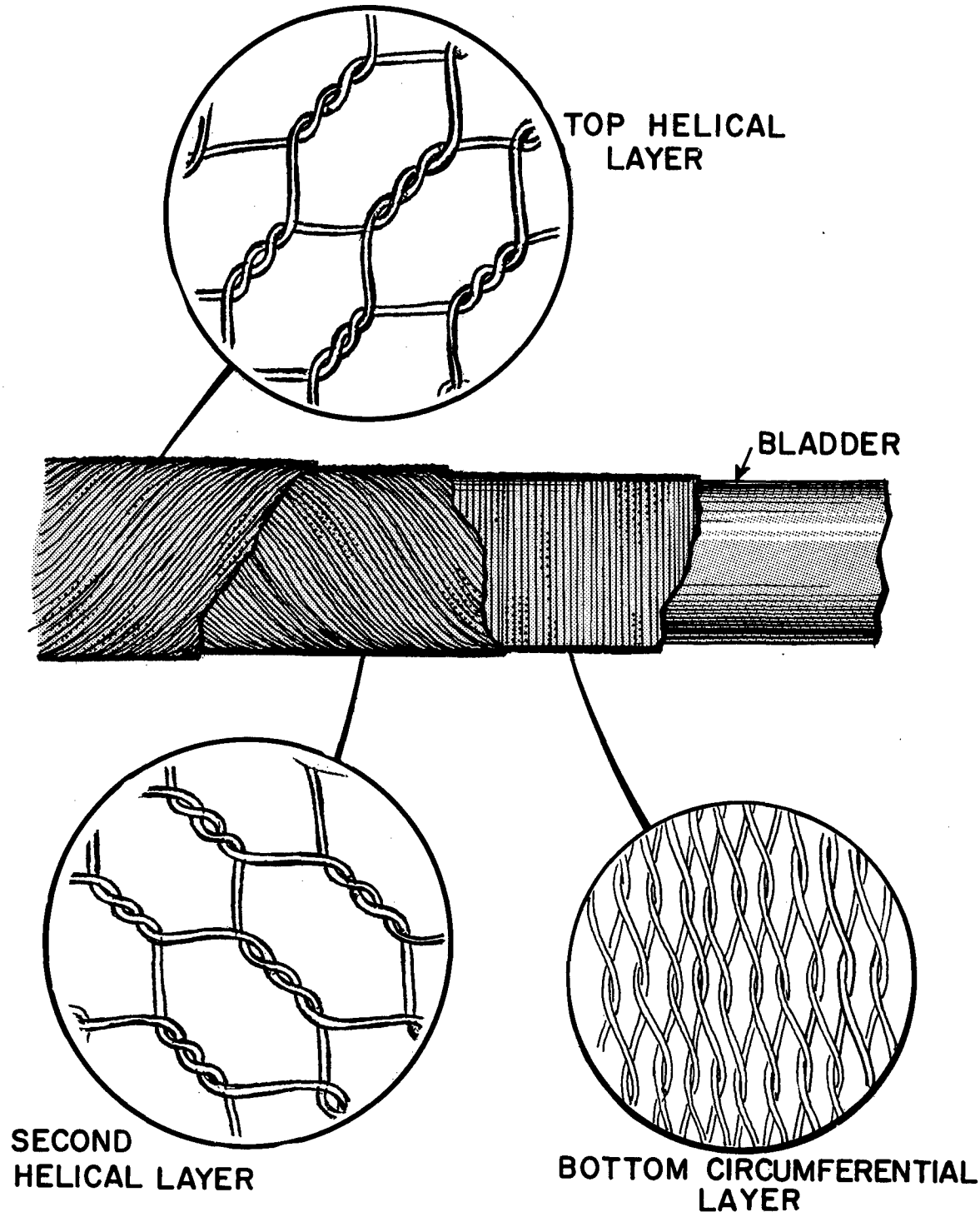

Figure 7. Typical Slip-Net Configuration

slip net is permitted to occur unconstrained, there is a tendency of the fibers to bunch in the region of maximum distortion as shown in figure 8. In this event the system can become locked in the deformed state and depressurization is required before the fibers can be restored to the undeformed geometry. This problem was eliminated during the experimental development by introducing knot lines along which the two slip-net layers are attached. The knot lines are located along positions at which, during deformation, there should be no slip action. In an elbow, wrist, or knee joint this line is defined by the intersection of the plane of bending and the body surface (see figure 9). Further benefit was obtained by introduction of knotted lines in the slip-net designs. First, the method of fabrication of the braided fabric produces a natural knot line which must be accommodated in the assembled joint. Previously, the braided fabric was folded so that this natural knot line was positioned at the end of tubular samples. In the current design, folding of the basic fabric into a slip net is accomplished so that the natural knot line is positioned at the outer extremity of the deformed bend. Secondly, the required knot line at the inner extremity is a natural position for zippers if desired. This property was utilized in the wrist sample. The diameter and therefore the required deformation forces were reduced to minimum values by introducing a zipper in the wrist area (figure 3). The zipper can be opened so that the hand can pass through the small diameter wrist section and when closed, the wrist section maintains a snug fit.

In the shoulder region, the natural lines of no slip for up-and-down motion occur along the top of the shoulders running from the neck to the top of the arm, and along the sides of the torso running approximately 6 inches down from the armpit.

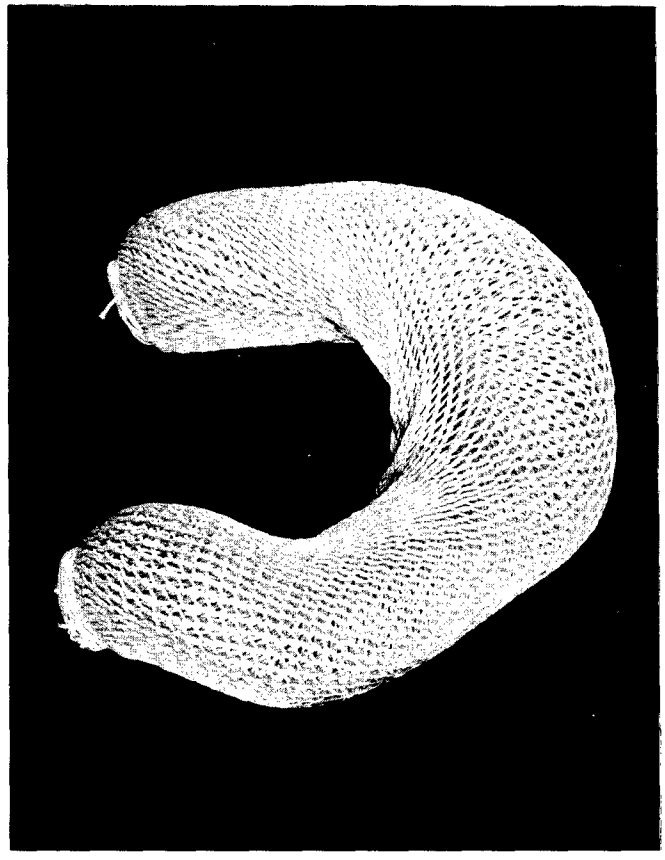

Figure 8. Typical Bunching Instability in Unconstrained Slip Net

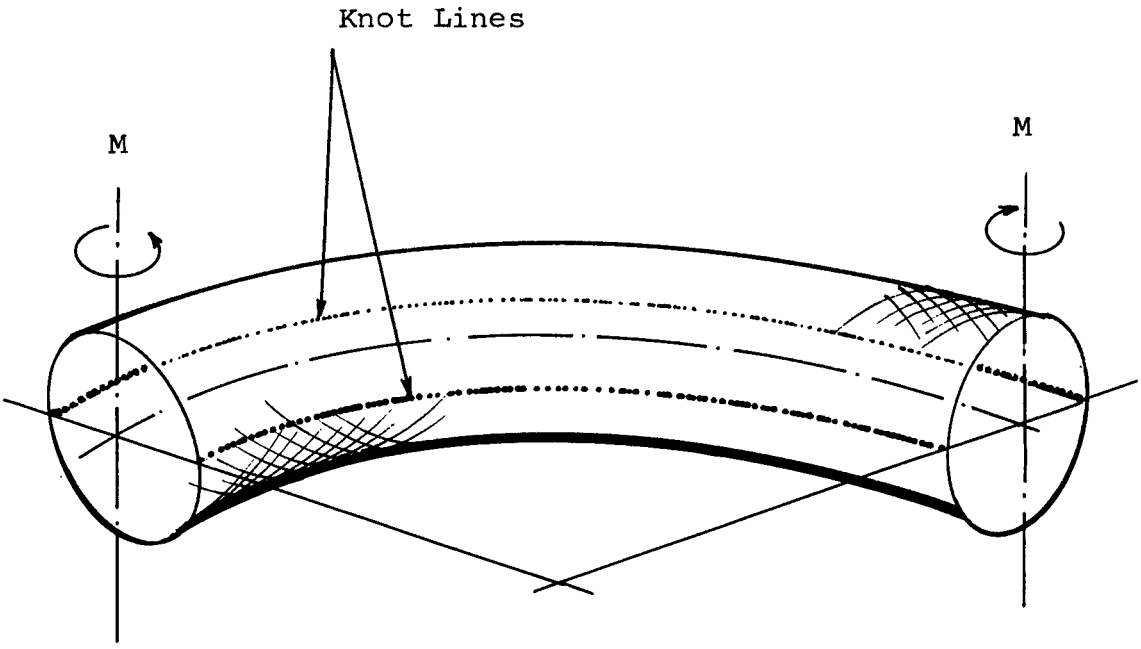

Figure 9 Knot Lines for Slip Net at Intersection of Bending Plane and Body Surface

SECTION IV, DESIGN OF DELIVERED COMPONENTS

The final design consists of four functional components integrated into an entire shoulder-arm assembly. The assembly was fabricated and installed as a unit in a Gemini G-2C-14 space suit replacing the entire right arm, right shoulder, and parts of the right chest and torso areas. The installed unit is shown in figure 1. A mitten with a palm constraint is attached to the end of the wrist to make the unit functional.

The entire unit employs the same basic material as the Gemini suit for an impermeable barrier to contain pressure. The pressure-barrier material in the Gemini suit is supplemented with a sleeve attached just above the usual position of the wrist disconnect and extending to a rubberized glove taken from a Gemini GG-4C-13 glove. The internal protective layer is also supplemented. Exterior to the pressure-barrier materials is a knitted contraint layer made from 20-lb Dacron roving. The function of this layer is to provide circumferential dimensional stability in the elbow and wrist components and shape stability in the chest region.

Wrist Component (figure 3)

The wrist component is made from 1-1/2-turn braided fabric in a slip-net configuration. The natural knot line is positioned at the back of the wrist running from the closure mitten to the forearm component. A pressure-sealing zipper 7 in. long serves as the knot line on the front of the wrist and, when open, allows the hand to slip through. The fabric fiber is 12-pound test, waxed, hot-stretched Dacron tufbraid. The length is 5.7 in. and the diameter varies from 3.3 in. at the base of the thumb to 3.0 in. at the forearm-wrist juncture. The mean fiber angle (as shown in figure 29) is $\beta = 35°$. (This is the angle between the mean fiber direction and circumferential lines in the wrist.) There are 52 fibers per inch measured along the natural knot lines and counting both layers.

Forearm Component (figure 3)

The forearm component is made from 1/2-turn braided fabric in a single-layer configuration. The wrist zipper extends 1.5 in. into this section. The fabric fiber is 50-lb test, waxed and hot-stretched Dacron tufbraid. The mean fiber direction is circumfer-

ential with $\gamma_1 = \gamma_2 = 35°$ (as shown in figure 29 for the 1-1/2-turn geometry). The shape of the forearm is a truncated cone of 4.3 in. height, with a maximum diameter of 4.0 in. and a minimum diameter of 3.0 in.

Elbow Component (figures 2 and 3)

The elbow is made with the same basic fabric as the wrist with the natural knot line positioned at the back of the elbow. It is 10 in. long and 4.0 in. diameter. A 50-lb test Dacron fiber is threaded through the fabric and wrapped to form the second knot line diametrically opposite the natural knot line. There are 52 fibers per inch measured along the natural knot line, counting fibers in both layers. A section similar to the forearm component connects the 4.0 in. diameter elbow component to the 5.0-in. diameter upper-arm section of the shoulder, serving also to increase the torsional compliance of the upper arm.

Shoulder Component (figure 2)

The shoulder component is made from two slip-net fabric pieces with knot lines running from the neck along the top of the shoulder and from the underarm down the side of the torso, as shown in figure 10. The knot line running from the armpit along the underarm is made with a 50-lb test Dacron fiber as was used in the elbow. The material and fabric are the same as in the wrist and elbow components. However, the mean fiber angle is 45° with respect to curves in the surface which are perpendicular to the knot lines. The basic dimensions are shown in figure 10. There are 46 fibers per inch measured along both knot lines, counting fibers in both layers.

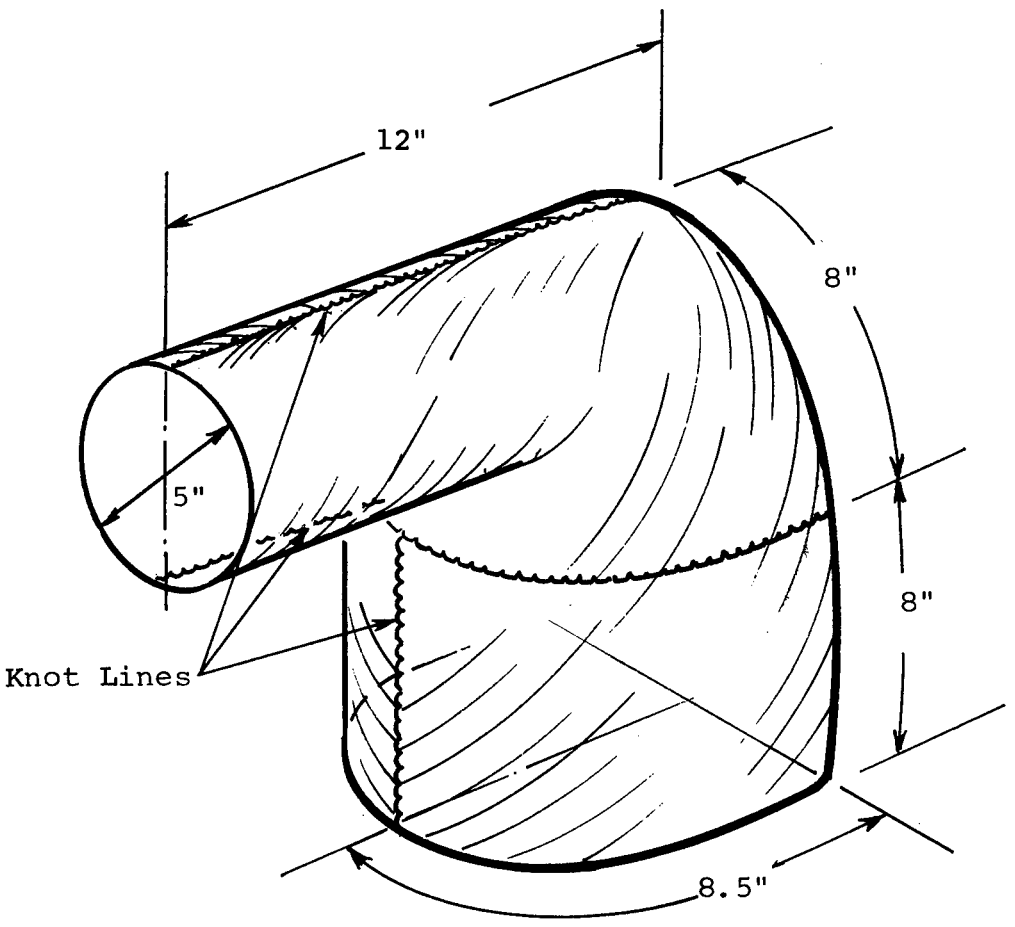

Figure 10. Construction and Dimensions of Shoulder Slip Net

SECTION V, PERFORMANCE OF COMPONENTS

A series of tests were run to evaluate the functional performance of the final design. Bending torque versus displacement measurements were taken during cantilever tests of the elbow, and torque-displacement measurements were obtained for the forearm. Volumetric change was measured during these tests, and measurements of dimensional stability were made during pressurization. Bending torque versus displacement measurements were taken during cantilever tests of the deliverable wrist section while installed in the Gemini suit. A 2000-cycle fatigue test was performed on the elbow-forearm-wrist section, and the section was proof tested successfully to 10 psig. The shoulder section has been pressurized to 5 psig.

A practical analysis of durability based on wear tests and stress analyses of the Dacron material is given in a separate section.

Description of Test Component

A duplicate of the integrated elbow-forearm-wrist final design was fabricated in order to measure its functional performance. The elbow section started approximately 4 in. from the shoulder and a mitten was attached to the end of the wrist to make the test sample functional. The impermeable layer used for test purposes was a one-piece surgical rubber glove. The overall length of the sample including the mittens was 25.5 in. The inner circumferential constraint layer was a knitted Teflon* stockinette which covered the entire sample from the top of the elbow section to the end of the wrist section.

The elbow was 10 in. long and 4 in. diameter. It was a 1-1/2-turn braided slip net with the natural knot line at the back of the elbow and a second knot line diametrically opposed (as in figure 3). The material was 12-lb test, waxed, hot-stretched Dacron tufbraid.

The forearm section was a 1/2-turn braided single-layer fabric made from 50-lb test, waxed, hot-stretched Dacron tufbraid. The mean fiber direction was circumferential with a bias angle, $\gamma_1 = \gamma_2 = 35°$ (see figure 29). The forearm section was a truncated cone 4.3 in. long matching the diameters of the elbow section (3 in.) and the wrist section (4 in.) at the two ends. The

zipper from the wrist section extended 1.5 in. into the forearm section.

The wrist section extended from the forearm to the base of the thumb, a total length of 5.7 in. The basic diameter was 3 in. It was a 1-1/2-turn braided slip net made of the same material as the elbow and with the natural knot line extending from the back of the hand to the forearm. A cloth-backed zipper replaced the knot line diametrically opposed to the natural knot line; it extended the entire length of the wrist section and into the forearm. The increase in diameter required near the base of the thumb was obtained by attaching a wedge of 1/2-turn braided single-layer fabric between the zipper and the slip net as can be seen in figure 3. The measurements of dimensional change during pressurization, the fatigue tests, and the proof pressurization tests were performed on this test sample. In order that the properties of the wrist with the deliverable zipper be reported, side-load bending tests were performed on the deliverable sample after it was installed in the Gemini suit.

The glove was a knitted mitten without a separate constraint layer. A flat aluminum ring was used for palm constraint.

Fatigue and Safety Test of Arm Sample

The elbow-forearm-wrist test article was attached to a fixture on the inside of an opening in a vacuum chamber. The setup was designed so that a man could insert his arm into the test article through the opening and move it in the partial vacuum environment (see figure 11). A vacuum of 10.2 in. Hg (Δp = 5 psi) was maintained in the chamber during testing.

A total of 2000 bending cycles of the elbow and wrist were performed with the bending angle in both sections cycling between zero and approximately 90°. Two pauses, one at 800 cycles and one at 1750 cycles, allowed exchange of test personnel and examination of the fabric.

After completion of the test, there was no visible damage to single fibers and no noticeable change in the response of the test article to further motion.

The test article was cycled to 10 psig several times before, during, and after the fatigue test with no damage to material or function.

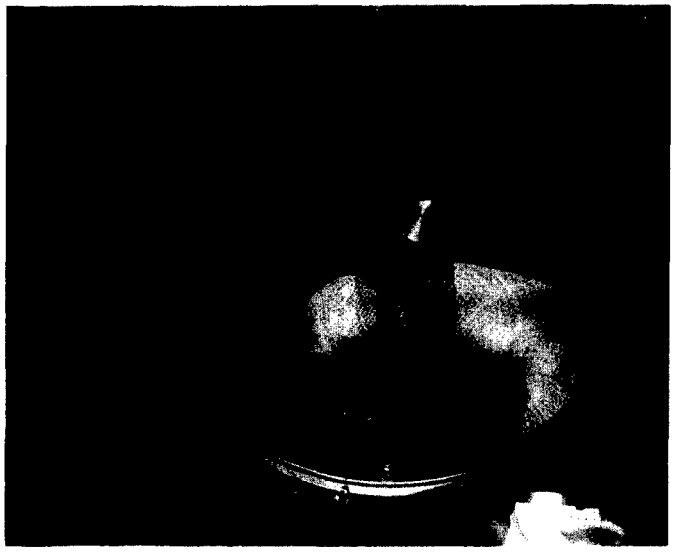

Figure 11. Elbow, Forearm and Wrist Components in Vacuum Chamber (5 psig)

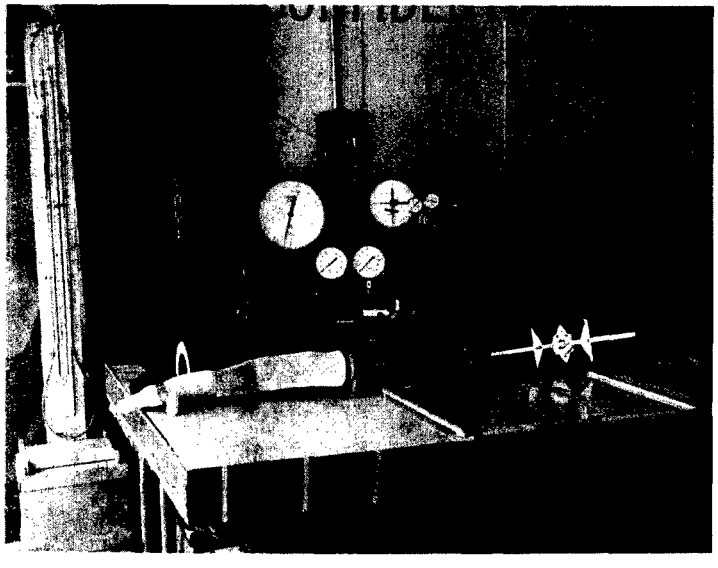

Figure 12. Test Setup for Arm Bending and Torsion Tests

Although applied force and energy expended could not be measured in the fatigue test, the test provided some general information about the performance of the arm sample. Starting relaxed, a man could bend his arm in the test article at a rate of approximately one cycle per second, 60 times (at Δp = 5 psi) before tiring seriously. Over a longer range, 900 to 1000 cycles per hour were performed in groups of ten consecutive cycles, without requiring excessive effort by either of the two right-handed testers.

Torsional motion of the wrist requiring angular twist in the forearm section was considerably more tiring. To a large extent this was due to the restricted mobility inside the vacuum chamber. The final delivery component installed in the Gemini space suit is more compliant in torsion. However, except for missions which require torsional mobility of less than 40° twist angle, the soft forearm is unacceptable and a disconnect such as the Gemini wrist disconnect is recommended.

Dimensional Stability

During the 2000-cycle fatigue test, the test article did not exhibit measurable dimensional change. A tendency of the fibers to bunch slightly in the regions of maximum distortion was observed. However, the joint functions were not affected by the bunching, and after less than 50 cycles, no further bunching was observed.

In order to measure dimensional change as a function of pressure differential, the test article was attached to a 4-in. diameter aluminum end plate which was mounted on a support table. The pneumatic system was the same as that used in the tubular sample test described in a later section, and the pressurized gas (N_2) was supplied through the end plate (see figure 12).

The elongation of the test article was measured as a function of internal pressure. The results of these measurements are shown in figure 13. An increase of 6.4 percent of the overall length was measured as the internal pressure increased from zero to 5 psig. This corresponds to 1.2 in. over the total length of the elbow-forearm-wrist components. The elbow component maintained a 10 in. length over the entire pressure range. The forearm increased in length from 3.6 in. to 4.3 in., and the wrist component increased from 5.2 in. to 5.7 in.

The circumference was measured at both ends of the forearm section (the two cross sections where the different fabrics join)

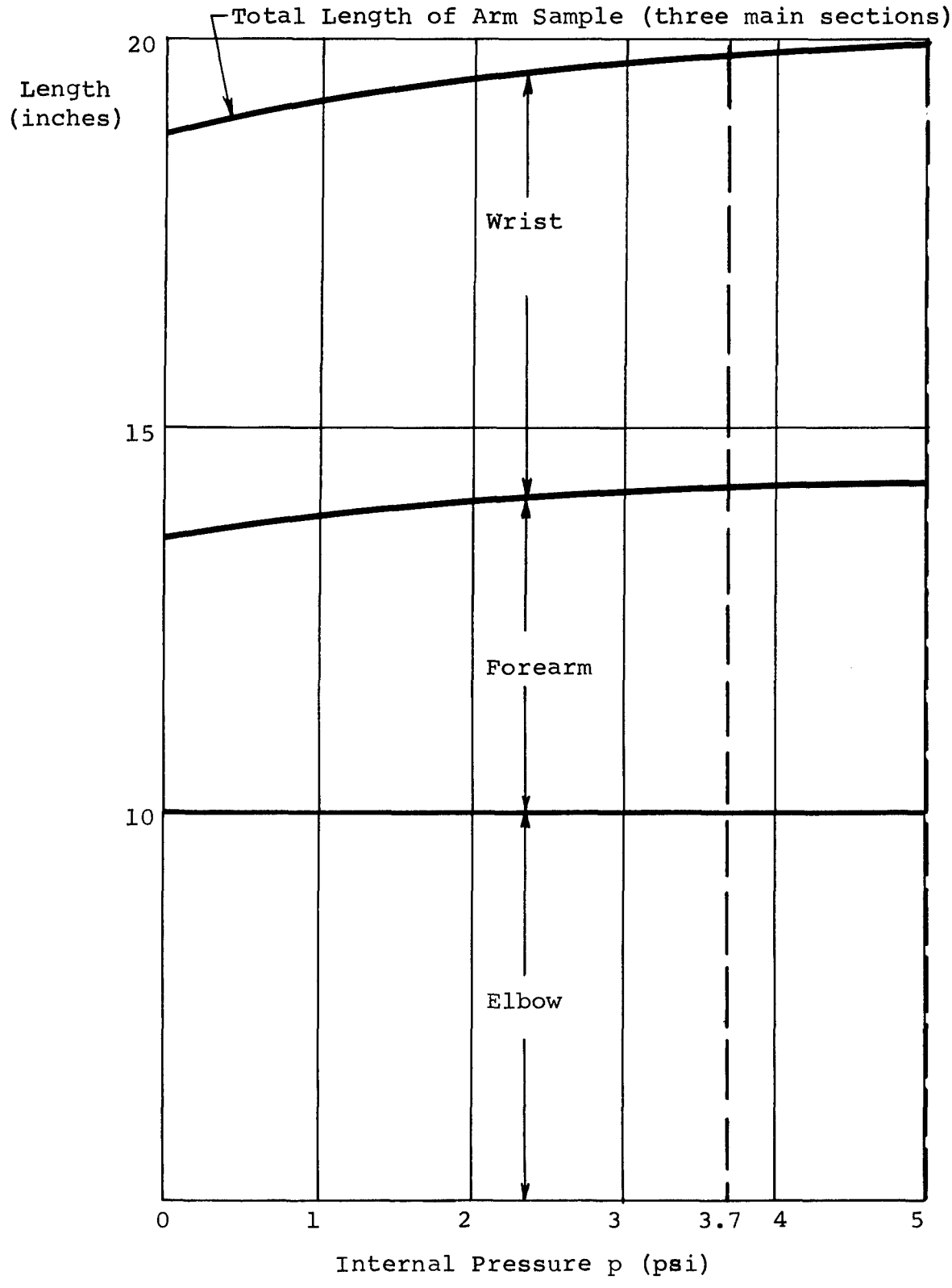

Figure 13. Elongation of Arm Sample as a Function of the Internal Pressure

at a near-zero pressure and at 5 psig. The circumference increased where the elbow and forearm join from 12 in. to 12.3 in., and it remained stable at 9.4 in. where the forearm and wrist join. This corresponds to a total change in volume of 21 $in.^3$, with an initial volume of 191 $in.^3$ and final volume of 212 $in.^3$ Thus, the volume change is 11 percent based on the volume at near-zero pressure and 10 percent based on the volume at 5 psig.

Load-Displacement Performance and Volume Change During Motion

The aluminum end plate, support table, and pressuirzation system used in the test to determine dimensional stability were also used in measuring the load-displacement performance for the elbow and forearm components. The same pressurization system was used in the side-load bending tests performed on the wrist. The forearm in this case was held fixed to a support table with a wooden clamp.

The inflated specimen was stiff enough to support its own weight when horizontally mounted (figure 12). In the torsion tests, the torque was applied by a specially designed and calibrated torque meter and a wooden block clamped to the palm constraint ring. The deformation was read on a protractor hung in a fixed position just above the wrist (figure 14) by means of a pointer and marking lines on the wooden block. The weight of the torque meter and the wooden block were compensated by the test technician using the fixed protractor as a reference for the axis of the sample during loading. The initial zero-load position was chosen with the palm facing downward (figure 14). The ring was twisted 180° clockwise (positive) and 90° counterclockwise (negative) corresponding to more than the maximum natural movements of the human hand. The measurements taken were torque and angle of twist.

In the side-load bending tests of the elbow (figure 15) the side load was applied directly to the palm constraint ring. The load, the lever arm, the radius of curvature at the elbow, the angular deformation, and the position angle were measured. In addition, pressure-change data from which volume change can be calculated was measured using the system described in the section titled Experimental Development Program. The arm was kept with the palm of the hand facing downward during the tests. It was bent inside to 150°, outside to -10°, slightly more than a man's arm can bend.

Figure 14. Initial Position for Torque Tests on Arm

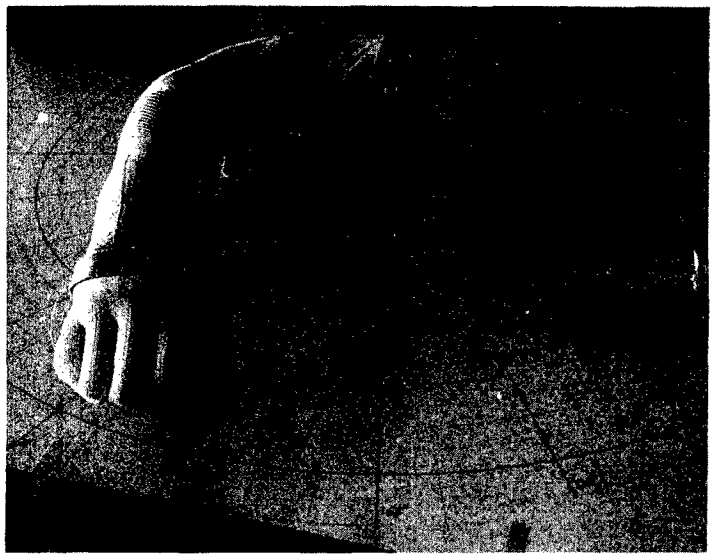

Figure 15. Deformed Position During Side-Load Bending Tests

In the side-load bending tests of the wrist, the side load was applied directly to the palm constraint ring. The load, the lever, arm, and radius of curvature, and the angular deformation were measured. The angular deformation was increased in 10° increments up to 80°.

The torsion test of the forearm and the side-load bending test of the elbow were performed with initial internal pressures of 3.7 and 5 psig. At each pressure a full-cycle load test was performed. In addition, at each pressure the sample was deformed in steps to increasing displacements and the load removed in order that the zero-load equilibrium position (no sustaining force) could be measured as a function of applied deformation. The side-load bending test of the wrist was performed at internal pressures of 3.7 and 5.0 psig. The pressure-sealing zipper degraded the performance to the extent that the motion was essentially elastic; thus a full-cycle loading test was not performed. Volume change data was not recorded because the tests were performed on the wrist while installed in the Gemini suit, in which leakage was large enough to render pressure-change data useless.

The results of the torsion tests are shown in figures 16 and 17. The torque-angular twist curves in figure 16 indicate that the torsional stiffness increases more rapidly at 5 psig than at 3.7 psig as the angle of twist is increased. The required torque for moderate angular deformations (of the order of 40°) is 14 in.-lb at 3.7 psig and 16 in.-lb at 5 psig. These loads are not excessive for the average man and this performance in combination with the zero-load equilibrium data on figure 17 is acceptable. For example, with the application of 16 in.-lb torque at 5 psig a 40° angle of twist is attained. After relaxing, figure 17 shows that the arm would remain twisted to 30°. Thus other movements and tasks could then be performed with the arm twisted 30° and all torsional sustaining force relaxed. Because of the change in slope of the curve on figure 17 at a zero-load equilibrium angle of 65°, operation above this value during moderate cyclic use would be rapidly tiring. This corresponds to an applied torque of 27 in.-lb at 3.7 psig and 32 in.-lb at 5 psig and requires a deformation angle of 100°. Consequently, the fabric forearm is unacceptable for missions requiring cyclic torsional motions such as those made in the use of a screwdriver. The characteristics shown in figure 17 indicate that for missions not requiring cyclic torsional motions but requiring a sustained torsional displacement of the hand of less than 60°, and particularly

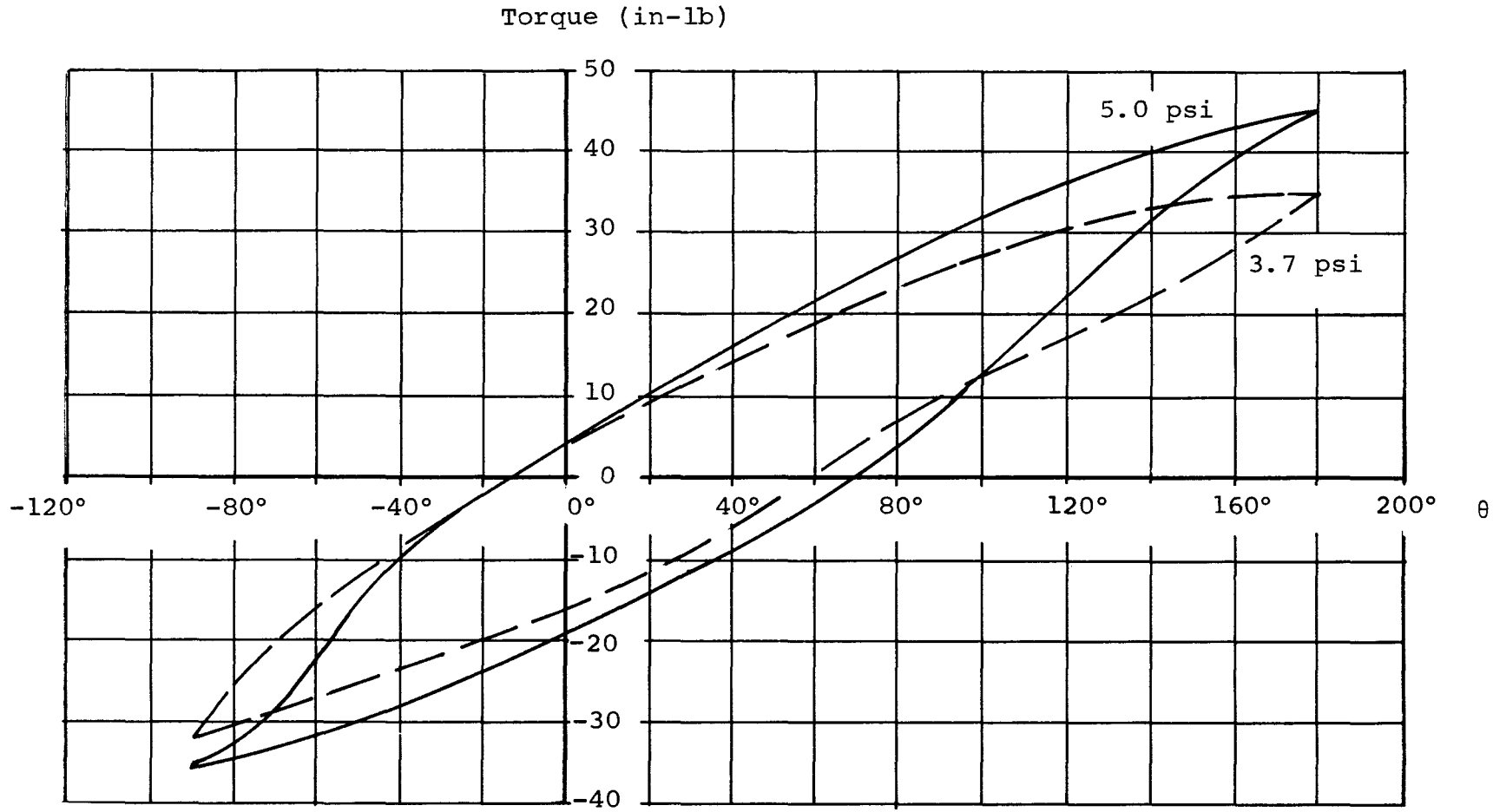

Figure 16. Torsion Tests of Arm Sample Torque versus Twist Angle, θ

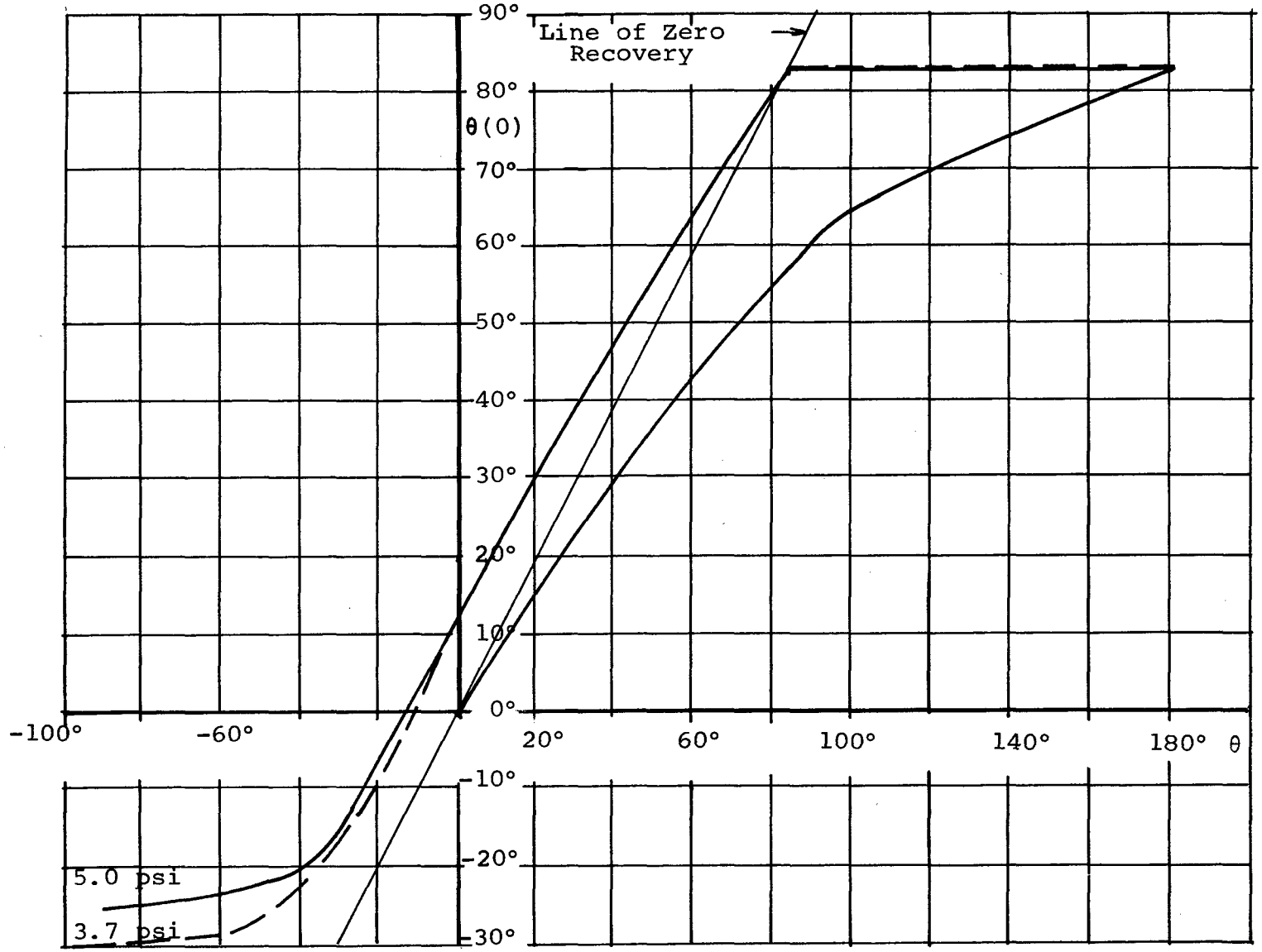

Figure 17 Torsion Test of Arm Sample: Recovery Angle θ(0) versus Twist Angle θ

less than 40°, the soft-forearm performance is acceptable. However, other factors dominate. The ability to remove the glove is a desirable characteristic, and if a wrist or forearm disconnect is employed, a twisting capability superior to the soft-fabric performance is easily built into the disconnect. Thus, unless there is an overriding requirement for an integral, all-soft arm component, a disconnect is recommended in place of the braided forearm for torsional compliance.

Results of the side-load bending tests of the elbow are given in terms of load versus α and load versus α_1. The angle, α, is the slope angle of the loaded end of the test article, and α_1 is the angle the secant between the base and tip of the test article forms with its initial position. These angles are shown in figure 18, which is a line-drawing reconstruction of bending deformations of the arm component.

The raw data, side load versus α_1, is given in figure 19. The positive slope of these curves throughout the increasing portion of the load cycle is contrary to the results of the development tests on tubular samples of knotted slip nets. This is caused in part by the forearm and wrist portions of the arm. The forearm has the bending characteristics of braided single-layer fabrics which are stiffer than slip nets, and the wrist section is knotted along lines which constrain bending in the direction of this test. The 10-in. length of the elbow component was determined as a result of a tradeoff between elbow component length for bending compliance and forearm length for torsional compliance. Based on the tubular-sample tests reported in a later section, if a disconnect and torsion bearing is used in place of the soft forearm as recommended, the length of the elbow component can be increased and the load shown in figure 19 should not exceed three pounds.

Reduction of the load-displacement data to bending torque-angular displacement curves results in the curves of figures 20 and 21. The moment arm used in reducing this data is the perpendicular distance between the load direction and the base of the arm sample. The load direction was maintained perpendicular to the loaded end as it traced out an arc as shown in figure 18. Figure 20 shows the moment as a function of α_1. In this figure, the hysteresis loop encloses the energy per cycle absorbed by the structure. The effect of pressure on the response of this arm is significant. Increase from 3.7 to 5 psig (35 percent) increased the maximum moment encountered in the load cycle from 28 in.-lb to 36 in.-lb, an increase of 29 percent.

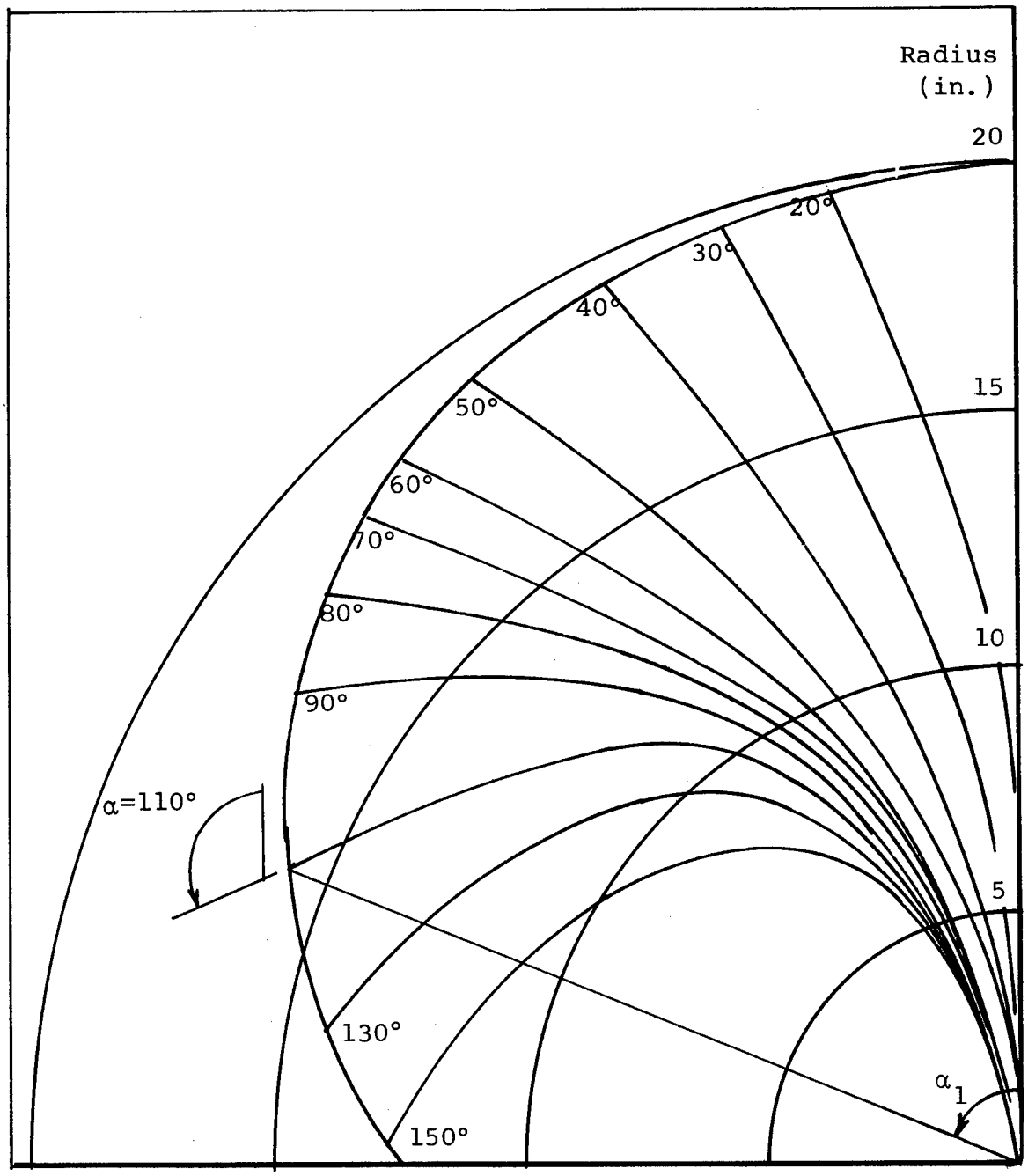

Figure 18 Reconstructed Bending Deformations of Arm Sample

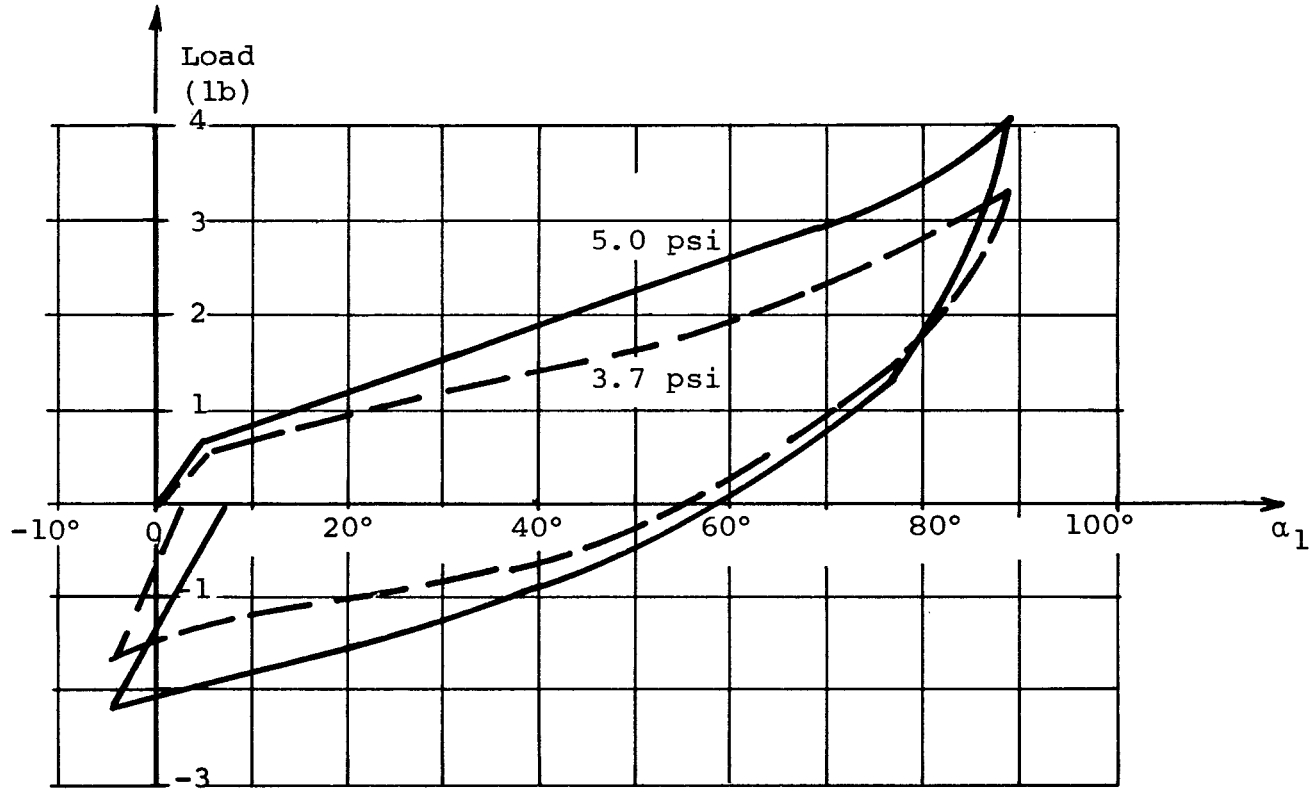

Figure 19 Side-Load Bending Test of Arm Sample
Load versus Deformation Angle α_1

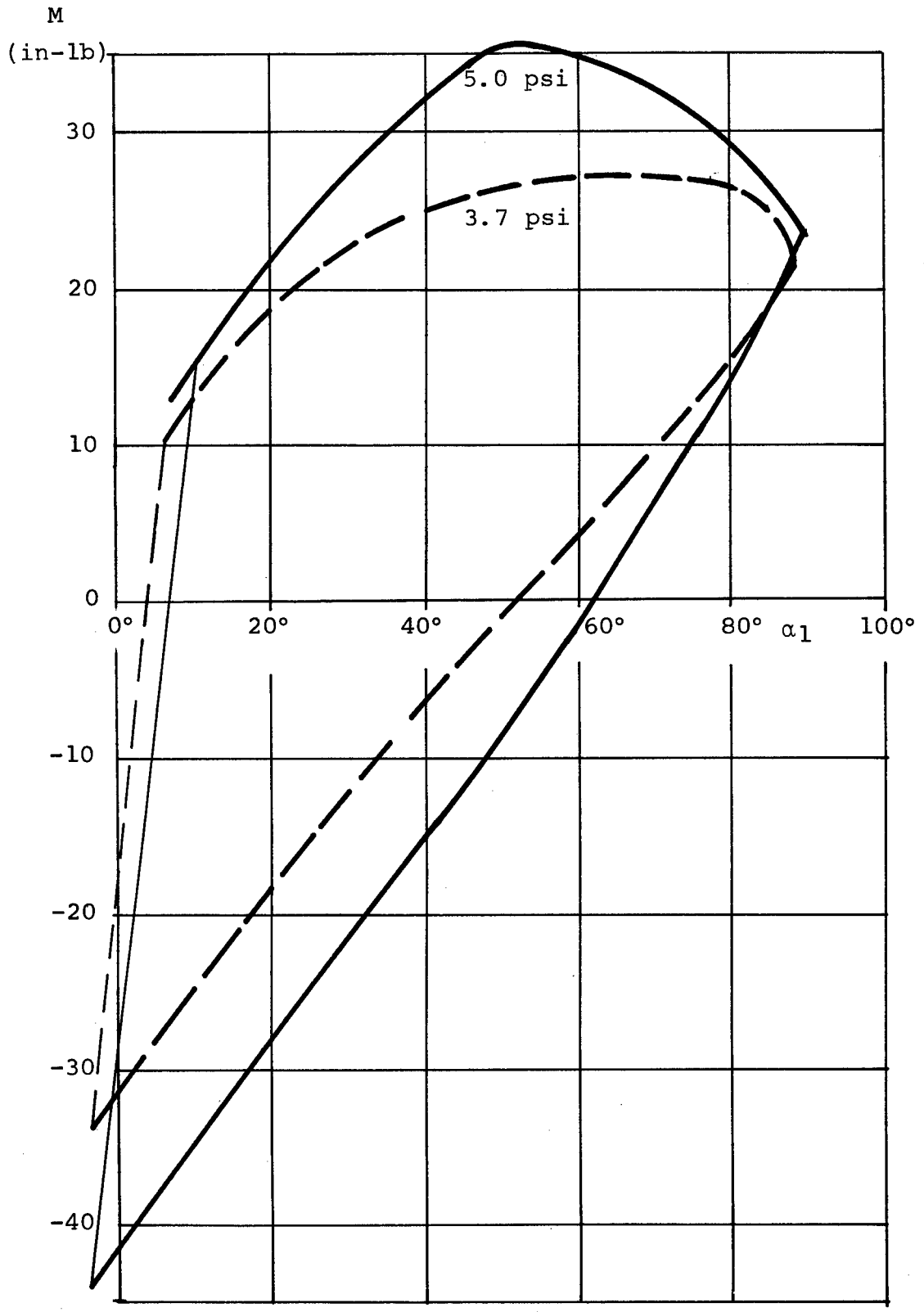

Figure 20 Side-Load Bending Tests of Arm Sample
True Hysteresis Loops

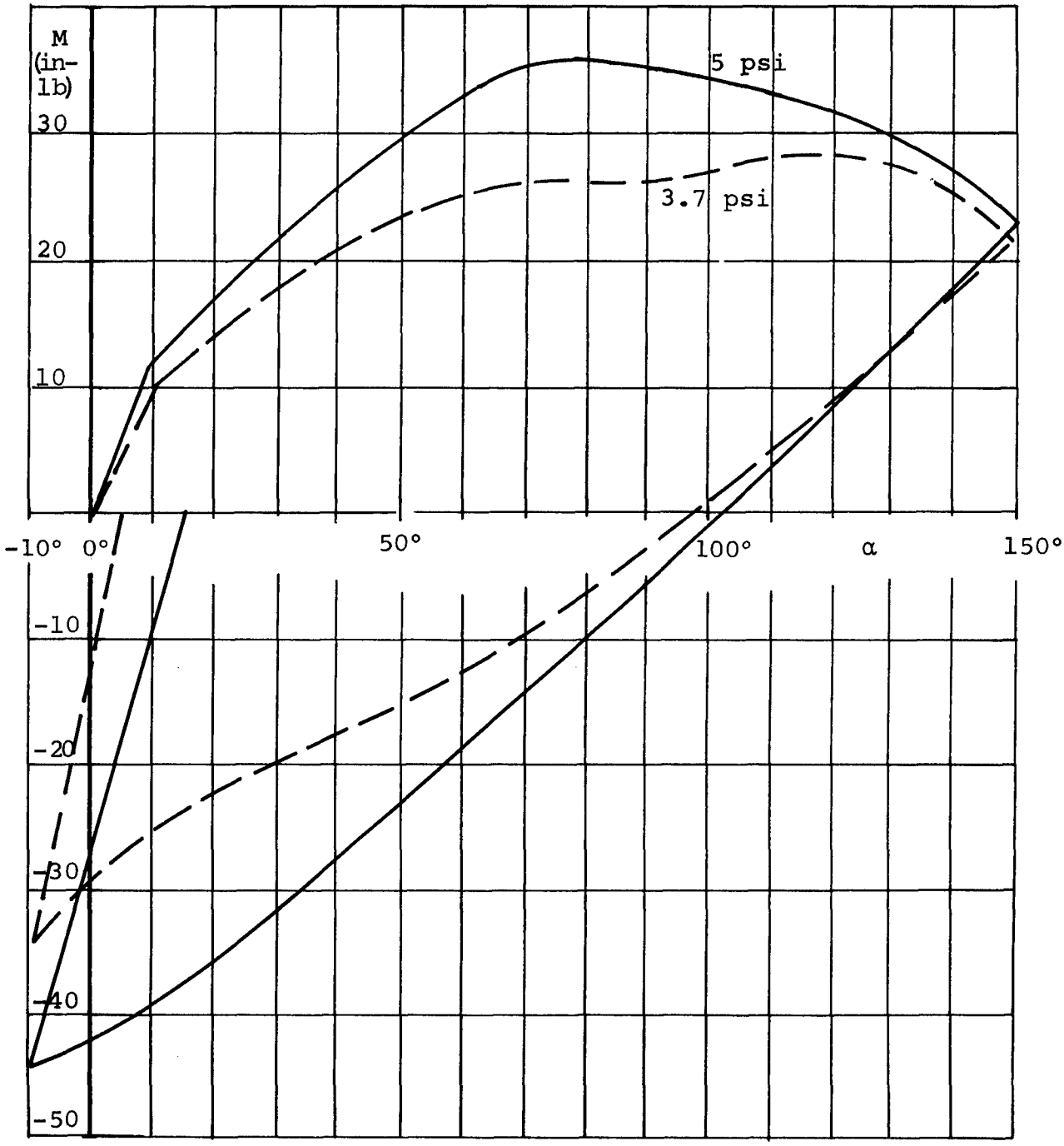

Figure 21. Side-Load Bending Test of Arm Sample—
Bending Torque M versus Total Deformation α

The volume change during deformation is shown in figure 22. For end-slope angles, $\alpha < 70°$, the volume increased with increasing load for internal pressure of 5 psig, thus displaying typical slip-net response. In this range of deformation, energy is extracted from the enclosed gas. For angular deflections larger than $\alpha = 70°$, the response is more typical of single-layer constraint garments. The volume decreases for $\alpha > 70°$, indicating that slip action has decreased or stopped. Thus, for displacement angles between $70° \leq \alpha \leq 150°$, work must be done on the confined gas during deformation. In returning to the nominally undeformed state, work is extracted from the confined gas until α has decreased to 70°,at which point the process reverses again. The response at 3.7 psig is similar except that the confined volume remained essentially constant during the loading cycle up to an angle $\alpha = 80°$.

Figure 23 demonstrates the capability of the elbow component to remain in deformed positions with no sustaining force. These are the results of tests at 3.7 and 5 psig internal pressure where the arm test article was deformed to an angle, α , and the load was released, and the resulting permanent deformation angle, $\alpha(0)$, recorded. Comparison with the line of zero recovery indicates that large percentages of any displacement can be maintained with no sustaining force. For example, at 5-psig operating pressure, the arm can be bent to $\alpha = 100°$ and then relaxed and maintained at $\alpha = 72°$ with no further force exerted. With reference to figure 21, the bending torque required to perform this task is 34 in.-lb.

This data was further reduced for comparison with performance of a molded convolute and an advanced constant-volume convolute. The data for comparison was obtained from NASA, MSC. The results are shown in figure 24. The moment arm used in calculating the torque reported in this figure is the measured perpendicular distance from the line of action of the deforming force to the position of maximum curvature in the elbow. The range (degrees) is the angle through which the elbow deforms in the near vicinity of the position of maximum curvature. The slip-net performance falls between the performance of the advanced constant-volume convolute (most compliant) and the molded convolute. Further description of the two NASA designs is not available. Comparison of the slip-net performance with the typical data reported in a survey paper[3]

---

3. "A Study of Techniques and Equipment for Evaluation of Extravehicular Protective Garments", AMRL-TR-66-4, February 1966.

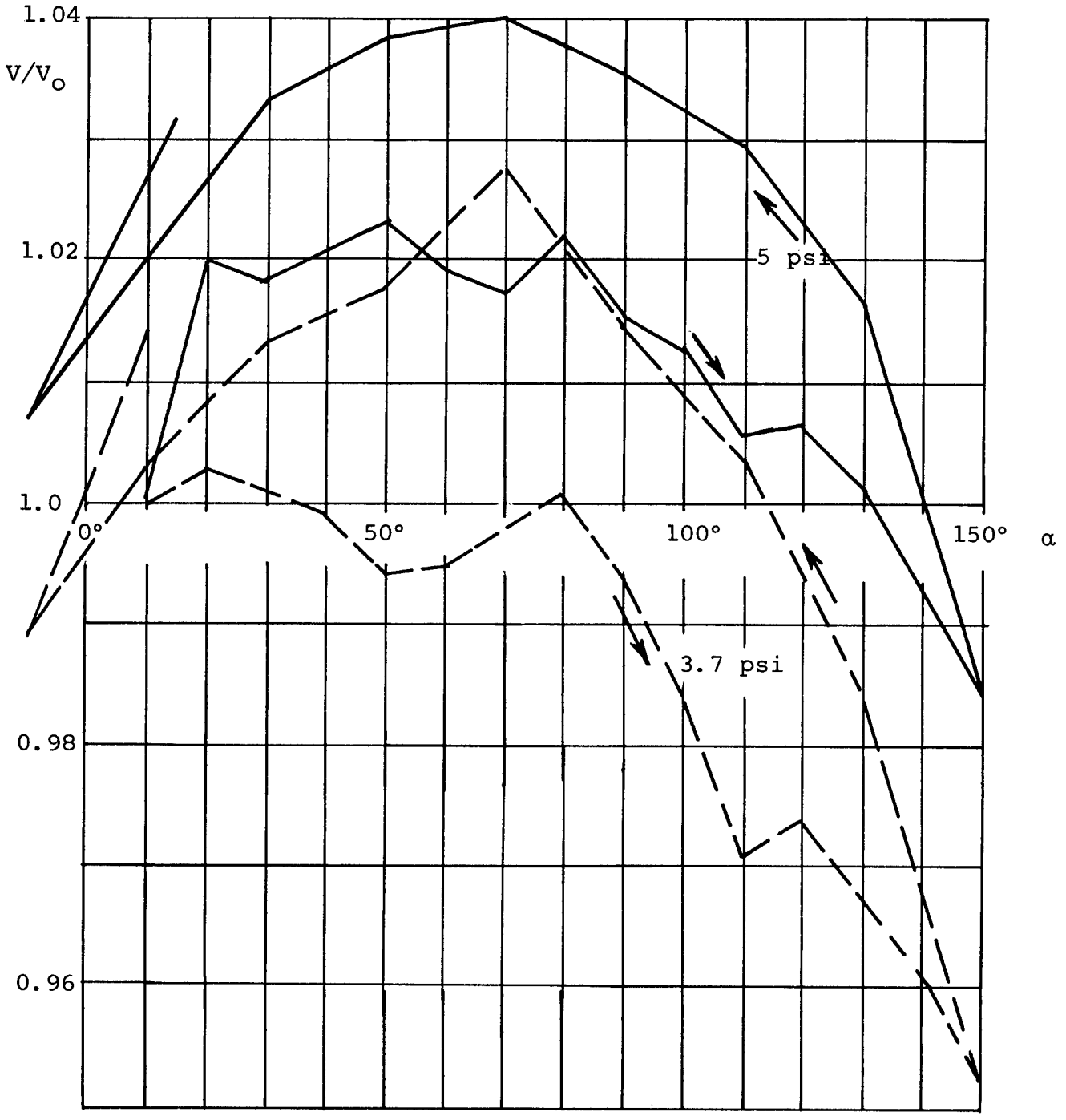

Figure 22. Side-Load Bending Test of Arm Sample - Volume Change, V/V_o versus Total Deformation Angle, α

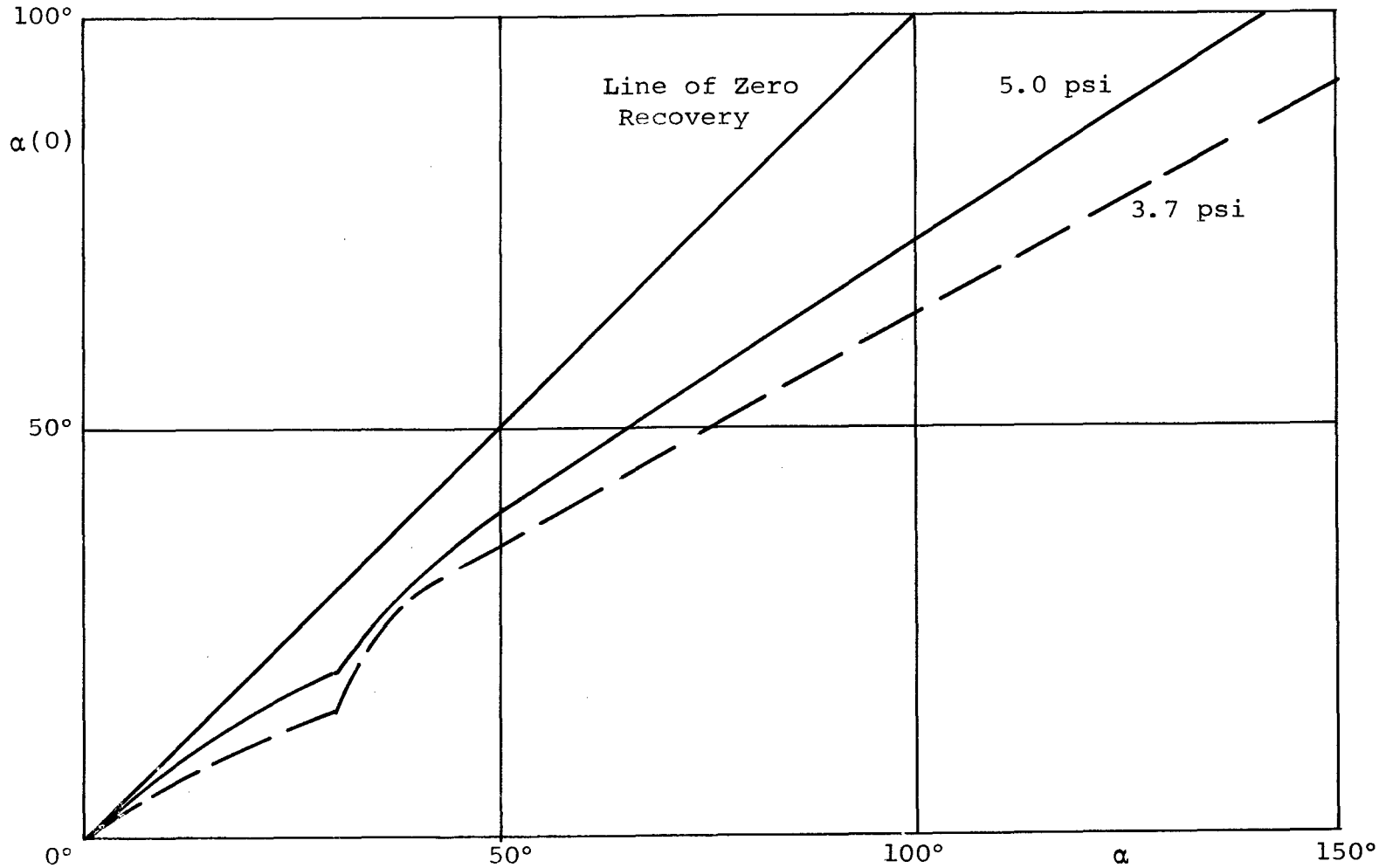

Figure 23 Side-Load Bending Tests of Arm Sample
Total Recovery Angle α(0) versus Total
Deformation Angle α

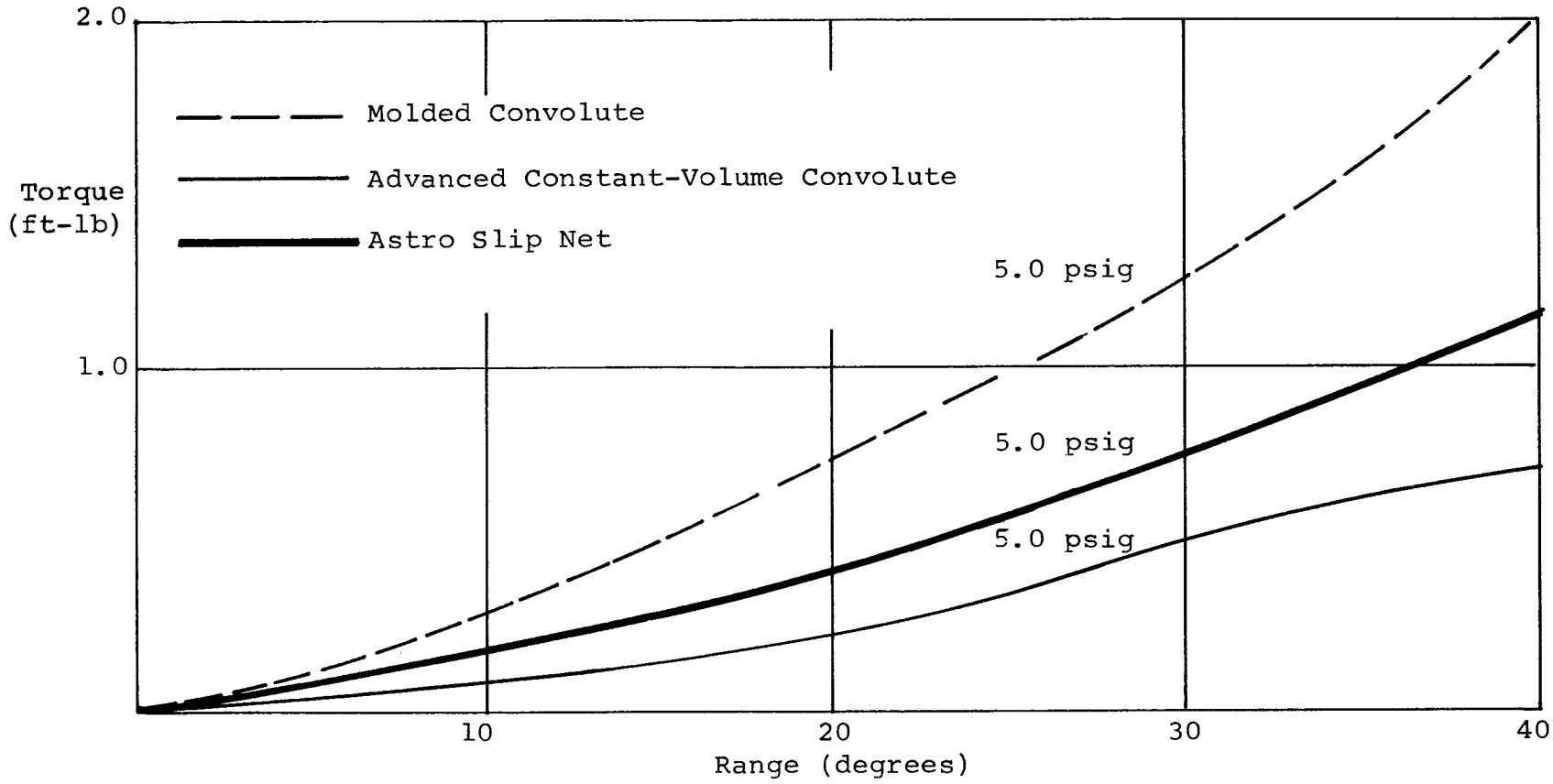

Figure 24 Comparison of Astro Elbow with Molded and Constrained Convolutes

demonstrates significant improvement. Maximum torque of 3 ft-lb in the slip net (see figure 21) compares with maximum torque of 6 to 8 ft-lb for the elbow joint data cited in the reference.

The results of the side-load bending tests performed on the wrist section are given in figures 25, 26, and 27. In figure 25 the load versus bending-angle data are plotted for both 3.7 and 5.0 psig internal pressure. The erratic behavior of the wrist section as evidenced by the scatter of the plotted points is due to the heavy zipper. During the test, the zipper actually buckled into a number of short arcs. This caused the load to oscillate about the lines drawn through the points. The type of buckling encountered can be seen in figure 4 at the inside bend radius of the wrist. The variation of moment arm with bending angle is shown in figure 26. From the data in figures 25 and 26, the bending torque can be computed. Figure 27 shows the variation of bending torque with bending angle for the wrist section. The scatter caused by the heavy zipper's buckling is also evident in this figure. The peak load, defined by the smooth curves, increases from 19 in.-lb at 3.7 psig to 24 in.-lb at 5.0 psig, an increase of 31 percent. Although the bending torque shown in figure 27 is higher than the torque required to displace the same wrist joint with a lighter cloth-backed zipper, it is still an improvement over the Gemini-glove wrist which it replaced.

Estimated Strength

The strength of the component is estimated by calculating the internal pressure each section can sustain statically.

$$P\ (T_{max}) = \frac{T_{max}\ n\ \sin\beta}{\pi\ r^2}$$

T_{max} is the admissible load for a single fiber, and it is standard to use one fifth of the nominal test load for the material, i.e., 2.4 lb for the 12-lb test Dacron and 10 lb for the 50-lb test Dacron tufbraid.

n is the total number of fibers crossing the circumference of each section and β is the angle between the fiber direction and the circumference (mean fiber direction for slip nets). For circumferentially wound braided single-layer fabrics $\beta = \gamma_1 = \gamma_2$). The sections are assumed to have circular cross sections, and the

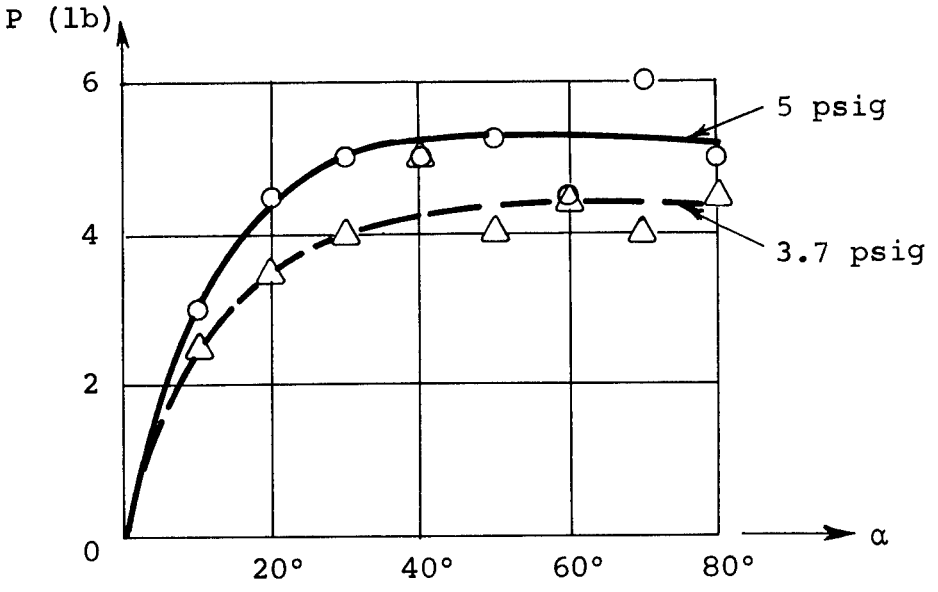

Figure 25. Wrist Section: Side Load Versus Bending Angle

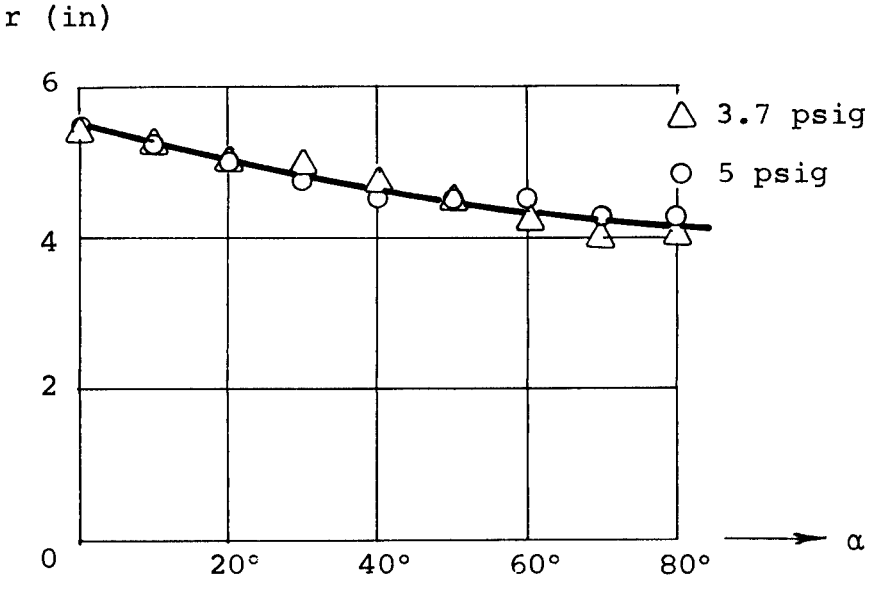

Figure 26. Wrist Section: Lever Arm Versus Bending Angle

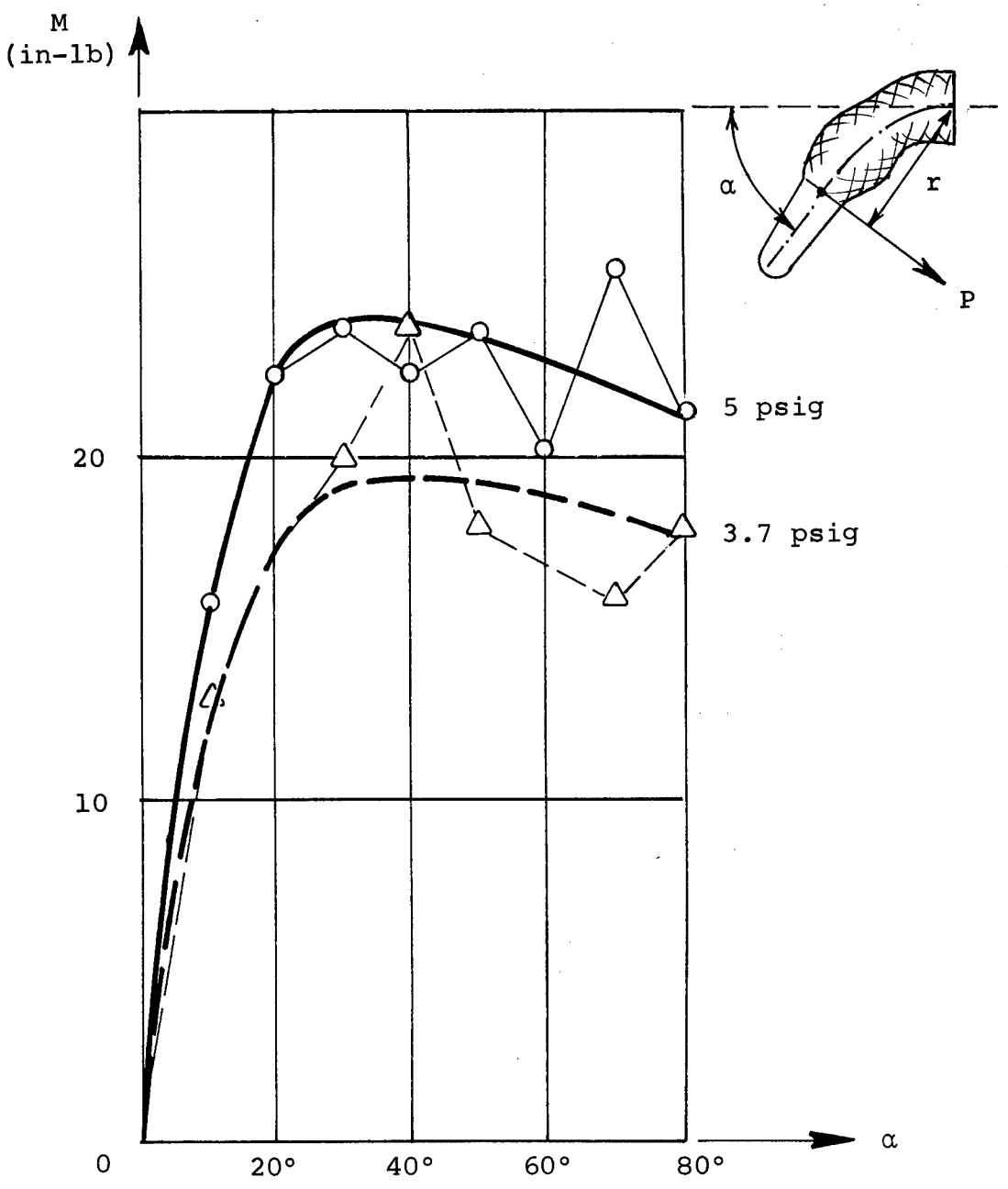

WRIST SECTION:

Figure 27. Bending Torque versus Bending Angle

equation above implies that the sum of fiber-load components in the axial direction of the section equilibrates the pressure force on the cross-sectional area. The axial component is preferred to the circumferential component because the underlayer carries part of the circumferential load but none of the axial load.

Table I lists the parameters for each section, the values for P_{max} , and the safety factor over the operating pressure of 5 psig.

The additional loads created during deformations are not accounted for. However, the sections with larger and more frequent motions also have higher safety factors.

TABLE I
Design Parameters and Strength Estimates for Delivered Components

Section	T_{max} (lb)	n	β	r (in)	$p(T_{max})$ (psig)	$\frac{p(T_{max})}{5 \text{ psig}}$
Wrist	2.4	294	35°	$\frac{8}{2\pi}$	80	16
Forearm	10	74	35°	2	34	6.8
Elbow	2.4	462	35°	2	51	10.2
Upper arm	10	94	35°	2.5	28	5.6
Shoulder	2.4	739	45°	$\frac{16}{2\pi}$	62	12.4
Chest*	2.4	784	45°	$\frac{17}{\pi}$	29	5.8

* The chest section is approximated by half a cylinder.

SECTION VI, WEAR TESTS AND DURABILITY ANALYSIS

In order to estimate the lifetime of the delivery sample, the wear of single fibers was studied and tested. This investigation included the two basic geometries of fiber crossover typical of the final design: the crossover of two fibers in the slip-net components (composed of two 1-1/2-turn braided crossovers as used in the elbow, the wrist, and the shoulder), and the crossover of two fibers in the braided single-layer components (composed of a 1/2-turn crossover as used in the forearm and upper arm).

The wear of the fabric in slip-net configurations caused by slip motion of one fabric over the other is negligible in comparison to the wear caused by relative fiber motions at crossovers within a layer. This is a result of the fact that wear life depends on the shearing (friction) load and consequently on the bearing load in the contact area between the wearing parts. The ratio of the bearing load between fibers in separate layers to the bearing load at crossover points within a layer is roughly proportional to the ratio of tube diameter to fiber diameter. In the wrist section this ratio is approximately 100 and it increases in all other components. As a consequence, wear between layers is ignored and only wear at crossover points within layers is treated.

Figure 28 shows sketches of the 1/2- and 1-1/2-turn crossover geometry and the kinematics of the test joints. Figure 29 is is a sketch of one slip-net layer and defines the notation used for both crossover geometries treated.

There are many parameters which influence the rate of wear and lifetime of stressed fabrics. Those which dominate the wear performance of the Dacron material in the space-suit components are fiber tension, T, the angle $(\gamma_1 + \gamma_2)$ between two fibers running into their common joint, relative motion between both fibers, and the speed or rate of motion. The fiber tension, the relative motion, and the angle $(\gamma_1 + \gamma_2)$ are controlled in the tests performed and can be estimated for motions of each of the components in the space suit. The rate of motion is significant in its effect on operational temperature in the fibers. However, during cyclic motions in the use of a pressure-constraint garment, the rate of motions and duration of cyclic loading are not large enough to cause frictional heating in the fabric. On the other hand, the necessity of completing the wear tests in a reasonable time required a rate of loading at which some heating was antici-

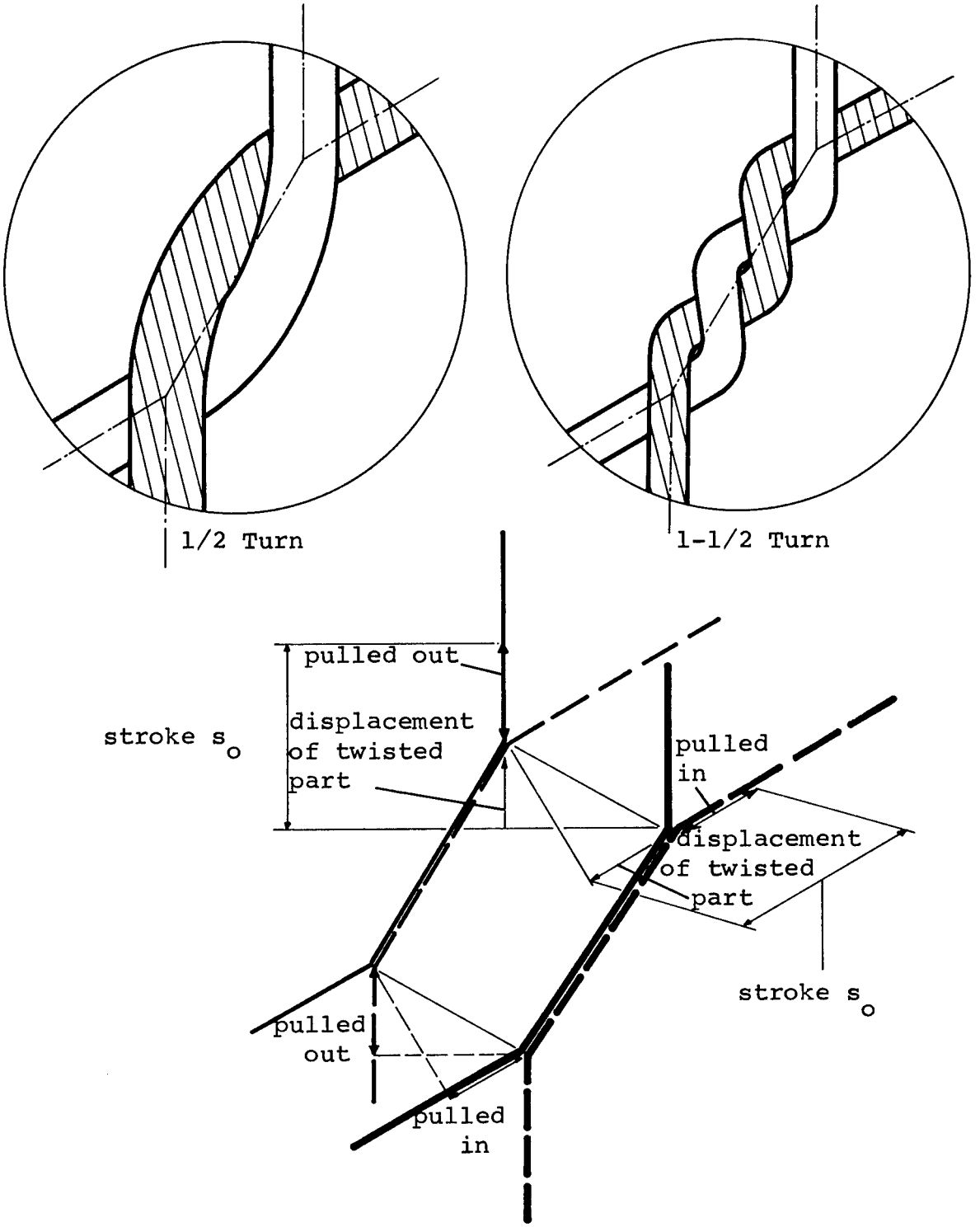

Figure 28. Geometry and Kinematics of Single Joint

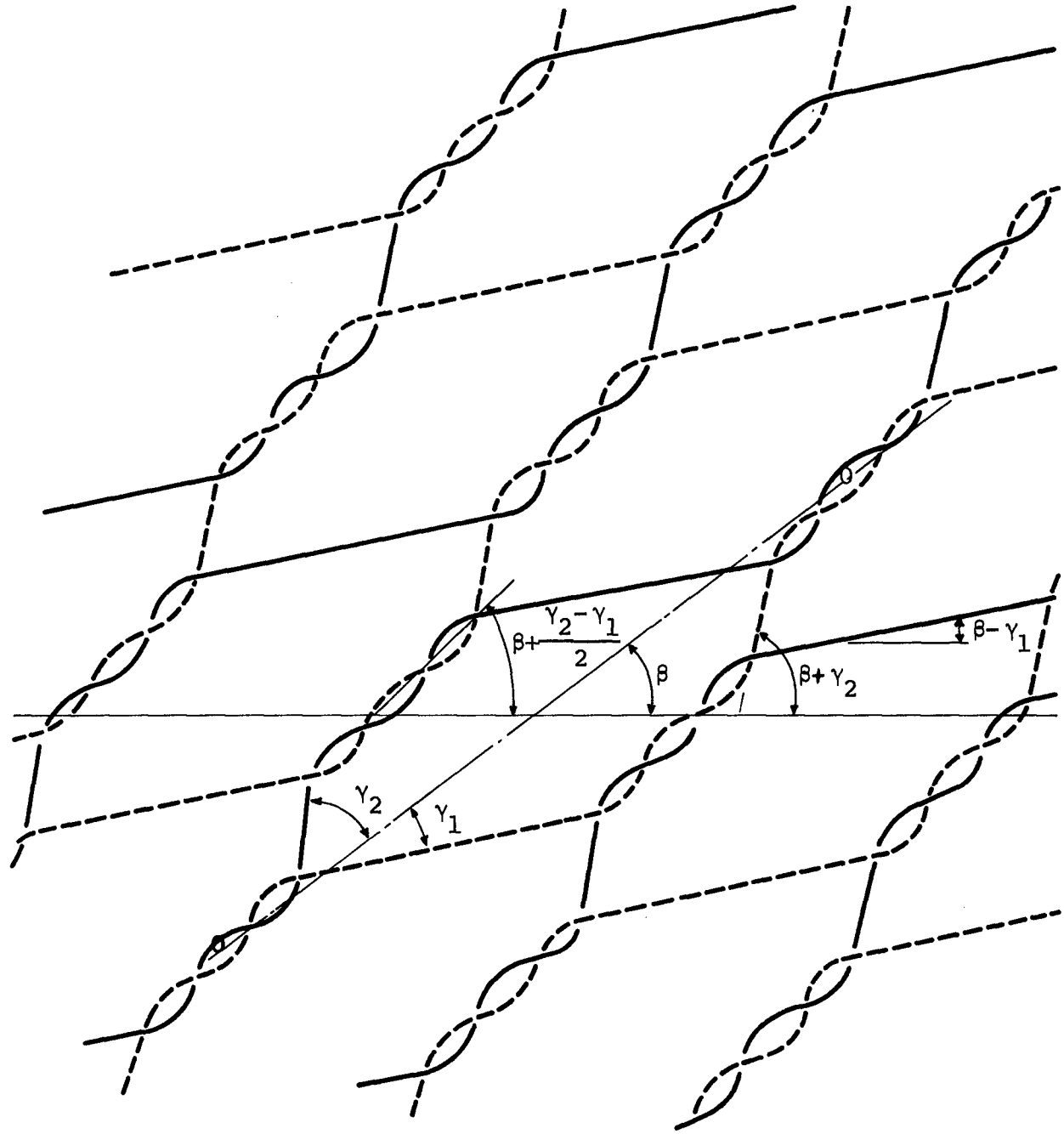

Figure 29. Angle Notation of Braided Nets

pated. The temperature variation was small, however, and not significant enough to alter the results. The test results can, therefore, be interpreted, and lifetime estimates of the fabric components can be made.

Test Setup

The test setup used is shown in figure 30. The ends of two fibers of the tested material were attached, one to the floor and one to the frame of a lathe while the other ends were attached to a weight-carrying and a stroke-inducing string, respectively. The stroke was produced by a pulley clamped eccentrically into the chuck of the lathe and moving in the plane of the string. Because this string was fixed at one end and running over a second pulley attached to the tool carriage of the lathe, the revolving pulley induced motion in the test joint causing wear of both fibers.

The stroke was varied by attaching the fixed string at different levels. The angle $(\gamma_1 + \gamma_2)$ at the joint of the filaments could also be varied by moving the attachment point on the floor and the stool supporting the weight-carrying string. The lathe was shut off automatically when one of the filaments broke. The number of cycles to failure was read on a counter registering the revolutions of the lathe spindle. Each cycle corresponded to a relative motion of the fibers at the crossover and a return to the initial geometry.

Tests Performed and Results

Two series of test were run, the first with 12-lb test, waxed, hot-stretched Dacron tufbraid turned 1-1/2 times at the joint, and the second series with 50-lb test, waxed, hot-stretched Dacron tufbraid with a simple 1/2-turn joint. The materials and joints correspond to those used in the delivery sample.

The first series was divided into three groups:

1. $(\gamma_1 + \gamma_2) = 60°$, load varied, stroke, s_o = 5/8 in.
2. $(\gamma_1 + \gamma_2) = 60°$, load varied, stroke, s_o = 1/4 in.
3. $(\gamma_1 + \gamma_2) = 30°$, load 53.5 oz., stroke, s_o = 1/4 in.

The parameters for the second series were

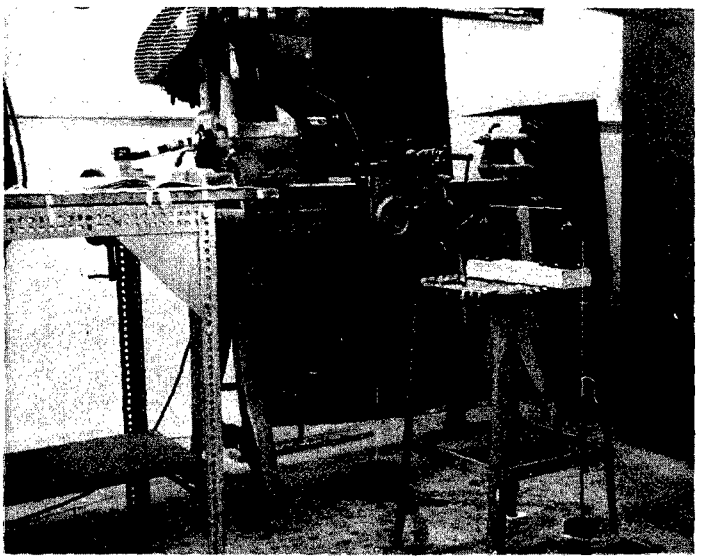

Figure 30. Apparatus for Filament Wear Tests

4. Angle $(\gamma_1 + \gamma_2) = (35° + 35°) = 70°$, load varied, stroke, $s_o = 1/4$ in.

All tests were run at a speed of 48 strokes per minute, and except for one low-load and long-duration test, at each load level a minimum of three filament couples was worn through.

The test results show the scatter range typical of wear and fatigue tests. The general shape of the load versus cycles-to-failure curve is also typical of tests of this type. In determining the fiber tension during testing, the dynamic loads were included. This was required because the weight at the end of one filament and the elasticity of the strings and fibers caused vibration with a frequency about four times that of the stroke. Therefore, due to inertial forces of the weight, W , the peak force, T_o , acting on the filaments is computed as

$$T_o = W\left[1 + \frac{s_o(4 \times 2\pi\nu)^2}{g}\right]$$

where ν is the stroke frequency (sec^{-1}) and g is the acceleration of gravity. Note that the observed amplitude happened to be equal to s_o .

Figures 31 and 32 show the results. The number of stroke cycles is plotted logarithmically versus the peak tensile load, T_o , for the two test series. The shaded area signifies the approximate range of scatter.

From the plotted results in figure 31, it is evident that a decrease in stroke length, i.e., less crimp exchange, lengthens the life of the single joint and the whole fabric. The same is true for decreasing the angle $(\gamma_1 + \gamma_2)$.

To determine from these results the expected lifetime of the space-suit sample, the geometry of the fabrics is required. For the braided slip net the general fiber direction, β , is 35° and the angle $(\gamma_1 + \gamma_2)$ is estimated to range from 60° to 70°. The stroke length, s_o , corresponding to the crimp exchange in the components is more difficult to estimate, but it is safe to assume that it does not exceed 1/4 in. in both fabric types.

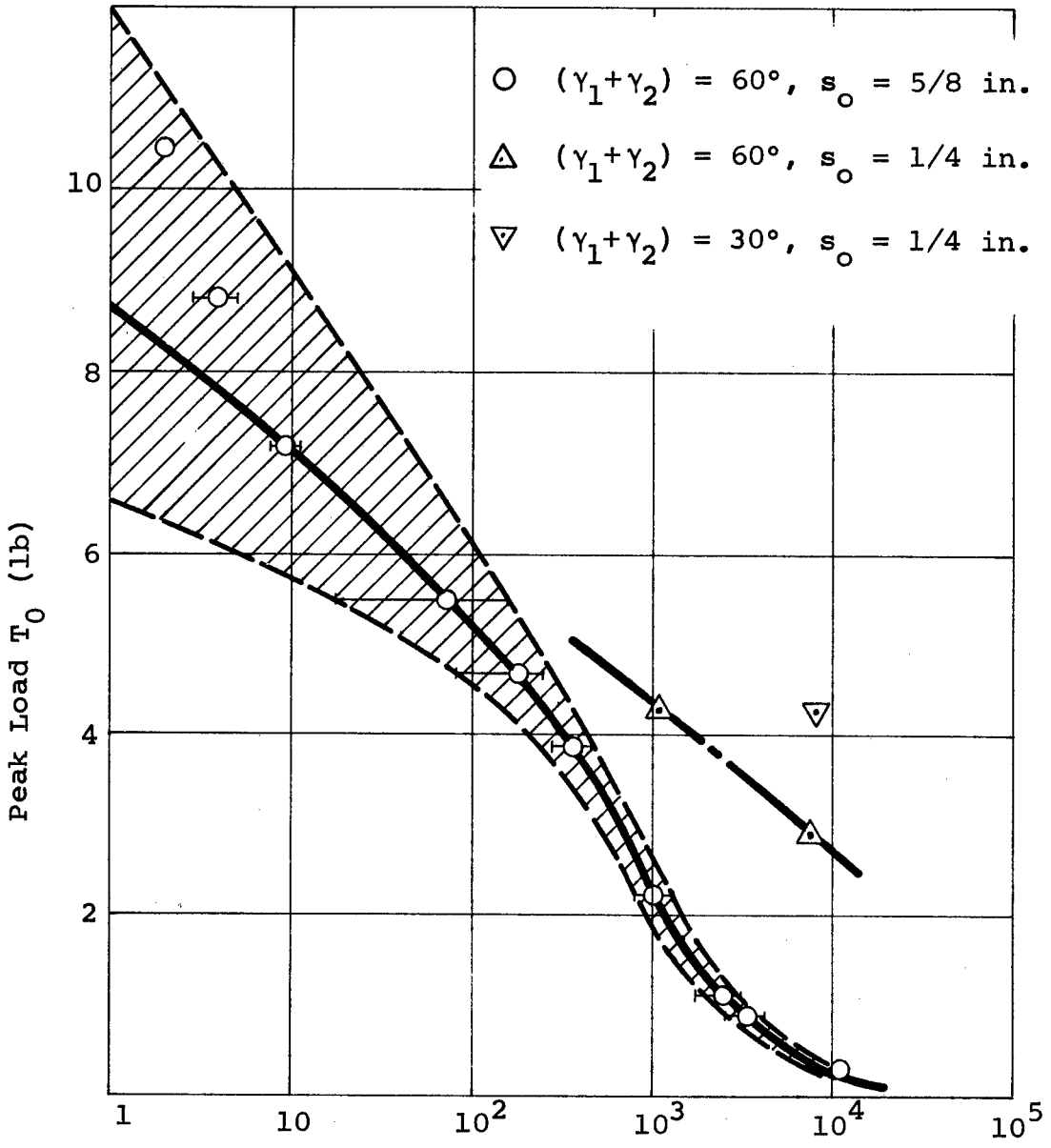

Figure 31. Wear of Braided Slip Net

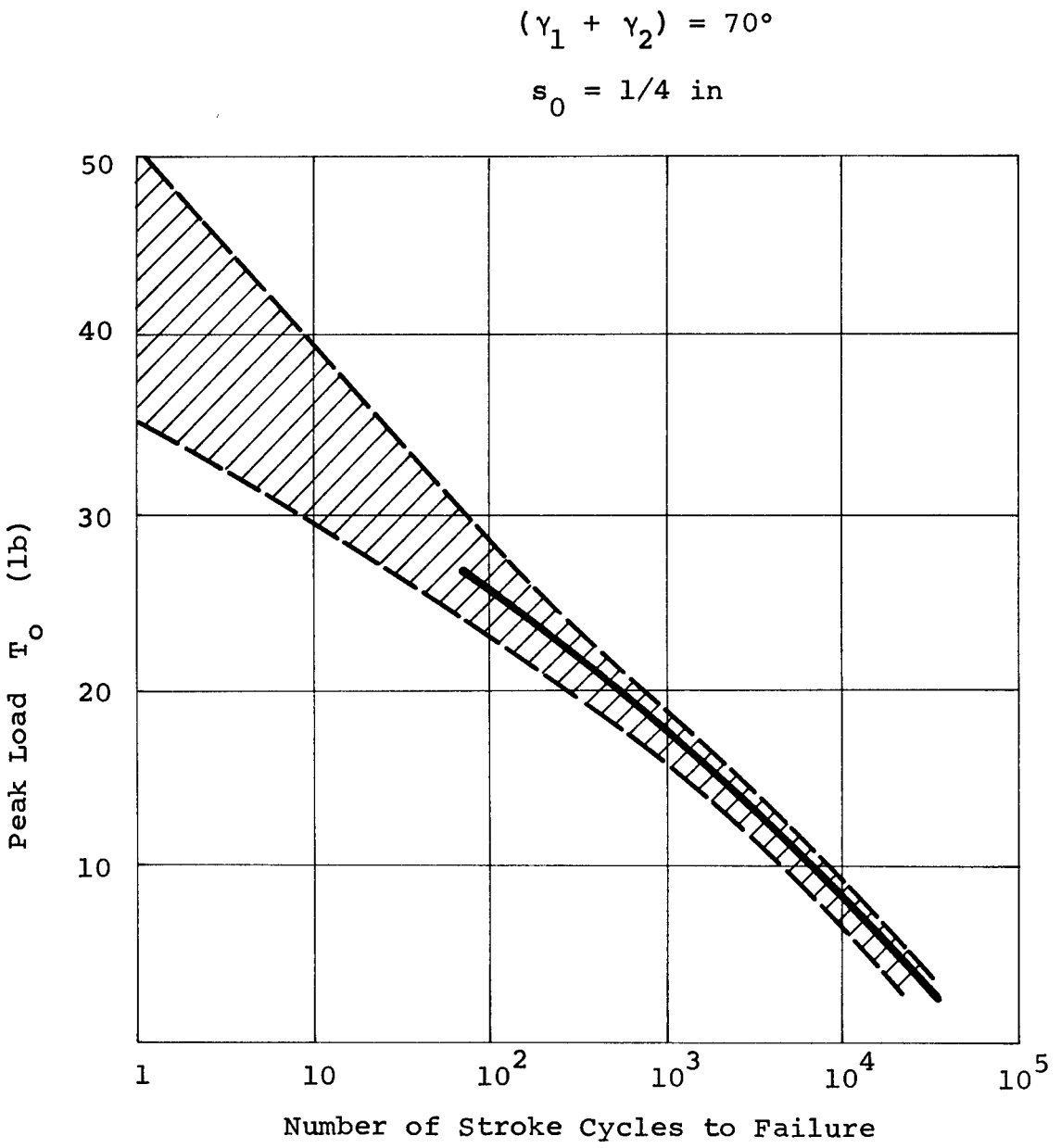

Figure 32. Wear of Braided Single-Layer Fabric

The tension of the single fiber is approximated by dividing the axial pressure force, πpr^2, by $\sin\beta$ and the number of filaments crossing the circumference ($n = 462$ for the braided slip net of the elbow, and $n = 74$ for the single-layer net). Thus a filament tension of 0.24 lb and 1.5 lb, respectively, is reached. Because this tension is derived from the static pressure only, four times this amount is allowed to take care of stress increase, irregularity in geometry, and general inaccuracy of the estimation.

With the parameters derived this way, $T_o = 1$ lb, $(\gamma_1 + \gamma_2) = 60°$, $s_o = 1/4$ in. for the slip net; and $T_o = 6$ lb, $(\gamma_1 + \gamma_2) = 70°$, $s_o = 1/4$ in. for the single-layer components. The life expectancy of the space-suit sample can be approximated as between 30,000 and 100,000 cycles for the slip nets and 16,000 cycles for the single-layer fabric. Both of these estimates are conservative because of the factor of 4 used to calculate the fiber tension. Reduction of this factor results in greatly increased lifetime predictions because of the flat nature of both curves in the range of load experienced by the components.

SECTION VII, MATERIALS SELECTION

Prior to the selection of waxed and hot-stretched Dacron as the basic material used throughout the program, a wealth of technical data was accumulated for a number of candidate fibrous materials. Organic and inorganic fibers were investigated, and where information was incomplete, supplemental tests were performed. Basic fabric suitability was measured on the bases of specific strength, elongation, heat and flammability resistance, chemical resistance, and availability in consistent quality. These data were compiled and reported.(4)

From the mechanical-performance viewpoint, a material with low elongation and hence dimensional stability, and with low friction and hence good mobility is desirable. Bulk and weight are minimized by choosing a material having the highest specific strength. Temperature, chemical, and flammability resistance are desirable properties. For tests on prototype samples, a material had to be chosen which represents a desirable balance of all of these requirements, and, in addition, is readily available in various sizes and of consistently reproducible quality.

On this basis, waxed and hot-stretched Dacron was chosen. This material is preferred to nylon or Nomex* because it has superior creep properties, an ultimate elongation of 10 to 12 percent, and a specific strength of approximately 1.7×10^6 in. This is shown in figure 33 where the specific stress of Dacron tufbraid is shown versus elongation. Its specific weight of 0.05 $lb/in.^3$ is comparable with that of most organic fibers. Yarn, tufbraid, and rovings are available in many sizes, and tufbraid was chosen due to its clean appearance and easy handling.

The most promising advanced material is Polybenzimidazole (PBI). However, coatings are required for material protection. Two candidate coatings are Teflon and Fluorel**, the latter being preferred because Teflon exhibits creep deformation under load.

---

4. "Research on Pressurized Elements for Space Suits", Astro Research Corporation report covering period April 1 to May 31, 1967, Contract No. AF 33(615)-67C-1586.

* Manufactured by E.I. DuPont de Nemours & Co.

** Manufactured by Minnesota Mining & Manufacturing Co.

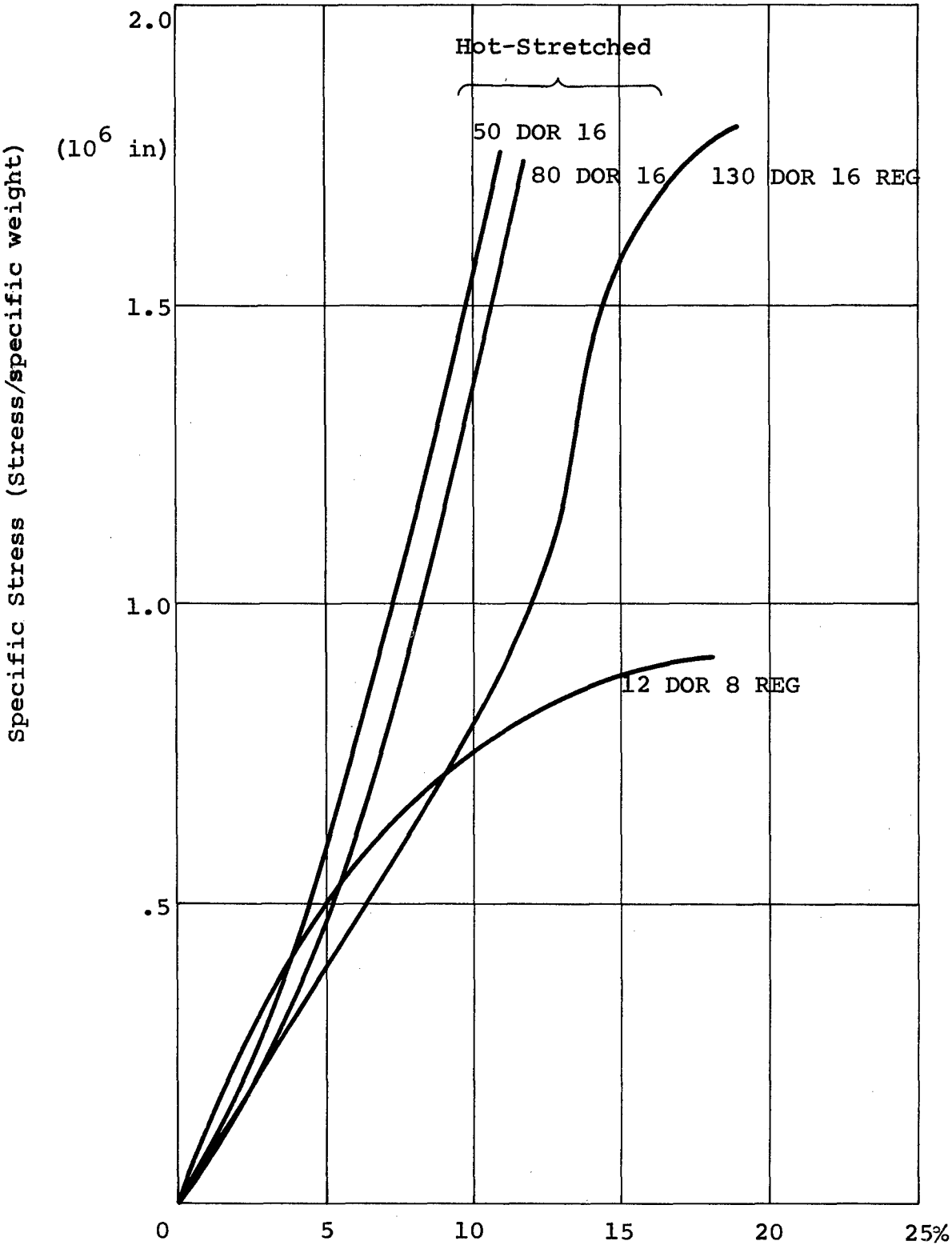

Figure 33. Specific Stress versus Elongation for Hot-Stretched and regular Dacron Tufbraids

SECTION VIII, EXPERIMENTAL DEVELOPMENT PROGRAM

The experimental development program consisted of a series of tests conducted on pressurized fabric cylinders 5 in. diameter and nominally 30 in. long. The object of the tests was to determine the response of slip-net and braided single-layer fabrics to load and deformation conditions typical of those in space-suit components, to improve the performance or response of these basic fabrics by modifications based on the tests, and to obtain comparative response data upon which the final design of the delivery space-suit-component joints could be based. The cylindrical tube was chosen for the basic test geometry because of its fundamental simplicity, ease of fabrication, and because it is representative of wrist and elbow components and a part of the shoulder component.

In all tests, one end of the tube was fixed to a table and the other end loaded. Large deformations were imposed to simulate actual limb motion. Torsional loading and cantilever bending by side load made up the major portion of the test program. An attempt was made to apply pure bending loads to the tubes but after numerous tests and modifications of the loading and measuring apparatus, this part of the program was abandoned. However, qualitative and comparative results were obtained from these tests, and they are reported below.

During the early tests, a bunching type of instability was observed in the slip-net response to large bending deformations (see figure 8). A separate program was conducted to eliminate this instability. Two modifications of the basic slip net were tested. First, constraint lines around the circumference of the tube were introduced, which restricted slip motion to only a segment of the tube. Then slip constraint or knot lines were introduced along the length of the tube at positions where theoretically no slip should occur during deformation. The latter modification proved best,and elimination of severe bunching detrimental to the slip-net performance was achieved.

The material tested was hot-stretched Dacron tufbraid in all but two tests. A knitted Nomex slip net was tested and compared with a knitted Dacron slip net during the tests to determine the material best suited for testing, and a knitted PBI slip net was tested in order to compare the mechanical response of this promising material to Dacron.

The test samples are described and identified with numbers in Table II. Identification numbers 1 through 6 correspond to slip nets, 7 through 12 to single-layer fabrics, and 13 through 15 to prototype samples with a slip-net section to simulate an elbow component attached to a single-layer fabric to simulate a forearm. The identification number 5 represents the five different section lengths, 5(a) through 5(e) tested in the attempt to eliminate bunching with circumferential constraints.

All fabric samples were mounted on a 5-in. diameter surgical rubber sheet 0.023 in. thick and 32 in. long. The ends of the tubes were closed with aluminum plugs. One sample was tested without any constraint layer on the tube; in the remaining cases either a 20-lb Dacron roving was wound helically on the tube with six windings per inch, or a knitted Teflon layer (stockinette) was pulled over the tube. The function of these constraint layers was to provide circumferential dimensional stability and to reduce friction between the fabric samples and the surgical rubber.

All tests on each sample were carried out at 5 psig and 3.7 psig. In addition to load and deformation data, pressure change during deformation was recorded so that volume change could be calculated as a function of deformation.

Description of Test Setup and Procedure

The test setup consisted of a rig to which the test samples and references to measure deformations could be attached, and a pressurization system to provide control and measurement of pressure change during deformation. The general setup is shown in figure 34, with the pure-bending-load apparatus assembled.

Figure 35 is a schematic diagram of the pressure system. Pressurized nitrogen was supplied from a bottle to a 4-way reduction valve. One exit was connected to the sample tube, the second exit to the accumulator and the pressure gauge, and the third to a bleed-air valve which served, together with the reduction valve, as a pressure regulator. The U-tube, filled with colored water, was connected so that it measured the pressure differential between the controlled accumulator and the test sample when Valve 2 was open and Valve 1 closed. The accumulator acted as a pressure sink for the gas displaced from the left leg of the U-tube during deformation. At the onset of each test, the entire system was pressurized to the desired test pressure. This was read on the pressure gauge. Valve 1 was then closed, isolating the test

TABLE II

LIST OF TUBULAR TEST SAMPLES

Identification Number	Type of Net	Type of Fabric	Material	Fiber Geometry	Constraints	Underlayer
1	Slip net	Knit and purl	Nomex	$\beta=55°$	None	Bladder with helically wound Dacron 20# rovings, 6 turns/in.
2	"	"	"	$\beta=35°$	None	"
3	"	"	Dacron 12# Waxed, hot-stretched	$\beta=35°$	None	"
4	"	"	"	$\beta=52°$	None	"
5(a)	"	Braided net (1½ turn)	Dacron 12# Waxed, hot-stretched	$\beta=35°$	5.0" Test length	"
5(b)	"	"	"	"	6.5" Test length	"
5(c)	"	"	"	"	7.5" Test length	"

(continued)

Identification Number	Type of Net	Type of Fabric	Material	Fiber Geometry	Constraints	Underlayer
5(d)	"	"	"	"	8.75" Test length	"
5(e)	"	"	"	"	10.0" Test length	"
6	"	"	"	"	Knotted side lines	"
7	Single layer	Braided net (½ turn)	Dacron 50# waxed, hot-stretched	Circumferential $\gamma_1=\gamma_2=$ 55° to 60°	None	None (plain bladder)
8	"	"	"	"	"	Bladder with helically wound Dacron 20# rovings, 6 turns/in.
9	"	"	"	$\gamma_1=\gamma_2=35°$	"	"
10	"	"	"	$\gamma_1=\gamma_2=$ 55° to 60°	6 Dacron 140# longitudinal constraints	"
11	"	"	"	$\gamma_1=\gamma_2=$ 20° to 25°	None	"

(continued)

Identification Number	Type of Net	Type of Fabric	Material	Fiber Geometry	Constraints	Underlayer
12	"	"	"	Longitudinal $\gamma_1=\gamma_2=55°$	None	"
13	Combination Slip net + Single layer	Braided net (1½ turn) Braided net (½ turn)	Dacron 12# waxed, hot stretched Dacron 50# waxed, hot stretched	$\beta=30°$ $\gamma_1=\gamma_2=35°$	Knotted side lines None	"
14	"	"	"	"	"	Stockinette, Teflon
15	Combination Slip net + Single layer	Knit and purl Braided net (½ turn)	PBI Dacron 50# waxed, hot stretched	$\beta=55°$ $\gamma_1=\gamma_2=35°$	None None	"

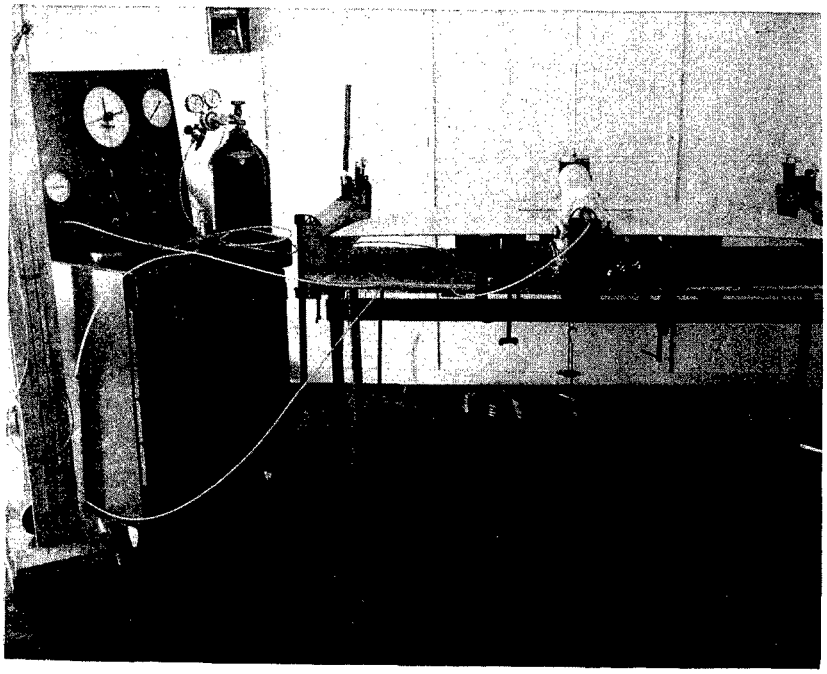

Figure 34a. Overall View of Test Equipment for Tubular Sample Tests

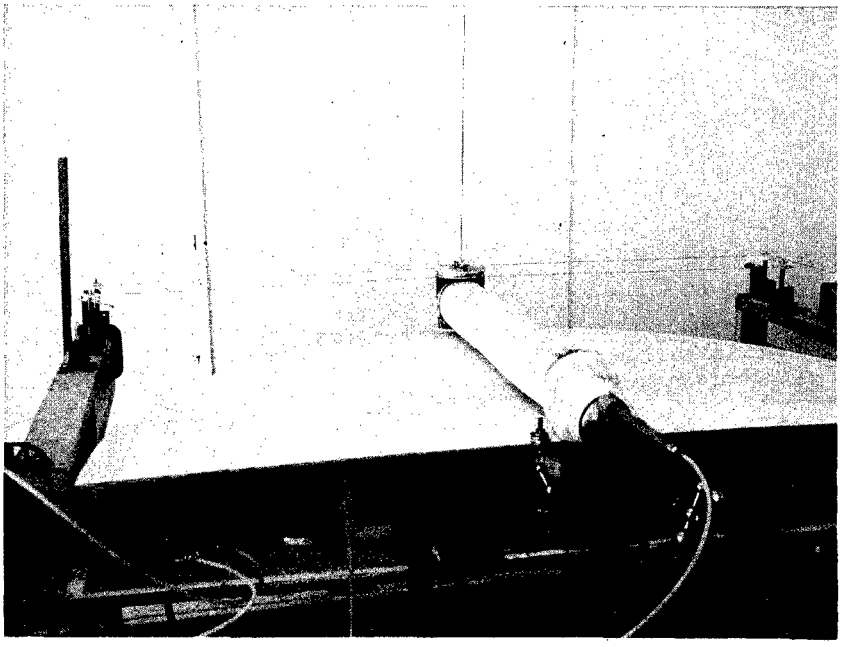

Figure 34b. Rig for Preliminary Bending Tests of Tubular Samples

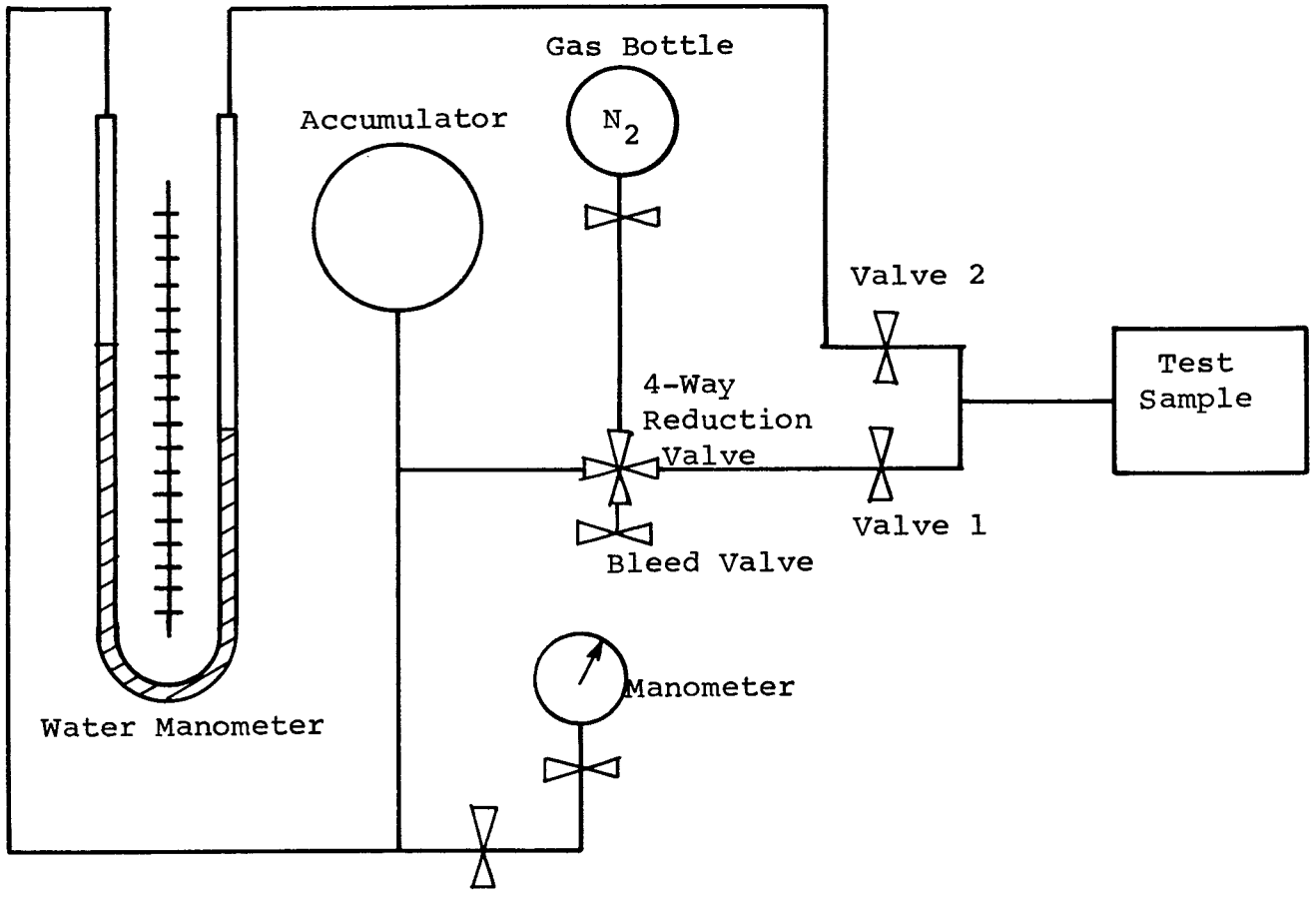

Figure 35. Pneumatic System for Tests of Pressurized Samples

sample from the pressure source. The water manometer then acted as a differential-pressure measuring device between the test sample and the accumulator which was maintained at the initial test pressure. The length of pressurized tube between the test sample and the water manometer, as well as the change in the system due to motion of the water in the 1/4 in. manometer tube, caused less than one percent of the differential pressure.

The setup to deform the samples as cantilever beams by side load is shown schematically in figure 36. One end was fixed to the table plate and the free end was supported by a caster roller. The load was applied to the end plate at the free end by a string. The load direction followed the deformation as shown in figure 36, always maintained perpendicular to the loaded end of the deformed specimen. The force was measured with a spring scale. The perpendicular distance between the load path and the fixed end of the specimen was measured with a tape measure attached to the table at the base of the tube. After pressurization to the desired test pressure, Valve 1 was closed and load applied. Two tests were run on each sample at both 5 and 3.7 psig initial pressure. In one test the sample was deformed continuously from $\alpha_1 = 0$ to $\alpha_1 = 110°$ to $\alpha_1 = -30°$ and returned to $\alpha_1 = 0$. The response, α_1, α_2, r and the U-tube manometer reading, was recorded at intervals $\Delta\alpha_1 = 10°$. The purpose of the other tests was to determine what fraction of the total deformation at any level would be sustained with no load applied. The deformation angle, α_1, was increased in 20° increments, and the load released after each increase. The position to which the sample returned after release of the load and the pressure variation were recorded.

For the torsion tests, one end of the tube was fixed to the table plate. The free end was suspended from above in such a way that it could turn about the tube axis. A bar was attached to the end plate with two holes matching the plug of a specially designed torque meter. Torque was applied by hand on the levers of the torque meter. The deformation angle was read by means of the suspension string on a scale attached to the end plate. To ensure the vertical position of this string, a plumb line was hung close to it.

Figure 37 shows the end plate of the tube with the dial mounted and the torque meter in place. In figure 38, the dial and suspension hook are removed so that the end plate and the torque meter can be seen separately.

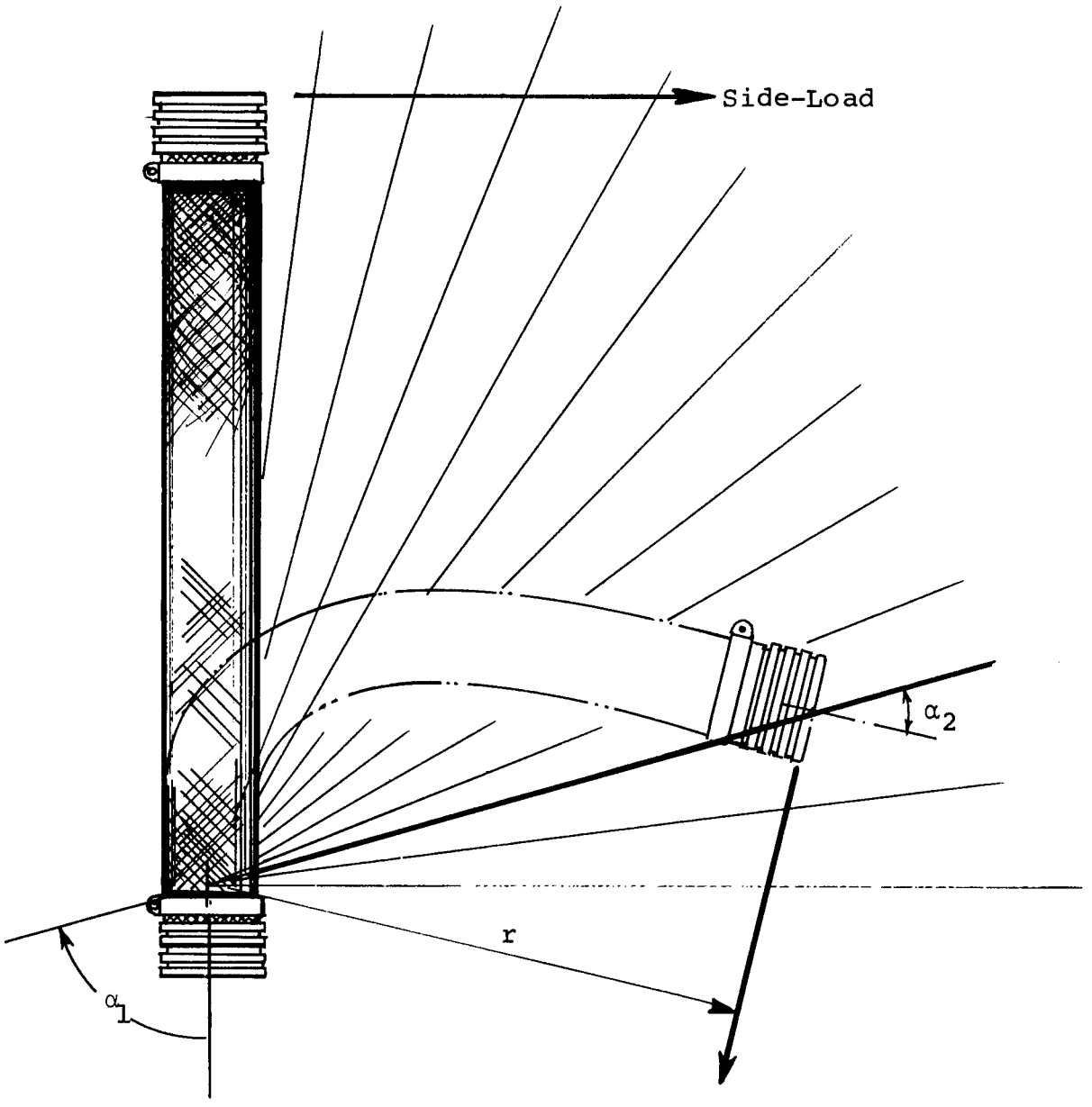

Figure 36. Sketch of Side-Load Bending Tests

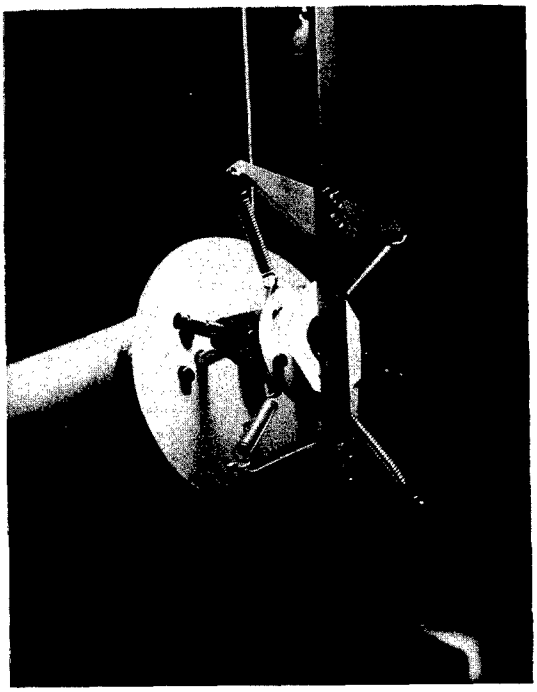

Figure 37. Torsion Test of Tubular Sample: Torque Meter in Place

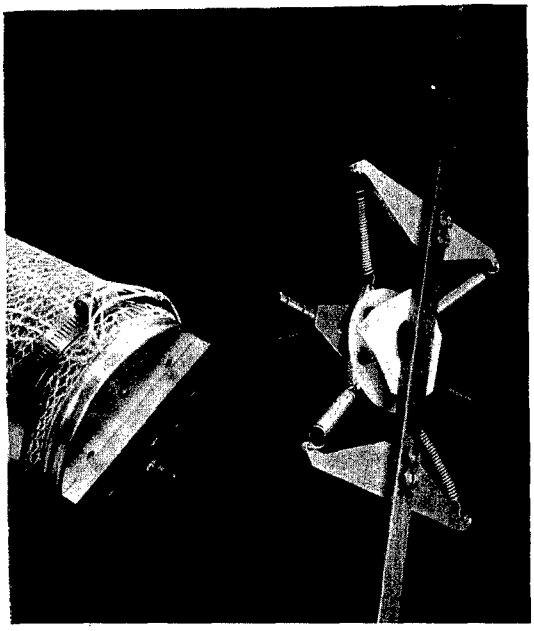

Figure 38. Torsion Test of Tubular Sample: End Plate with Plugholes Fitting Torque Meter

The test procedure was similar to the side-load bending tests except that torque and angular twist were applied and measured. A continuous single-cycle test was performed on each sample between total twist angles of approximately $\pm$ 220° for the single-layer fabrics and between torque loads of $\pm$ 130 in.-lb for the slip-net fabrics. The latter were too stiff in torsion to apply large deformations without damage to the fabrics. Zero-load equilibrium angles were measured by increasing the twist angle in increments of 10° and releasing the load after each increase. Pressure-change readings from the U-tube manometer were recorded throughout the torsion tests.

In the attempt to apply pure bending torque through large deformations, the fixed end of the sample was attached to a turn-table which rested on a sled. In principle, the sled could be moved during deformation of the tube so that reaction loads other than bending torque could be avoided.

The bending torque was applied by two pairs of parallel cables attached to a 5-in. diameter disk on top of the end plate of the tube, each cable pair running over pulleys to a crossbar where weights were applied. In order to allow the loaded end to move along the direction of the cables, the end plate was suspended as shown in figure 34(b) from a trolley traveling parallel at the ceiling. The deflection with respect to the fixed end, α_1, could be read on a large protractor mounted on the turntable. The total deflection was obtained from the sum of this angle, α_1, and an angle, α_2, between the axis of the tube at the loaded end and the cord connecting both tube ends.

The test procedure was essentially the same as in the other tests. However, zero-load equilibrium tests were not performed.

The results of the cantilever side-load bending tests are shown in figures 39 through 46. In figure 39 the side load is plotted versus the deformation angle, α_1, at 5 psig internal pressure for the knitted Dacron slip net and for the series of tests used to evaluate the effect of circumferential constraints on the braided-fabric slip nets. The improved performance of the braided fabric over the knitted fabric shown on this figure was the basis for its selection in the final design. An increase in bending compliance with distance between circumferential constraints is evident from this figure. For Sample 5(e) with 10 in. of test length between constraints, the slip net deforms at nearly constant load of 2 lb. As the unconstrained section length is

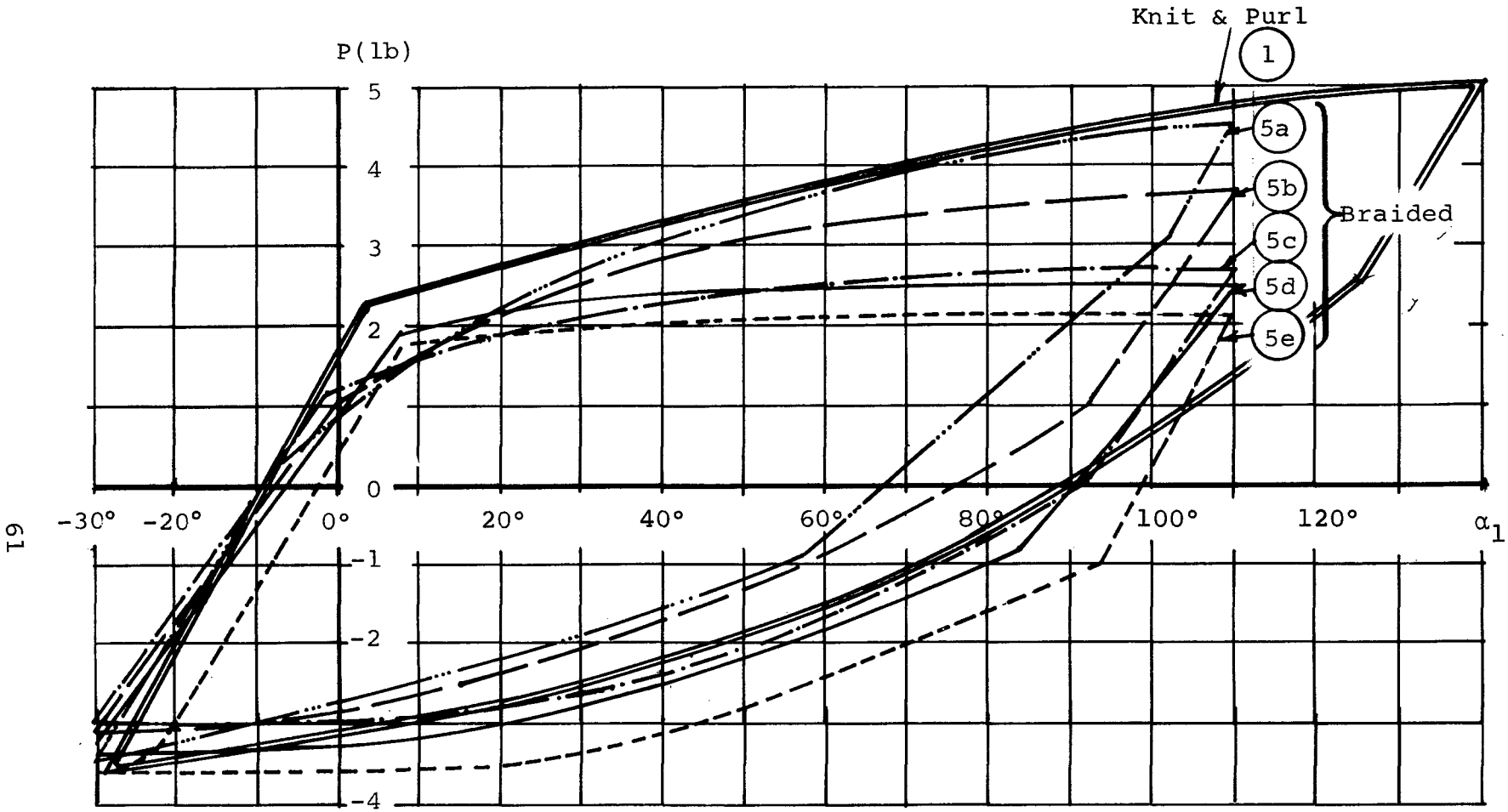

Figure 39. Side-Load Bending Tests of Tubular Samples
Load versus Deformation Angle α_1
for Slip Nets at 5 psi Internal Pressure

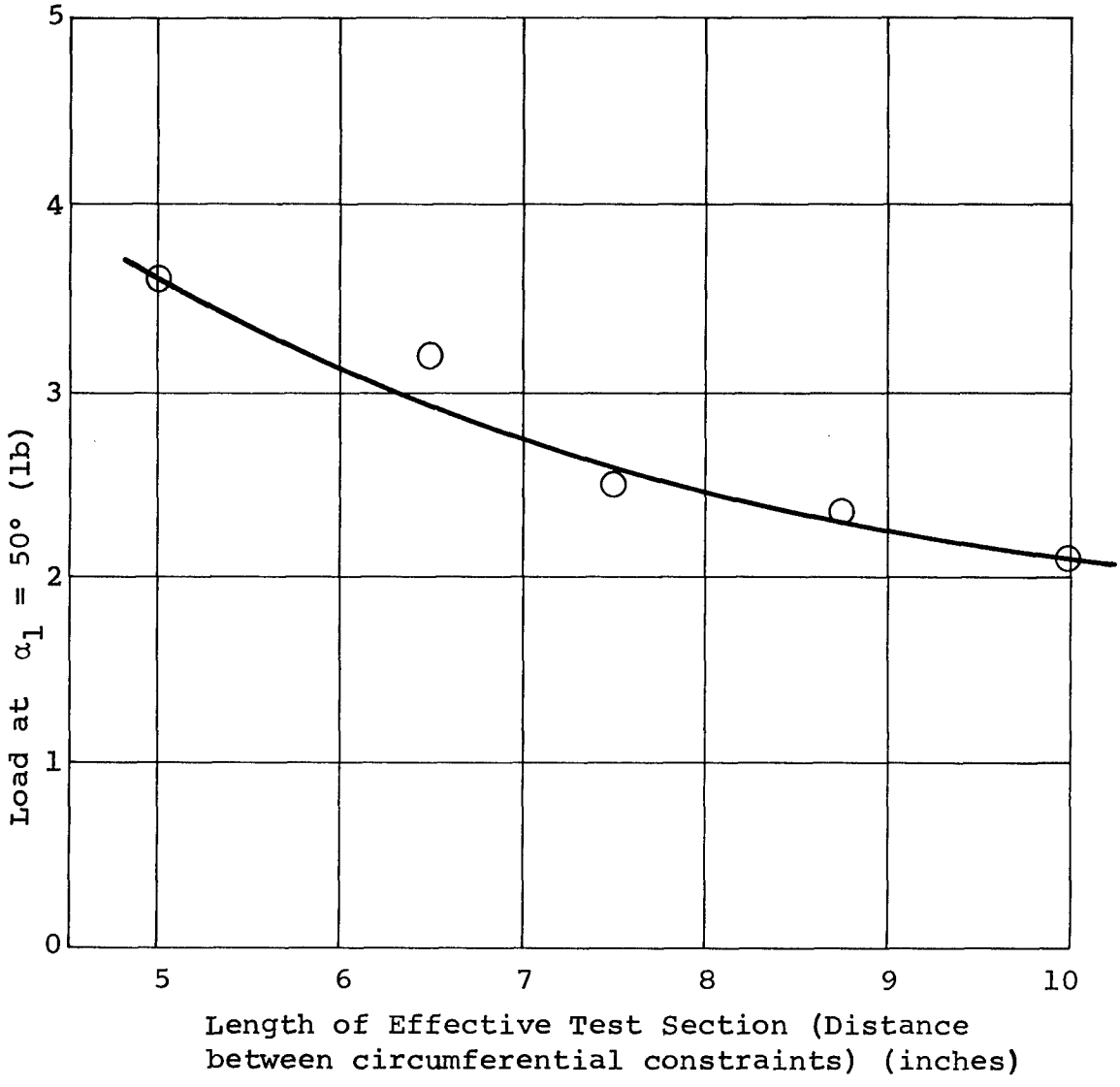

Figure 40. Effect of Test-Section Length on Load for Braided Slip Nets (Tests 5a, b, c, d and e)

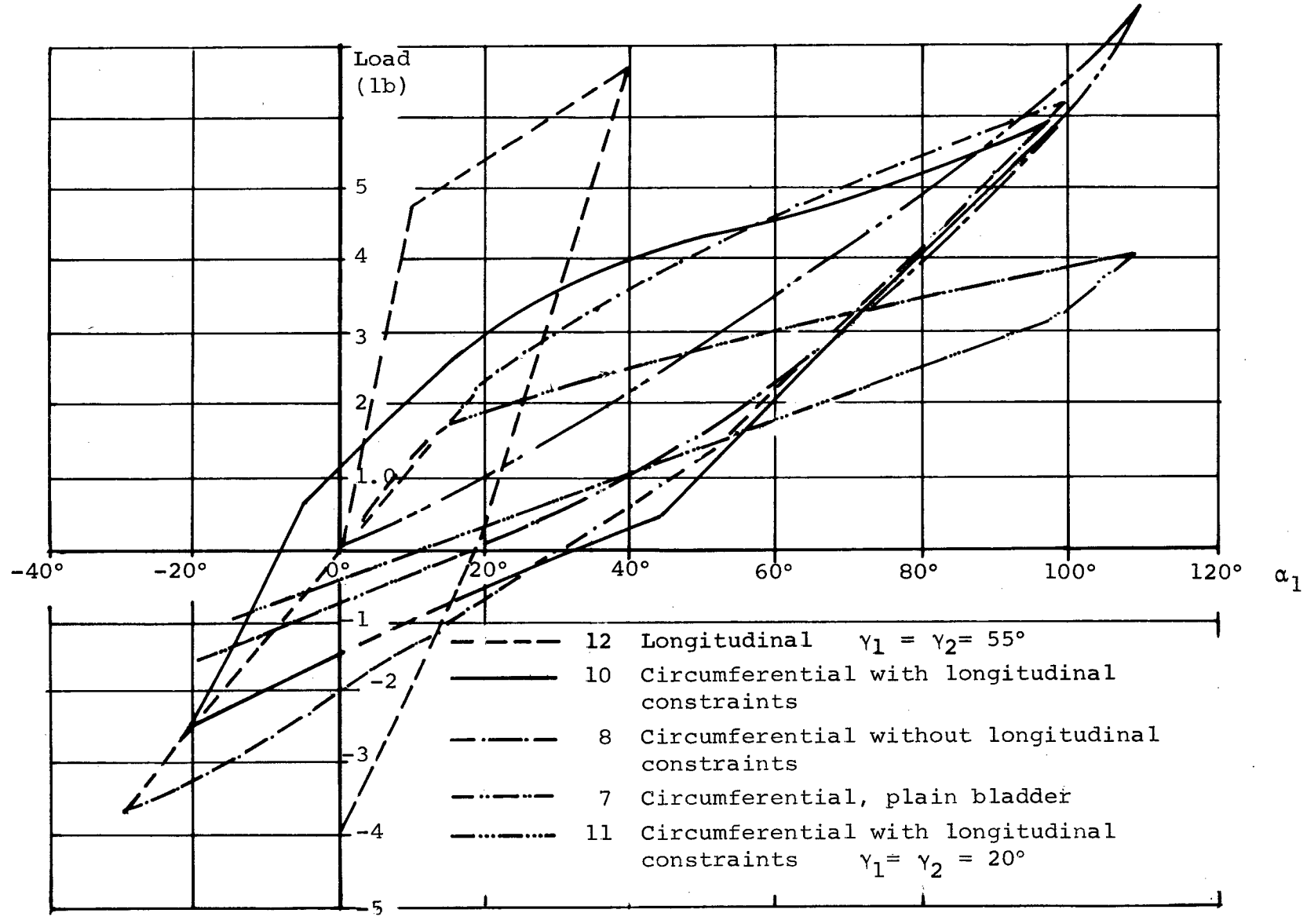

Figure 41. Side-Load Bending Tests of Tubular Samples
Load Versus Deflection Angle, α_1, for Braided Single-Layer Fabrics at 5 psi Internal Pressure

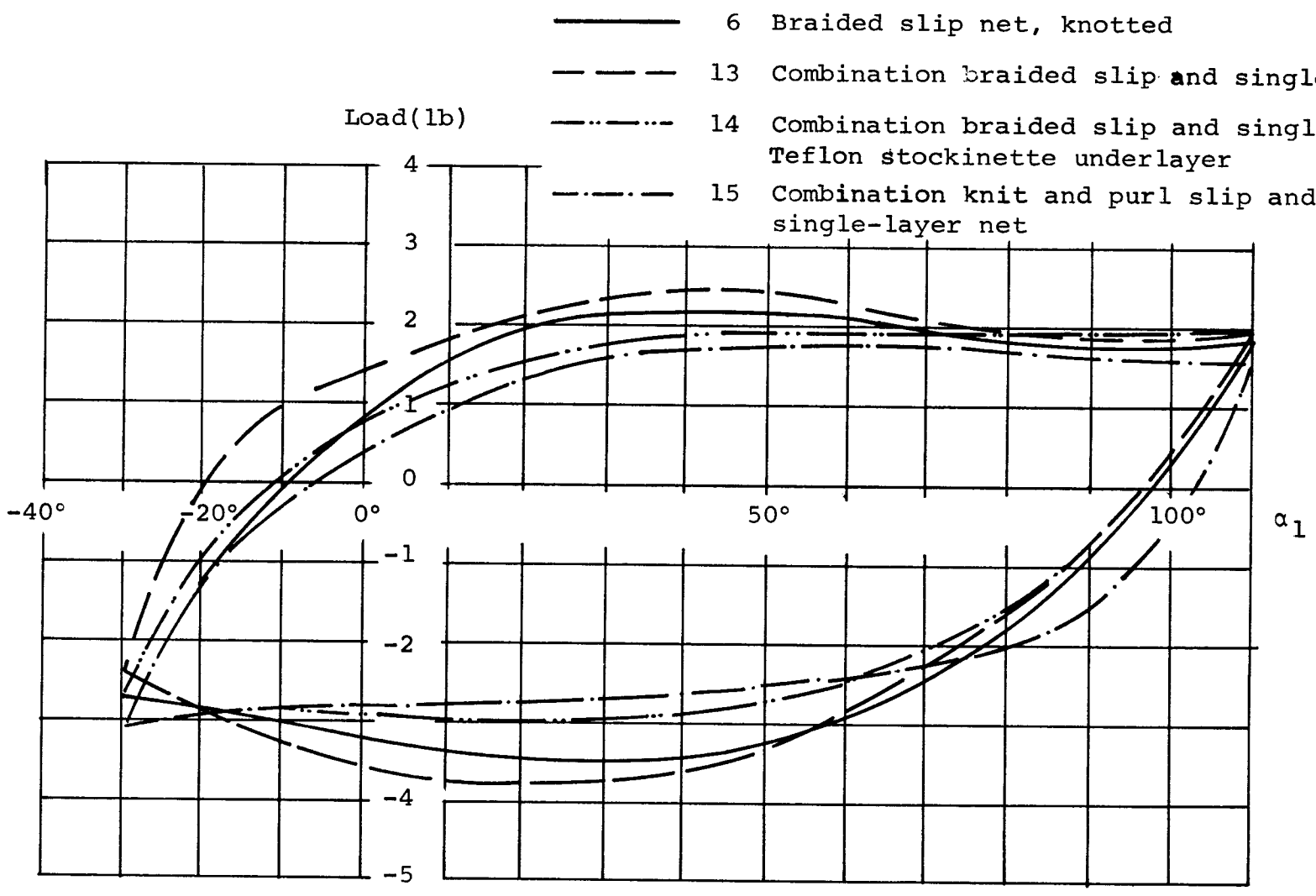

Figure 42. Side-Load Bending Tests of Tubular Samples
Load versus Deflection Angle, α_1, for Slip Nets and Combinations of Slip and Single-Layer Nets at 5 psi Internal Pressure

decreased, the compliance decreases and more elastic-type behavior is obtained as evidenced by the positive slope of the curves. Figure 40 is a plot of the load required to deform the circumferentially-constrained braided slip net to $\alpha_1 = 50°$. The increase of compliance with test length is again apparent; however, gross bunching occurred for lengths above 10 in. A series of cyclic load tests were also performed on Samples 5(a)-(e) in order to identify the test length below which bunching would not occur. This value was determined to be between 7.5 and 8.75 in. Thus, the curve corresponding to 5(c) on figure 36 is the best performance displayed by a circumferentially-constrained braided slip net without bunching.

The load-versus-angular-deflection (α_1) response of the braided single-layer fabrics is summarized in figure 41. The best bending performance was obtained from Sample 11, a 1/2-turn braided fabric with fiber direction around the circumference and 6 longitudinal constraint fibers -- 3 along each intersection of the neutral plane of bending with the sides of the test sample. The torsional compliance of this fabric was also higher than all the other single-layer fabrics tested (see figure 47). However, the concentrated longitudinal load in the longitudinal constraints precludes its use in integrated designs with slip nets. All other braided single-layer fabrics demonstrated approximately the same response to side-load bending tests with peak loads of 6 lb at $\alpha_1 = 100°$. The sample with fiber direction along its length was clearly inferior to the fabrics with circumferentially directed fibers.

The side-load versus angular-deflection performance of the various knotted slip-net single-layer combinations is shown in figure 42. The performance of the knotted slip net covering the entire sample is included on this figure. The knitted PBI slip-net braided single-layer net with a knitted Teflon stockinette used for the constraint layer exhibits the best performance. The effect of the change from the helically-wound Dacron constraint layer to the Teflon stockinette is displayed by the difference between the results for numbers 13 and 14. The results shown on this figure can be summarized as follows. The decrease in test length caused by replacing part of the knotted slip net with a simulated single-layer forearm section did not substantially affect the performance. Replacing the circumferentially wound constraint layers with a knitted Teflon constraint layer increased the compliance of braided slip-net configurations but not significantly. On the contrary, the performance of the knitted slip-

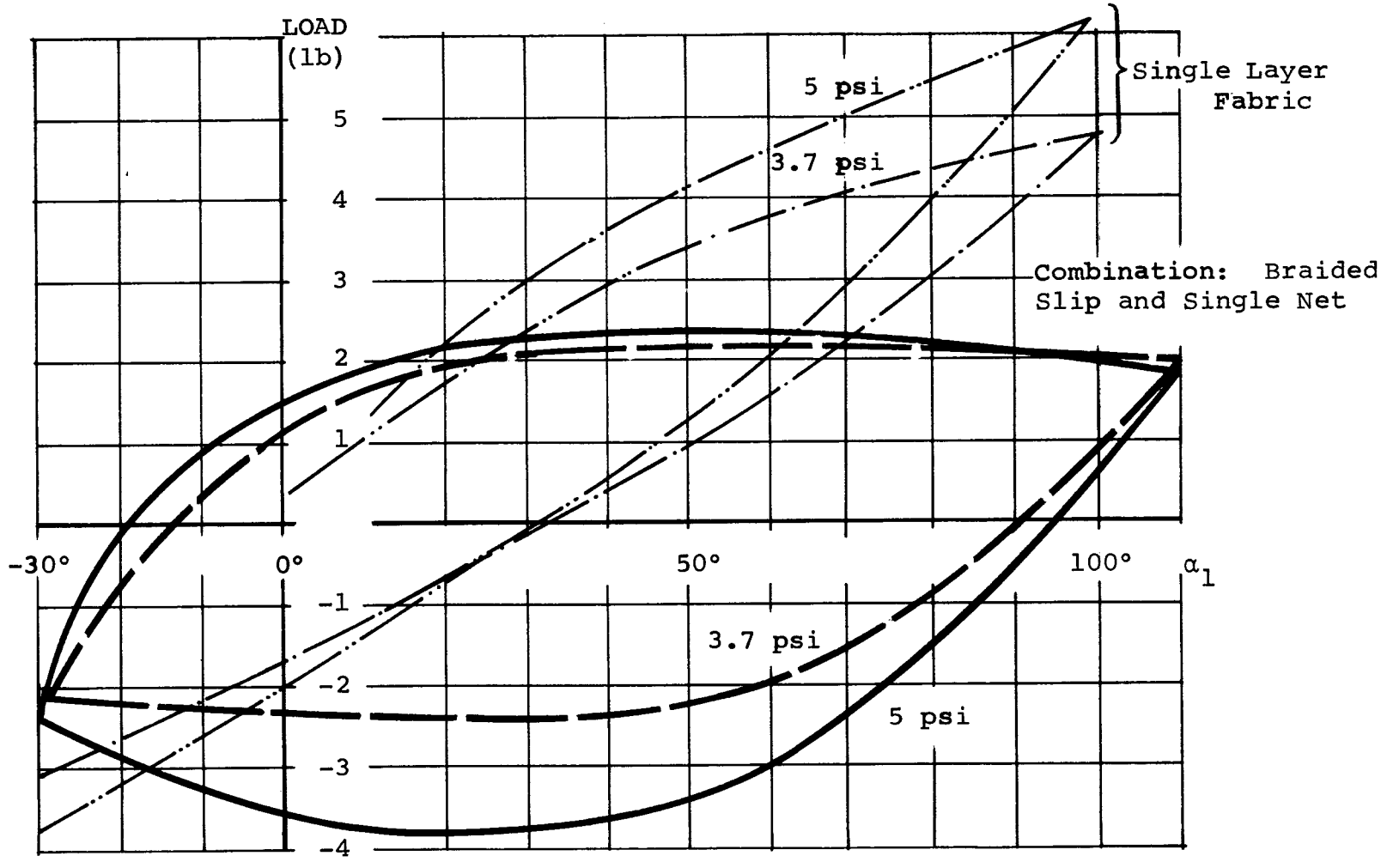

Figure 43. Side-Load Bending Tests of Tubular Samples
Load Versus Deflection Angle α_1 of Two Typical Fabrics at
Different Internal Pressures

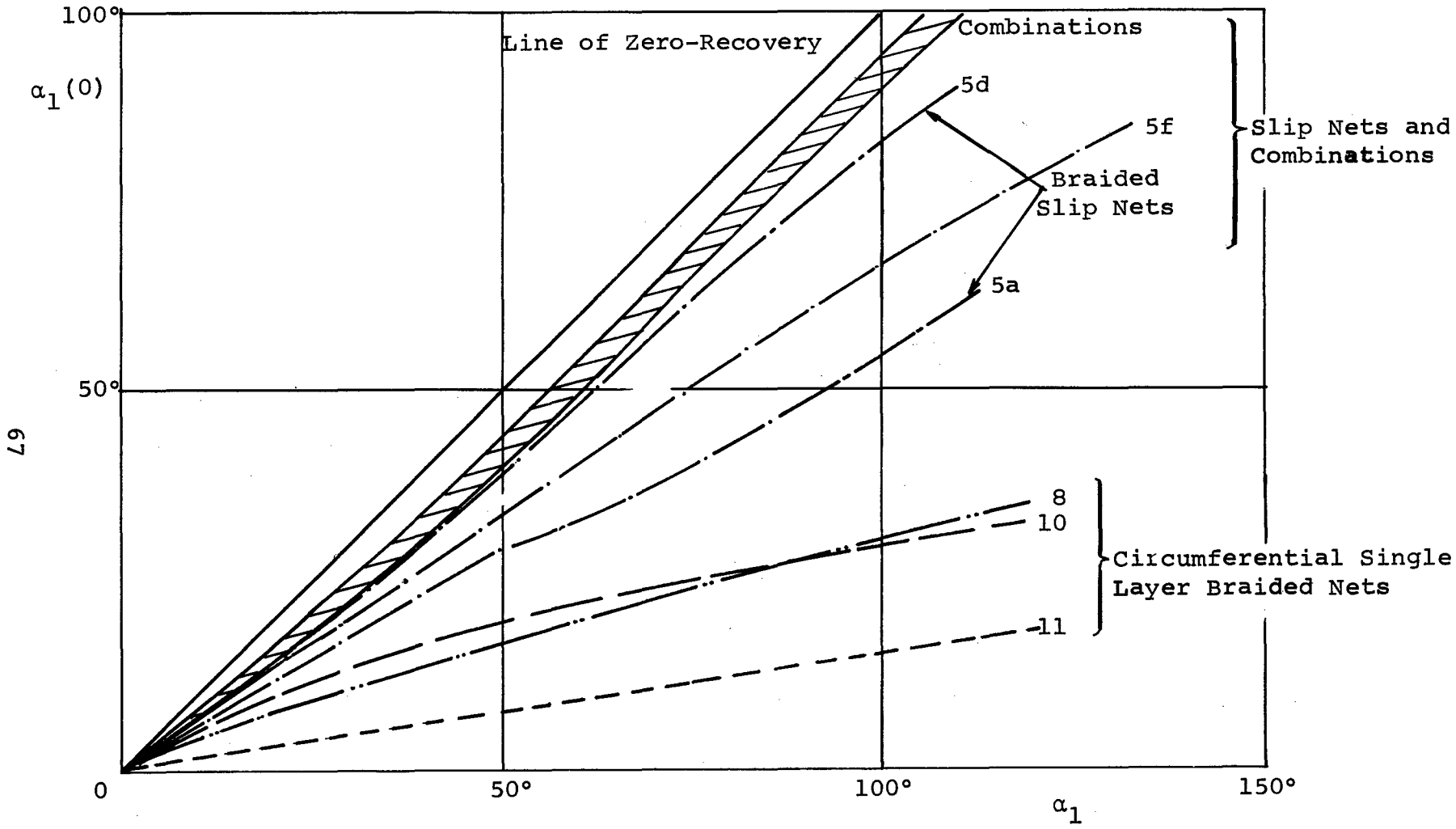

Figure 44. Side-Load Bending Tests of Tubular Samples
Recovery Angle $\alpha_1(0)$ versus Deformation Angle α_1 at 5 psi Internal Pressure

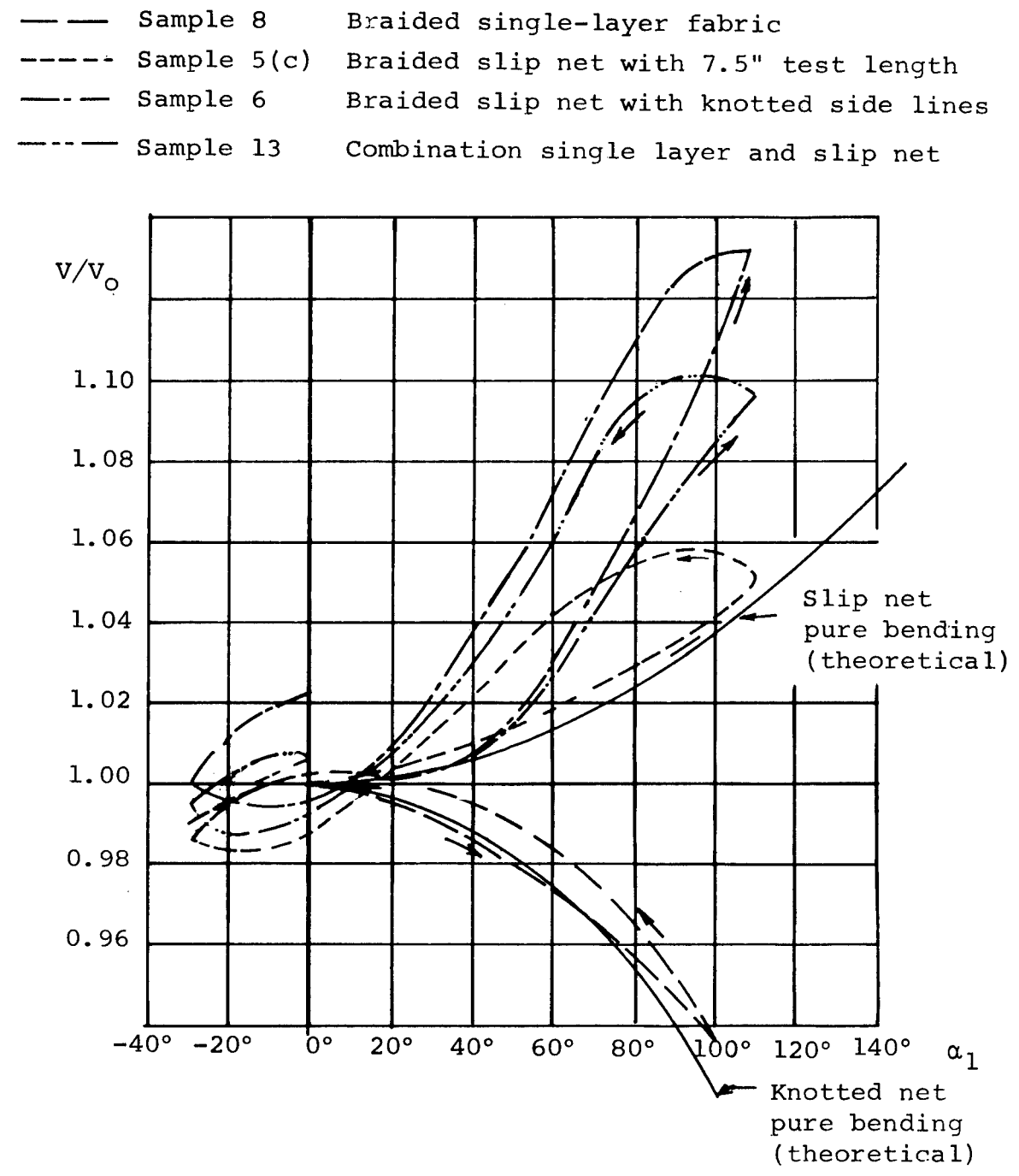

Figure 45. Volume Change During Side-Load Bending Tests at 5 psi Internal Pressure

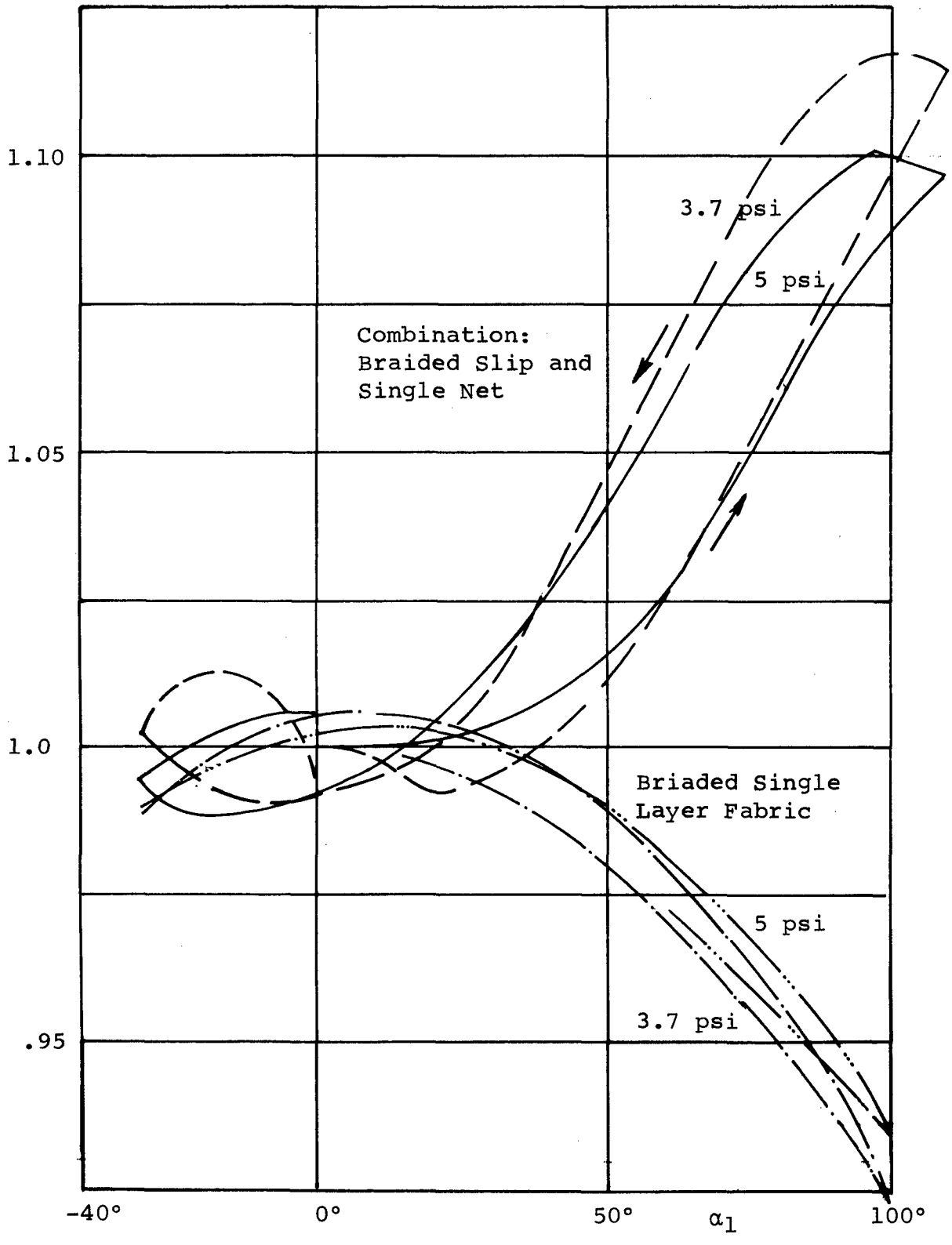

Figure 46. Volume Change for Two Typical Fabrics at Different Internal Pressures during Side-Load Bending Tests

net configuration was significantly improved by changing from Dacron to PBI in the slip-net fabric and replacing the Dacron hoop wraps by a Teflon constraint layer. This is evidenced by comparison of the performance of Sample 1 in figure 39 with that of Sample 15 in figure 42. If it were not for the poor creep properties of Teflon, the combination of a Teflon constraint layer and a knitted Teflon slip net would no doubt display the best performance in bending compliance. When available, Fluorel-coated PBI fibers could be expected to display similar bending properties as well as high flammability resistance, and should be investigated.

In order to compare the bending response of the two fabric types, typical results at both 3.7 and 5 psig for slip-net and single-layer net are shown in figure 43. The slip net requires significiantly lower loads to attain large deformations; however, in returning to the straight position, higher returning load is required. At 3.7 psig the maximum load level required for both deformations and return in the slip net is of the order of 2 lb. At 5 psig the deformation load is essentially unaffected; however, the load required to return to the straight position increases to nearly 4 lb. This is attributed to the higher fiber loads which cause more slip in the slip net at 5 psig. Thus the sample is aided in attaining deformations but inhibited from returning. This phenomenon is also evident from the results in figure 39. As the unconstrained length is increased, the deforming load decreases, but the magnitude of the required restoring force increases because more slip is permitted by the increased length. Against this undesirable property must be traded off the ability of the slip-net joints to remain in deformed geometries with no sustaining force. This property is displayed in figure 44 where the zero-load equilibrium angle is plotted versus the deformation angle achieved before the load was released. Included in this figure are typical results for slip-net, circumferential braided single-layer nets, and the combinations of the two. The slip-net capability for permanent deformation is significantly better than the single-layer nets and, in conjunction with the low deforming load required, was the basis for selection of slip-net wrist, elbow, and shoulder components in the final design.

The variation of enclosed volume with deformation angle, α_1, is shown in figure 45. The behavior of the two fabric types is qualitatively as predicted by the pure bending theory. The theoretical curves for idealized slip nets and braided single-layer nets are included in the figure (see the following section for

discussion of these theories). The braided single-layer nets represented by Sample 8, display a decrease in volume for increasing deformation angle. This indicates that work is done on the confined gas during loading and is recovered during unloading. The braided slip nets, represented by Samples 5(c), 6, and 13, display an increase in volume for increasing deformation angle. This indicates that energy was extracted from the gas during loading and, therefore, work had to be done on the gas as the tubes were forced back to their initial shape. The data plotted in figure 46 is included to display the marginal effect of initial pressure on volume change in both braided single-layer nets and slip nets.

The torsion tests revealed no serious problems. During testing of the braided single-layer fabrics, regular deformation was observed to be distributed uniformly along the tube axis. The slip-net samples showed a slight tendency to bend at the loaded end, displaying a dimensional instability under the large loads applied.

The results of the torsion tests are given in figures 47, 48, and 49. Figure 47 shows the variation of torque with angle of twist per unit length. The slip-net constraint layer is obviously too stiff for use as a torsion joint such as the forearm. The sample with circumferential fiber direction and longitudinal constraints (number 11) displays the highest torsional complaince. However, the longitudinal constraints cannot be used in integrated designs because they will introduce concentrated loads into adjacent sections.

The zero-load equilibrium angles for the three braided single-layer nets are shown in figure 48. The desired performance is the reverse of that displayed in figure 47. Thus the stiffest tube displays the largest zero-load equilibrium-angle positions, and the most compliant tube the smallest zero-load equilibrium angles. The effect of initial pressure is included in figure 48 and is seen to be relatively unimportant in its effect on zero-load equilibrium angles. Figure 49 is included to show typical dependences of torsional load-deformation angle response to initial internal pressure. Though not negligible, the effect is not pronounced.

In spite of the high loads displayed in figure 47, the braided single-layer fabric with circumferential fibers and no longitudinal constraint fibers was chosen for the forearm and upper arm components because of its zero-load equilibrium performance shown in figure 48.

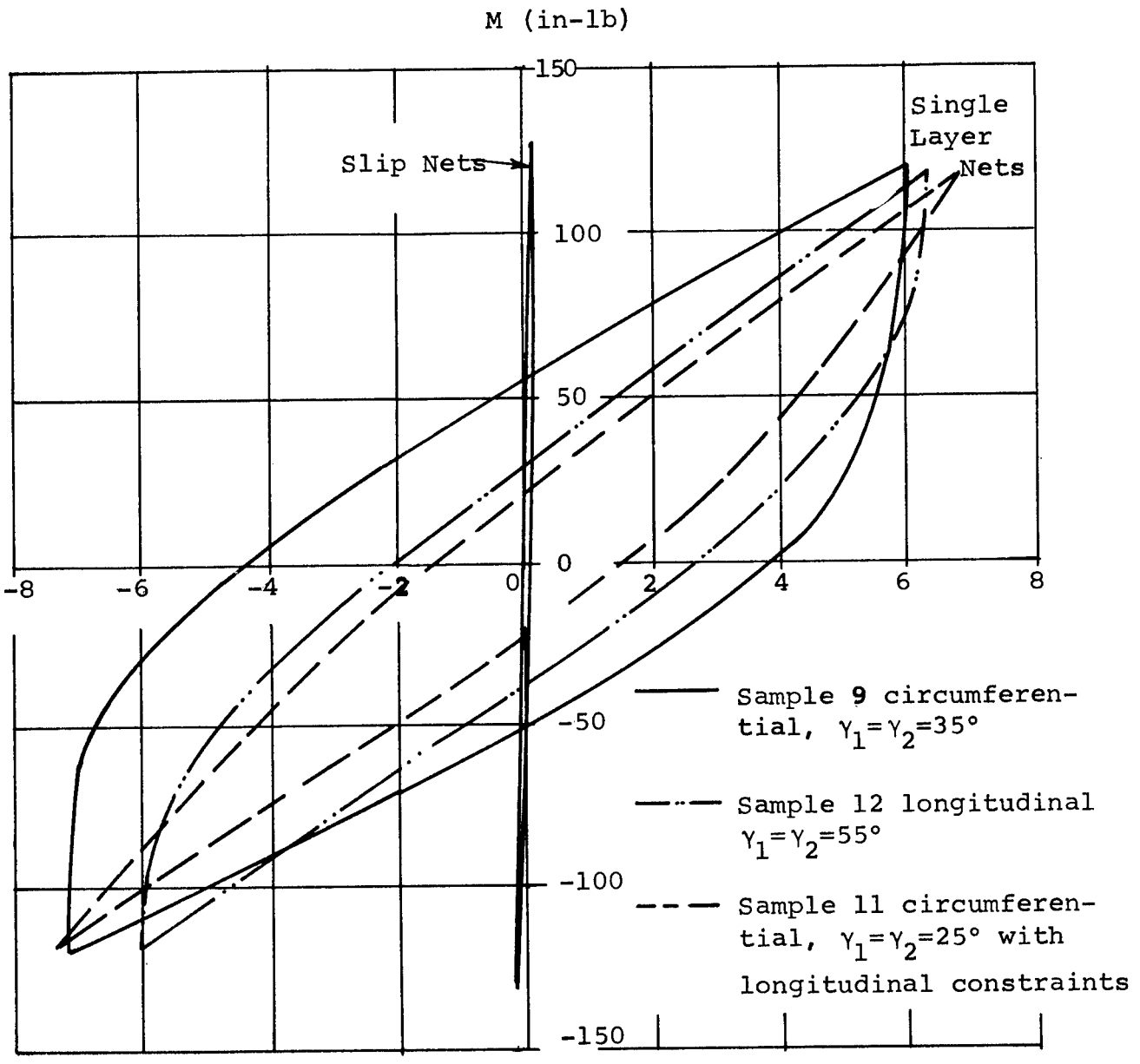

Figure 47. Load-Deformation Response to Torsional Loading

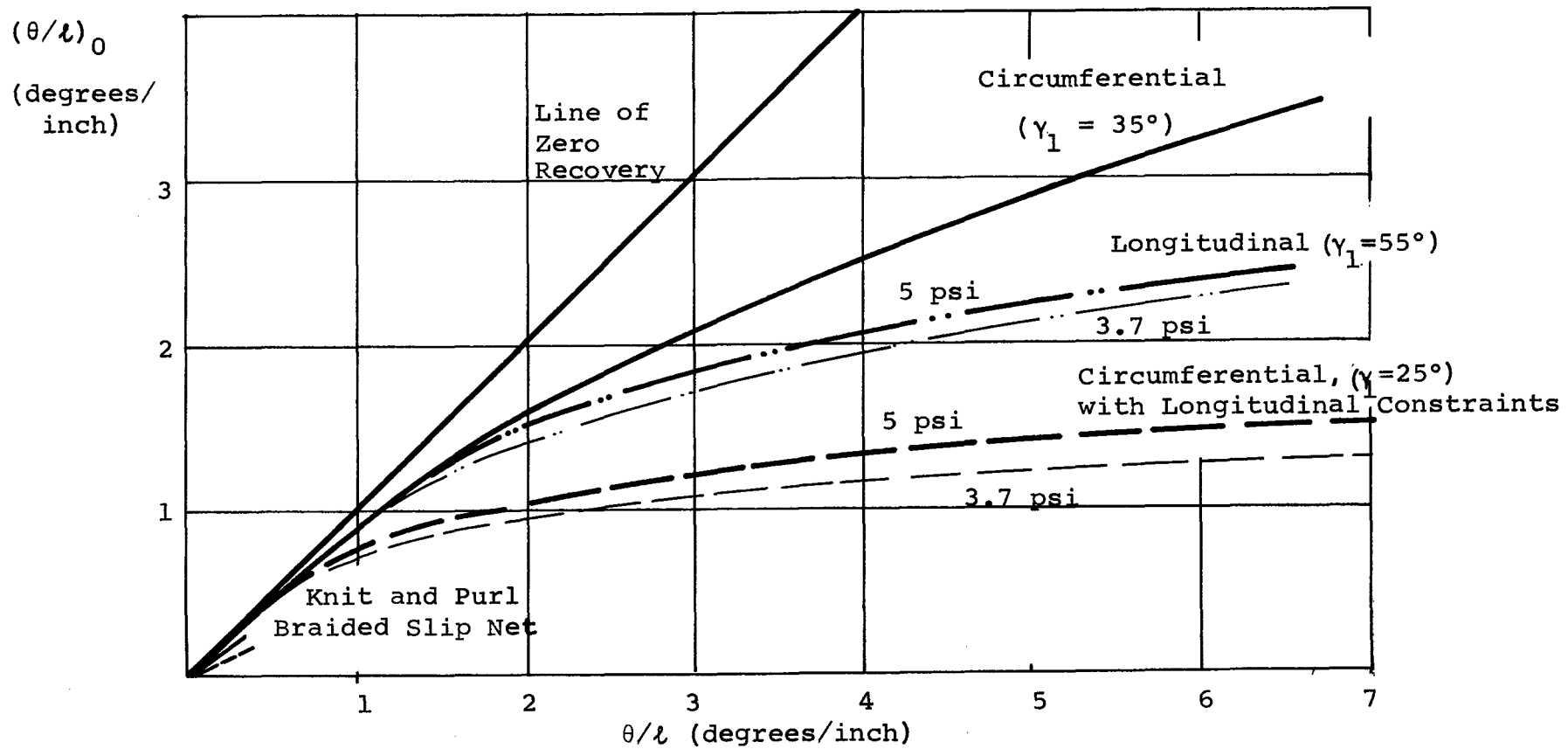

Figure 48. Zero-Load Equilibrium Values of Twist Angle in Braided Single-Layer Fabrics

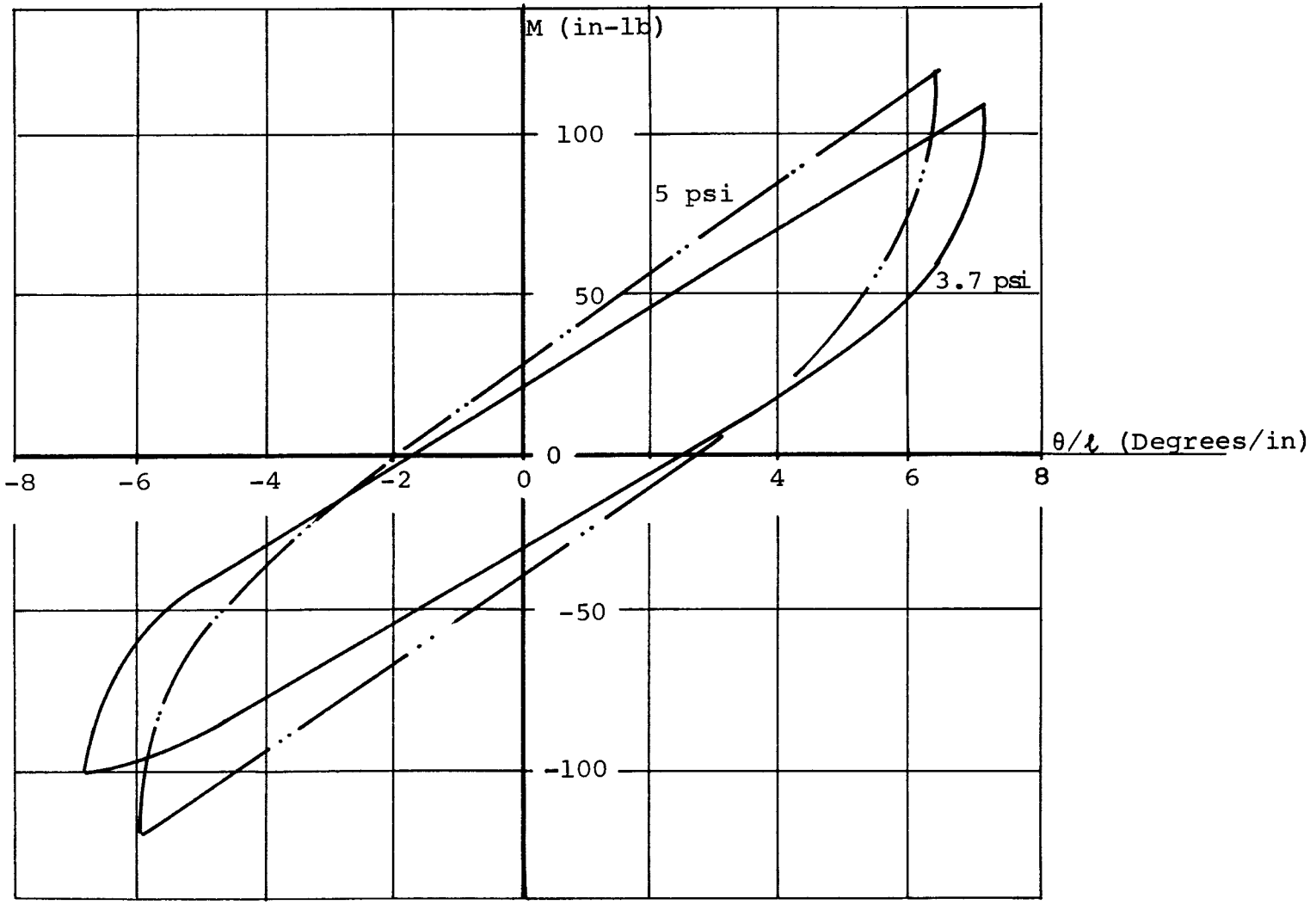

Figure 49. Pressure Influence on Torsional Response of Braided Single-Layer Fabrics

The results of the attempt to load the samples with a pure bending moment through large deformations is reported in figure 50 for slip-net constraint layers, and in figure 51 for the braided single-layer constraint layers. The shaded region in figure 50 covers the scatter range of three tests performed on Sample 3. The results cannot be interpreted quantitatively because the true load conditions are not known. However, they serve to confirm the qualitative behavior observed in the bending by side-load tests.

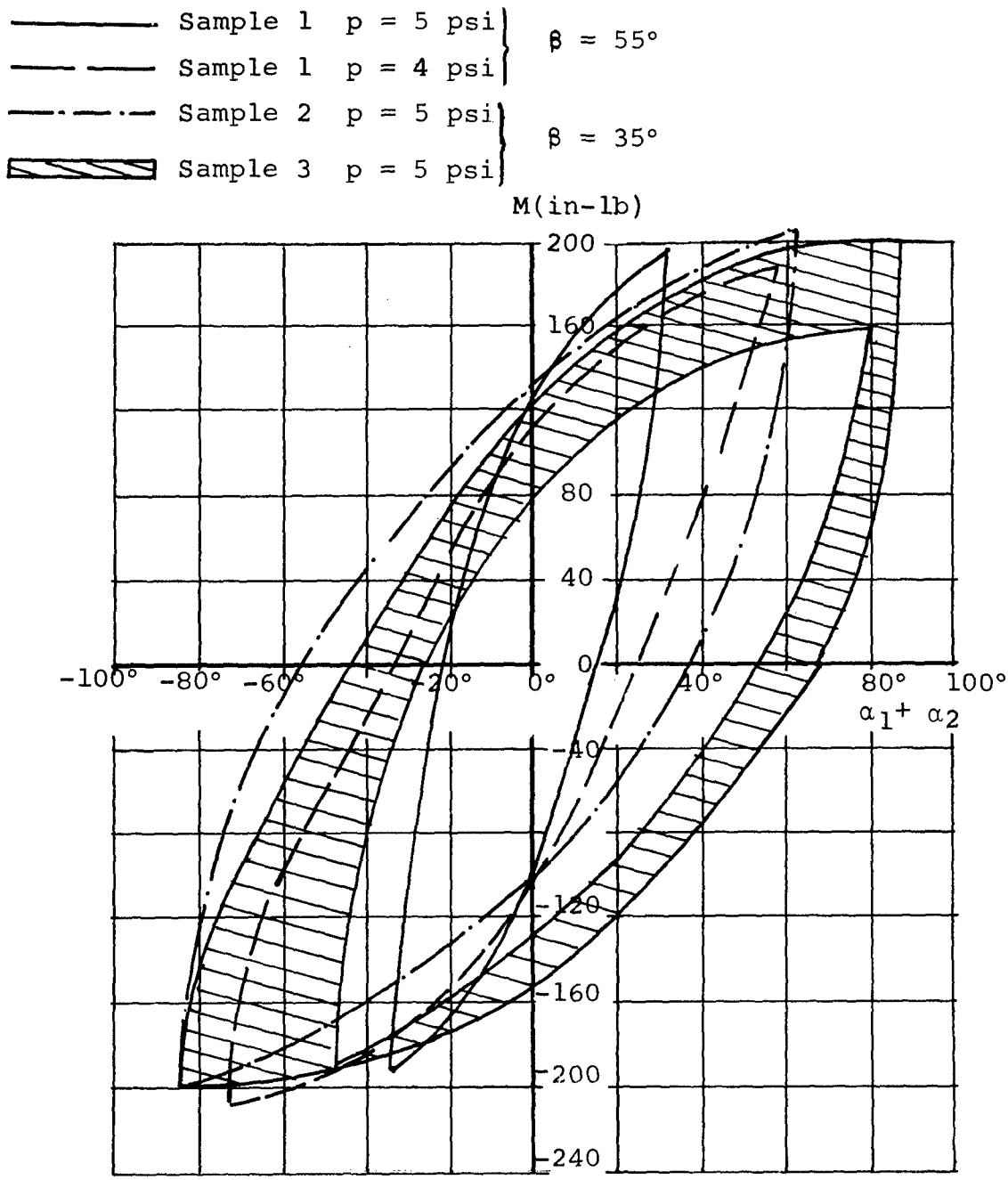

Figure 50. Preliminary Bending Tests of Tubular Slip-Net Samples

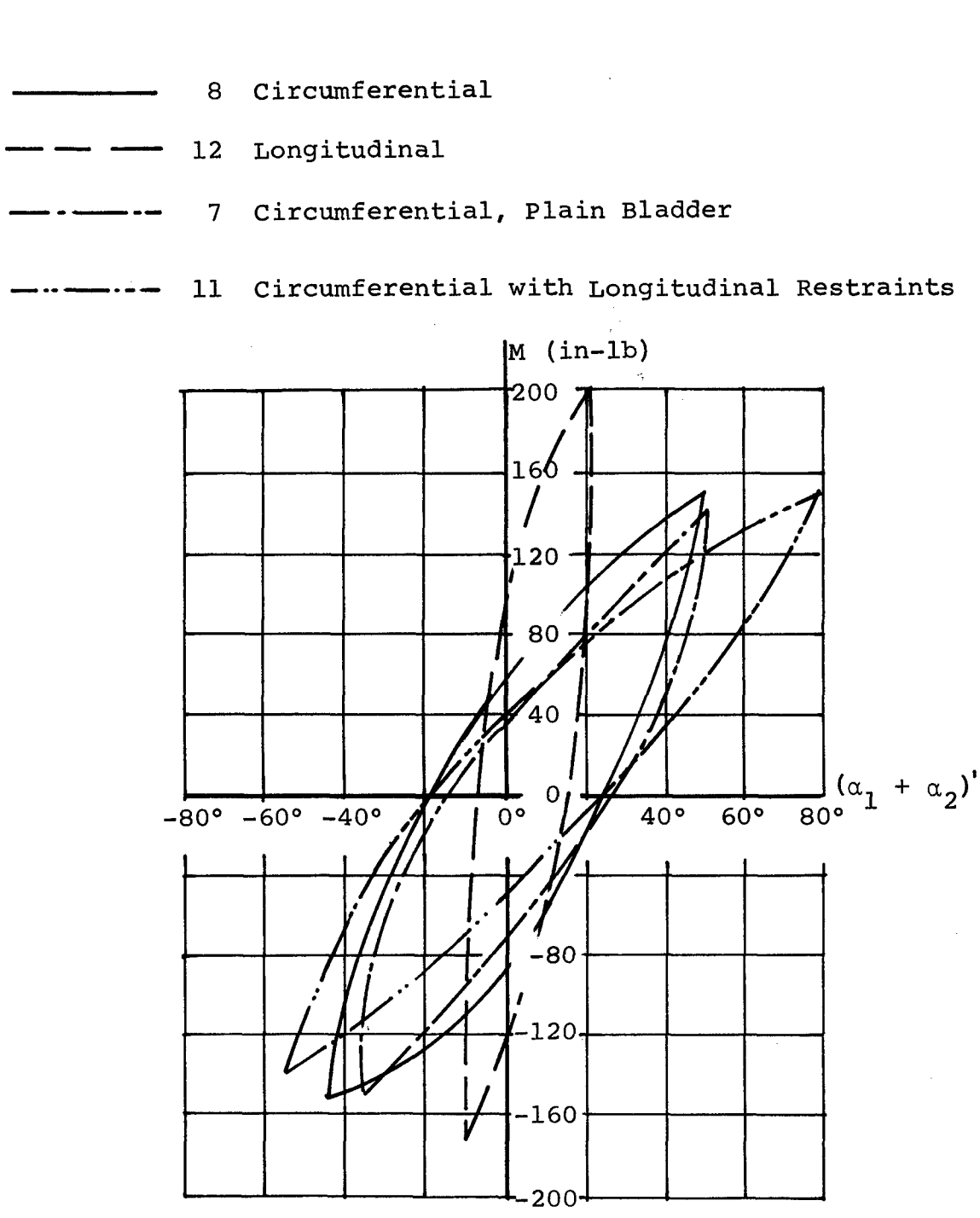

Figure 51. Preliminary Bending Tests of Tubular Samples 1/2-Turn Braided Single-Layer Fabrics at 5 psi Internal Pressure

$(\alpha_1 + \alpha_2)'$ = Sum of Deformation Angles Reduced to Standard Tube Length of 30 Inches

SECTION IX, BENDING ANALYSES OF PRESSURIZED FABRIC TUBES

Theoretical bending analyses of both slip-net and single-layer pressurized fabric tubes have been made under separate contract to the National Aeronautics and Space Administration (Contract No. NAS7-427). The results of this work are contained in two company notes.(5 & 6)

Volume changes as a function of bend angle have been calculated and are shown in figure 52 for the two fabric types. In this figure, V/V_o represents the ratio of volumes after and before bending of the initially straight tubes. $\alpha_{2\pi}$ is the bending angle subtended by a section of the bent tube. This section is the length (measured along the tube) traversed by a fiber as it completes one turn about the tube. β_o is the helical fiber angle on the originally straight tubes.

The cross section is initially circular and is assumed to remain circular during deformation. The fibers are assumed to be inextensible and the load is a pure bending torque. The slip net is approximated in the analysis by two sets of fibers following geodesics on the bent tube and they remain on geodesics by sliding over one another without friction as the tube deforms. The braided single layer is represented in the analysis by two sets of fibers which are counterwound helices on the unbent tube and are knotted at fiber intersections. These knots are equivalent to high friction preventing the fibers from relative motion. The analyses are based on the assumption that the tube deforms into a series of segments of circular tori with the radius of the circular cross section constant, and with the length of the segments and large radii of the tori determined by the fiber kinematic constraints described above, and equilibrium considerations.

---

5. "Volumetric Change of Circular Torus Segments Under Pure Bending", Astro Research Corporation, P.O. Box 4128, Santa Barbara, California. TM No. 145a, June 8, 1967.

6. "Volumetric Change and Bending Moments", Astro Research Corporation, P.O. Box 4128, Santa Barbara, California. TM No. 162, September 8, 1967.

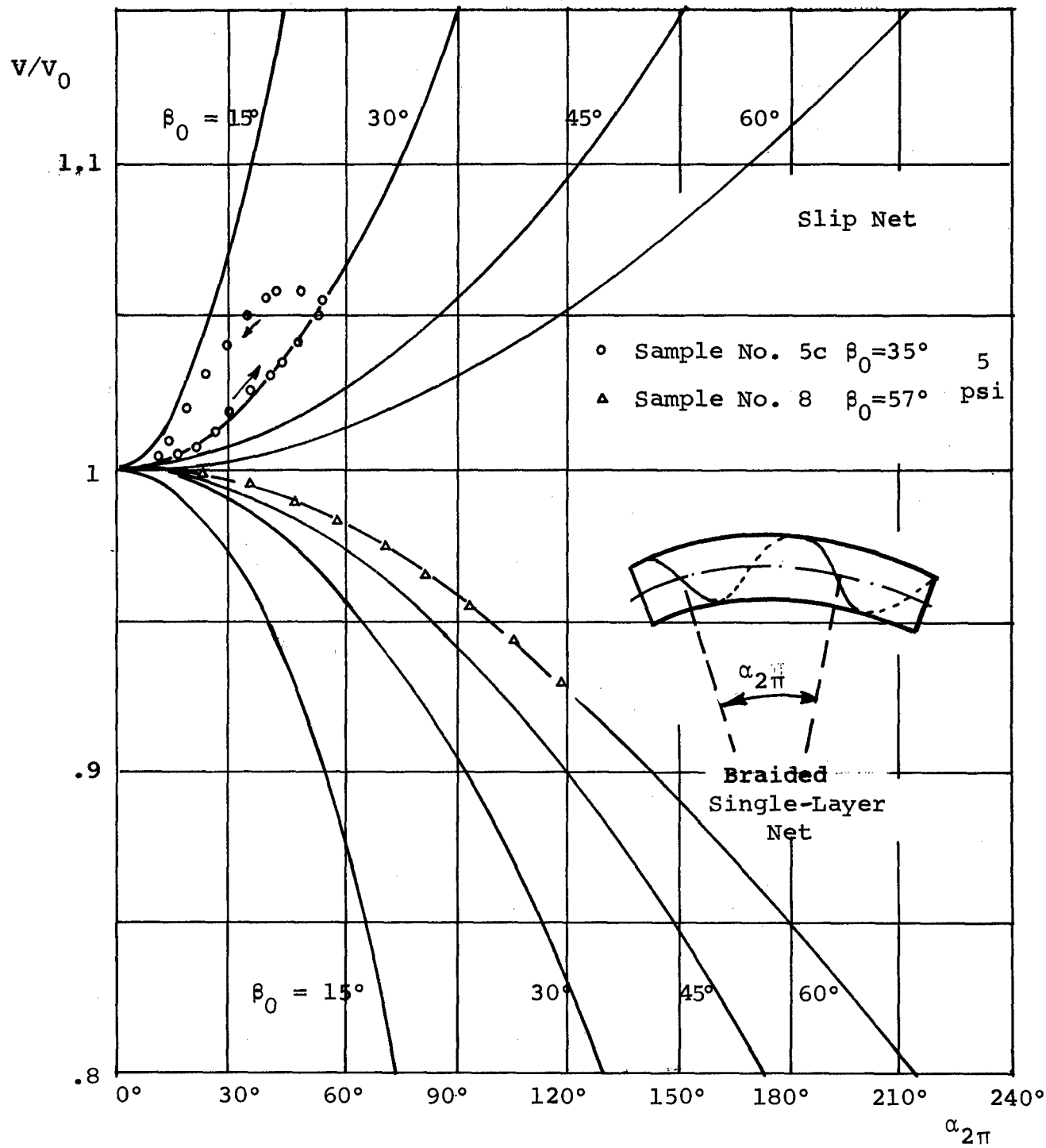

Figure 52. Volumetric Change of Slip-Net and Braided Single-Layer Net Tubes Under Pure Bending

Based on these inputs, the volumetric changes shown in figure 52 are determined as a function of the bending angle $\alpha_{2\pi}$. The solution involves elliptic integrals of the first, second,and third kind,and iterative or graphic evaluation. Based on the results shown in figure 52 the bending moment may be determined if desired from the relation

$$M = -p \frac{dV}{d\alpha} = -p_o \left(\frac{V_o}{V}\right)^n \frac{dV}{d\alpha}$$

where p_o is the initial pressure, $1 < n < \gamma$, and γ is the adiabatic constant (1.4 for O_2, N_2, etc., and 1.667 for inert gas).

The results demonstrate the gross difference in response of the two fabric types to bending deformations. The volume contained by a slip-net fabric increases with increased deformation thus the bending torque (from the equation above) is negative and a force must be applied to stop the tube from further deformation. The volume contained by the braided single-layer fabric decreases with increasing deformation thus the moment is positive and a force must be applied to maintain a given deformation. In an actual fabric tube, friction in the slip-net configuration will oppose slip and therefore will decrease magnitude of volume increase. On the other hand, the braided joints are not as stiff as actual knots thus the fibers will slip within the fabric layer and the volume decrease shown on figure 52 will not be as large.

For comparison, the reduced data of two representative tests are plotted in figure 52. Although these tests were side-load bending tests, the agreement with the theoretical values is surprisingly good. The test data was reduced by computing $\alpha_{2\pi}$ from the total deflection (α_1 and α_2) .

$$\alpha_{2\pi} = (\alpha_1 + \alpha_2) \frac{\pi d \tan \beta_o}{\ell}$$

where d is the diameter and ℓ the length of the tubular sample. The value for β_o corresponds in the case of the slip net to the angle between the meridian and the mean fiber direction, β . For the single-layer fabric β_o is equivalent to γ_1 and γ_2 when the mean fiber direction is circumferential.

In figure 52, the volume change of the single-layer fabric (Sample No. 8) is represented by a single row of points only, because the response was essentially elastic and the hysteresis loop is very small. The slip net (Sample No. 5c) exhibited a considerable difference (see also figure 45) with a large hysteresis loop.

SECTION X, CONCLUSIONS

The slip-net wrist and elbow as developed during this program are ideally suited for use in soft pressure suits. Either braided or knitted fabrics can be used. The performance of the braided fabrics is superior; however, the knitted fabrics are less costly. If production braiding machines are developed, the cost difference can be eliminated. The degradation in performance of the wrist after change to the heavier zipper can be eliminated by use of lighter zippers. For example, a plastic spiral zipper has been developed by the Scovill Manufacturing Company which has comparable strength and is considerably more flexible. It is recommended that this zipper be considered for use in any future designs in which the pressure bladder is not cut along the zipper line.

Though the functions of the soft forearm for wrist-forearm torsional compliance is acceptable for limited motion, a disconnect similar to the Gemini wrist disconnect but positioned halfway between the elbow and the wrist is recommended. The performance advantage of the disconnect is supplemented by the fact that the gloves can be taken off with ease. This is a major improvement in user comfort over an integral design. The position of the disconnect halfway between the wrist and elbow is ideal both for space suits and Boyle's Law-type pressure garments. In the human arm, torsional motion in the area forward of the elbow takes place entirely in the forearm, and the wrist actually goes through a rigid body-twisting motion. Thus, particularly in Boyle's Law garments, where pressure is applied through tubes bearing on the skin, the constraint layer should perform its twisting motion as close as possible to where the arm twists to minimize relative motion between the skin and the pressure tubes. Placing the disconnect at the middle of the forearm also allows the improved slip-net wrist to be properly designed by leaving the required length of soft fabric in the wrist area.

The combination of the slip-net shoulder and the braided single-net upper arm is recommended for soft shoulder pressure-suit components over the single-layer design in the Gemini suit. It is more comfortable, requires less force to deform, and has a significantly larger range of motion. However, there is good indication that further development of the slip-net concept will improve performance of the shoulder components. The problem centers on compatibility of both displacements and fiber load distribution between the knitted underlayer and the slip net.

The slip action did not permeate into the chest and back areas because compatibility has not been completely achieved in the current design. As a consequence, part of the slip net is slack, the major portion of the biaxial load in these regions being carried by the undergarment. In other regions, the undergarment is slack and the entire biaxial load is carried by the slip net. Ideally, the undergarment will carry the major part of the circumferential component of stress in the chest, back, and underarm areas. The slip-net fiber paths and knot lines can then be positioned such that the changes in load distribution during motion are accommodated by slip in the outer net rather than changes in fiber load level.

Security Classification

DOCUMENT CONTROL DATA - R & D

(Security classification of title, body of abstract and indexing annotation must be entered when the overall report is classified)

1. ORIGINATING ACTIVITY (Corporate author)	2a. REPORT SECURITY CLASSIFICATION
ASTRO Research Corporation 1330 Cacique, P.O. Box 412B Santa Barbara, California 92703	UNCLASSIFIED 2b. GROUP N/A

3. REPORT TITLE

SLIP NET MOBILITY JOINTS FOR PRESSURE SUITS

4. DESCRIPTIVE NOTES (Type of report and inclusive dates)

Final Report, 1 April 1967 - 31 May 1968

5. AUTHOR(S) (First name, middle initial, last name)

A.F. Fraser
P.R. Preiswerk

6. REPORT DATE	7a. TOTAL NO. OF PAGES	7b. NO. OF REFS
November 1968	83	0

8a. CONTRACT OR GRANT NO. F33615-67-C-1586 b. PROJECT NO. 7164 c. Task No. 716411 d.	9a. ORIGINATOR'S REPORT NUMBER(S) ARC-R-286 9b. OTHER REPORT NO(S) (Any other numbers that may be assigned this report) AMRL-TR-68-94

10. DISTRIBUTION STATEMENT

This document is subject to special export controls and each transmittal to foreign governments or foreign nationals may be made only with prior approval of Aerospace Medical Research Laboratories, Wright-Patterson Air Force Base, Ohio 45433.

11. SUPPLEMENTARY NOTES	12. SPONSORING MILITARY ACTIVITY
	Aerospace Medical Research Laboratories Aerospace Medical Div., Air Force Systems Command, Wright-Patterson AFB, OH 45433

13. ABSTRACT

The results of a 1-year experimental program to develop and evaluate fabric constraint layers for pressurizable suits are described. The principal object of the development was to produce soft-pressure-suit components with minimum constraint to motion and with maximum range of motion. A secondary goal was to develop joint designs that allow the user to maintain displaced positions of the limbs with minimum use of sustaining force.

DD FORM 1 NOV 65 1473

Security Classification

14. KEY WORDS	LINK A		LINK B		LINK C	
	ROLE	WT	ROLE	WT	ROLE	WT
Pressure suits						
Pressure suit mobility						
Pressure suit design						
Joint mobility						
Slip-net materials						
Dacron tufbraid						
Pressurization tests						
Fatigue tests (fabric)						
Gemini II space suit						